

**KATG AS A DEFENSE AGAINST HYDROGEN PEROXIDE TOXICITY:
FROM A REDUNDANT C-TERMINAL DOMAIN TO
THE PARADOXICAL SYNERGY OF
TWO MUTUALLY ANTAGONISTIC ACTIVITIES**

by

Haijun Duan

A dissertation submitted to the Graduate Faculty of
Auburn University
in partial fulfillment of the
requirements for the Degree of
Doctor of Philosophy

Auburn, Alabama
December 13, 2014

Copyright 2014 by Haijun Duan

Approved by

Douglas C. Goodwin, Chair, Associate Professor of Chemistry and Biochemistry
Holly R. Ellis, Associate Professor of Chemistry and Biochemistry
Eduardus C. Duin, Associate Professor of Chemistry and Biochemistry
Christopher J. Easley, Knowles Associate Professor of Chemistry and Biochemistry

Abstract

Catalase-peroxidases (KatGs), first discovered in 1979, are heme-dependent enzymes mainly found in bacteria, archaea and fungi. They are capable of decomposing H_2O_2 by catalatic and peroxidatic pathways. KatG has garnered considerable attention due to its role in activation of the front-line antitubercular drug isoniazid. Mutations to the *katG* gene in *Mycobacterium tuberculosis* are frequently associated with isoniazid resistance. Moreover, periplasmic catalase-peroxidases from highly pathogenic bacteria such as *Escherichia coli* O157:H7, *Yersinia pestis* and *Legionella pneumophila* have been implicated as virulence factors. The robust catalase activity of KatG that even rivals the canonical catalase is astounding given that the enzyme bears a peroxidase-like protein core with little if any resemblance to the canonical catalases. Indeed, the active site of KatG is almost superimposable to peroxidases such as cytochrome *c* peroxidase and ascorbate peroxidase. Nevertheless, KatG is the only enzyme in the entire superfamily that has appreciable catalase activity. One of the most important structural features that distinguish KatG from its relative peroxidases is an extra C-terminal domain which is proposed to have originated from gene duplication and fusion. It has been observed that the C-terminal domain maintains the active site architecture of KatG that is essential for both catalase and peroxidase activity. It appears to prevent the otherwise spontaneous coordination of the distal histidine to the heme iron. However, the mechanisms by which the C-terminal domain does this from a distance no closer than 30 Å from the active site remains to be elucidated. The research reported in this dissertation evaluated the roles of C-terminal domain in KatG function. In particular, the

interface between N-terminal domain harboring the active site and C-terminal domain within each subunit reveals two strictly conserved H-bond networks, namely distant- and near-network based on their distance from the active site. With C-terminal domain's ability to reactivate the N-terminal domain being employed, stand-alone domain proteins targeting these conserved H-bond interactions in both networks were generated by site-directed mutagenesis and characterized by spectroscopic and kinetic studies. It was shown while the reactivation process was largely unaffected by substitutions, the resulting domain variants exhibited distinct properties from the unmodified domain proteins. Substitution of Arg 117 and Arg 479 substantially shifted the heme species from predominantly narrow rhombic to broad rhombic high-spin. Although catalase activity was diminished to different extent ranging from 24% to 99%, it appeared to have no significant correlation with low-spin contribution observed in the reactivated domain variants. Moreover, substantially impaired peroxidase activity was observed in near-network variants with either Asp 482 or Arg 479 substitution. These results suggest that the C-terminal domain modulated catalase and peroxidase activity of KatG by low-spin-independent mechanisms. In light of peroxidatic electron donors (PxEDs) of peroxidase activity in KatG, it was strikingly observed that instead of inhibiting catalase activity as expected based on the current proposed mechanism, PxEDs stimulated catalytic turnover of the periplasmic catalase-peroxidase from *E. coli* O157:H7 (KatP) by reduced apparent K_M and enhanced apparent k_{cat} . The acidic conditions under which PxED-assisted catalytic turnover was optimal are well mirrored in host immune responses where bacteria are challenged with copious H_2O_2 in the acidic environment of phagolysosomes. With the model organism *E. coli*, we constructed single, double and triple mutants with *ahpCF*, *katE* and *KatG* null mutation and demonstrated that KatG played the pivotal role in aerobic growth of *E. coli*. To evaluate the stimulatory effect observed *in vitro*, we

complemented *katE/katG* and *ahpCF/katE/katG* mutants with fully active wild-type *katG* gene and Y229F *katG* gene from *M. tuberculosis*. Our results suggest that in the presence of PxEDs, catalase-inactive Y229F KatG with an even enhanced peroxidase activity was not sufficient to alleviate H₂O₂-induced growth inhibition. Conversely, PxEDs stimulated the catalase activity of KatG as evidenced by that wild-type *katG* complemented *katE/katG* mutant recovered from H₂O₂ challenge within 2 hours in the presence of TMB compared to a lag period of 12 hours when TMB was absent. Our work provides the first evidence that PxEDs remarkably enhanced bacterial defenses against H₂O₂ by specifically stimulating the *catalase* activity of KatG thereby contributed to bacterial survival under H₂O₂ assaults.

Acknowledgments

My deepest gratitude goes to my advisor Dr. Douglas Goodwin. He has been a huge influence on me growing up as a researcher which in turn paved the way for my career down the road. He has also been a role model for future mentors, nurturing and patient, always encouraging his students to take initiative and work independently. He has mentored me not just on a scientific ground but also on a philosophical level which manifest the true meaning of Ph.D.

My appreciation further extends to my honored committee, Dr. Holly Ellis, Dr. Eduardus Duin and Dr. Christopher Easley for their excellent support and valuable suggestions. Dr. Ellis has always been inspiring and supportive on my research with her enthusiasm and persistence. Dr. Duin has been a tremendous help in my EPR experiments with his friendliness unmatched anywhere. Dr. Easley has shown me the path from a new PI to an accomplished professor with his motivation and energy. Moreover, I am especially thankful and privileged to have worked at the Suh Lab. Dr. Sang-Jin Suh has offered me lots of valuable suggestions on my project and his radiant personality touches everybody who knows him.

I would also like to thank my colleagues Dr. Carma Cook, Dr. Robert Moore, Dr. Shalley Kudalkar, Dr. Yu Wang and Dr. Elizabeth Ndontsa from the Goodwin lab, Zhou Tong, Bingyu Li from the Suh Lab for their magnificent support and encouragement.

My sincere appreciations also go to my parents and sisters for their everlasting caring and love throughout my entire life.

Table of Contents

| | |
|---|----|
| Abstract..... | ii |
| Acknowledgments | v |
| List of Figures..... | xi |
| List of Tables | xv |
| Chapter One Literature Review | 1 |
| 1.1 The Evolution and Activation of Oxygen | 1 |
| 1.2 Reactive Oxygen Species and Cellular Damage | 1 |
| 1.3 Sources of Reactive Oxygen Species | 4 |
| 1.3.1 Endogenous sources | 4 |
| 1.3.1.1 Photosynthesis | 4 |
| 1.3.1.2 Aerobic respiration | 5 |
| 1.3.1.3 Autoxidation of flavoproteins..... | 5 |
| 1.3.2 Exogenous sources | 6 |
| 1.3.2.1 Antibiotic action | 6 |
| 1.3.2.2 Oxidative burst | 8 |
| 1.4 Cellular Responses to Oxidative Stress | 9 |
| 1.4.1 Defensive mechanisms | 9 |
| 1.4.1.1 Superoxide scavengers | 9 |
| 1.4.1.2 Hydrogen peroxide scavengers..... | 12 |

| | |
|--|----|
| 1.4.1.2.1 Alkyl hydroperoxide reductase..... | 12 |
| 1.4.1.2.2 Monofunctional heme catalases | 14 |
| 1.4.1.2.3 Bifunctional catalases | 16 |
| 1.4.2 Immune Responses | 28 |
| Chapter Two Essential Role of Distant Interdomain H-bond Interactions in Heme Environment and Catalytic Function of KatGs | 32 |
| 2.1 Introduction | 32 |
| 2.2 Materials and Methods | 38 |
| 2.2.1 Reagents | 38 |
| 2.2.2 Cloning and expression of KatG ^N , KatG ^C and their variants of the distant-network.. | 39 |
| 2.2.3 Purification of KatG ^N , KatG ^C and their variants of the distant-network..... | 40 |
| 2.2.4 Domain combination and incubation..... | 41 |
| 2.2.5 UV-visible absorption spectra and activity assays | 41 |
| 2.2.6 Circular and magnetic circular dichroism | 42 |
| 2.2.7 Electron paramagnetic resonance spectroscopy | 42 |
| 2.3 Results | 42 |
| 2.3.1 Circular dichroism and UV-visible spectroscopy..... | 42 |
| 2.3.2 Magnetic circular dichroism..... | 44 |
| 2.3.3 Electron paramagnetic resonance | 47 |
| 2.3.4 Reactivation and steady-state kinetics..... | 50 |
| 2.4 Discussion..... | 54 |
| Chapter Three Integral Role of Interdomain Interactions 20 Å from Active Site in Heme Environment and Catalytic Function of KatGs | 65 |
| 3.1 Introduction | 65 |

| | |
|---|-----|
| 3.2 Materials and Methods | 67 |
| 3.2.1 Reagents | 67 |
| 3.2.2 Cloning and expression of KatG ^N , KatG ^C and their variants of the near-network..... | 69 |
| 3.2.3 Purification of KatG ^N , KatG ^C and their variants of the near-network..... | 70 |
| 3.2.4 Domain combination and incubation..... | 71 |
| 3.2.5 UV-visible absorption spectra and activity assays | 71 |
| 3.2.6 Circular and magnetic circular dichroism | 72 |
| 3.2.7 Electron paramagnetic resonance spectroscopy | 72 |
| 3.3 Results | 73 |
| 3.3.1 Circular dichroism and UV-visible spectroscopy..... | 73 |
| 3.3.2 Magnetic circular dichroism..... | 73 |
| 3.3.3 Electron paramagnetic resonance | 76 |
| 3.3.4 Reactivation and steady-state kinetics..... | 78 |
| 3.4 Discussion..... | 84 |
| Chapter Four Effect of Peroxidatic Electron Donors on the Catalase Activity of Pathogen- derived Periplasmic Catalase-peroxidase | 95 |
| 4.1 Introduction | 95 |
| 4.2 Materials and Methods | 97 |
| 4.2.1 Reagents | 97 |
| 4.2.2 Cloning and expression of KatP | 98 |
| 4.2.3 Purification of KatP | 98 |
| 4.2.4 UV-visible absorption spectra and activity assays | 99 |
| 4.2.5 Catalase activity assay by O ₂ production | 99 |
| 4.2.6 Comparison of PxED radical production and H ₂ O ₂ consumption..... | 100 |

| | |
|---|-----|
| 4.2.7 Circular dichroism | 100 |
| 4.3 Results | 101 |
| 4.3.1 Peroxidatic electron donor enhances the catalytic turnover of KatP at neutral pH. .. | 101 |
| 4.3.2 PxED stimulation of KatP catalase activity at acidic pH. | 103 |
| 4.3.3 Effect of pH on PxED-assisted catalase activity of KatP. | 103 |
| 4.3.4 NADPH marginally assisted catalase activity of KatP at pH 5.0. | 107 |
| 4.3.5 Production of ABTS radical is minimal and even negligible compared to the production of O ₂ even at peroxidase optimal condition. | 108 |
| 4.4 Discussion..... | 108 |
| Chapter Five Peroxidatic Electron Donors Enhance Bacterial Defenses Against H ₂ O ₂ During Oxidative Stress in <i>Escherichia coli</i> | 119 |
| 5.1 Introduction | 119 |
| 5.2 Materials and Methods | 122 |
| 5.2.1 Reagents | 122 |
| 5.2.2 Strain constructions | 122 |
| 5.2.3 Bacterial growth studies | 125 |
| 5.2.4 KatG expression analysis | 127 |
| 5.2.5 H ₂ O ₂ challenge assays | 127 |
| 5.3 Results | 128 |
| 5.3.1 KatG plays the critical role for bacterial defenses against H ₂ O ₂ during aerobic metabolism. | 128 |
| 5.3.2 Peroxidatic electron donors ABTS and TMB pose no adverse effect on aerobic growth of <i>katG</i> complemented strains..... | 130 |
| 5.3.3 PxEDs afford a more effective and quick response to oxidative stress for mutant strains complemented with the fully active wild-type <i>katG</i> gene. | 131 |
| 5.3.4 PxEDs enhance bacterial defenses against H ₂ O ₂ by stimulating the <i>catalase</i> | |

| | |
|--------------------------|-----|
| activity of KatG | 133 |
| 5.4 Discussion..... | 136 |
| Chapter Six Summary..... | 142 |
| References | 149 |

List of Figures

| | |
|---|----|
| Figure 1.1 The sequential univalent reduction of oxygen (A) and reactive oxygen species (ROS) induced oxidative damage to DNA, lipids and proteins (B) | 3 |
| Figure 1.2 Two pathways of autoxidation of FADH ₂ in flavoproteins | 7 |
| Figure 1.3 Active site of <i>Escherichia coli</i> KatE (as known as HPII) (A) and catalytic cycle of canonical catalases (B) | 17 |
| Figure 1.4 Active sites of lignin peroxidase (LiP) (A), manganese peroxidase (MnP) (B) and horseradish peroxidase (HRP) (C) | 20 |
| Figure 1.5 Catalytic cycle of canonical peroxidases | 21 |
| Figure 1.6 Active sites of cytochrome <i>c</i> peroxidase (CcP) (A), ascorbate peroxidase (APx) (B) and catalase-peroxidase (KatG) (C) | 23 |
| Figure 1.7 Unique structural features of KatGs: an extra C-terminal domain (A); two Large Loops (B); Met-Tyr-Trp covalent adduct and the mobile arginine (C) | 25 |
| Figure 1.8 Current proposed catalytic cycle of catalase activity of KatGs | 29 |
| Figure 2.1 Catalytic cycles of catalase-peroxidases | 33 |
| Figure 2.2 Comparison of active sites: canonical catalase (A) and catalase-peroxidase and canonical peroxidase overlaid (B) | 35 |
| Figure 2.3 Interactions between the N-terminal domain BC interhelical loop and the C-terminal domain B'C' interhelical loop, E' helix in KatG | 37 |
| Figure 2.4 Far-UV circular dichroism spectra of KatG ^N and its variants (A) and KatG ^C and its variants (B) in the distant-network | 43 |
| Figure 2.5 UV-visible spectral comparison of distant-network reactivated variants with inactive KatG ^N and fully active wtKatG in their native state | 45 |
| Figure 2.6 MCD spectral comparison of distant-network reactivated variants with inactive KatG ^N and fully active wtKatG in ferrous state of heme | 46 |

| | |
|---|----|
| Figure 2.7 EPR spectra of distant-network reactivated variants without Q600 substitutions along with KatG ^N and KatG ^N +KatG ^C for comparison | 48 |
| Figure 2.8 EPR spectra of distant-network reactivated variants with Q600 substitutions along with KatG ^N and KatG ^N +KatG ^C for comparison | 49 |
| Figure 2.9 Effect of H ₂ O ₂ concentration on catalase activity of distant-network domain variants and unmodified KatG ^N +KatG ^C for comparison..... | 56 |
| Figure 2.10 Correlation between catalase activity k_{cat} and low-spin contribution in reactivated distant-network variants (●) with KatG ^N and KatG ^N +KatG ^C as two endpoints (■) | 61 |
| Figure 2.11 Correlation between peroxidase activity k_{cat} and low-spin contribution in reactivated distant-network variants (●) with KatG ^N and KatG ^N +KatG ^C as two endpoints (■): H ₂ O ₂ -dependent peroxidase activity (A) and ABTS-dependent peroxidase activity (B) | 62 |
| Figure 2.12 Correlation between H ₂ O ₂ -dependent peroxidase activity and catalase activity with respect to k_{cat}/K_M in reactivated distant-network variants (●) with KatG ^N and KatG ^N +KatG ^C as two endpoints (■)..... | 63 |
| Figure 3.1 Near-network Interactions between the N-terminal domain BC interhelical loop and the C-terminal domain B'C' interhelical loop in KatG | 68 |
| Figure 3.2 Far-UV circular dichroism spectra of KatG ^N and Y111A ^N (A) and KatG ^C and its variants (B) in the near-network | 74 |
| Figure 3.3 UV-visible spectral comparison of near-network reactivated variants with inactive KatG ^N and fully active wtKatG in their native state..... | 75 |
| Figure 3.4 MCD spectral comparison of near-network reactivated variants with inactive KatG ^N and fully active wtKatG in ferrous state of heme..... | 77 |
| Figure 3.5 EPR spectra of near-network reactivated variants along with KatG ^N , and KatG ^N +KatG ^C for comparison..... | 79 |
| Figure 3.6 Effect of H ₂ O ₂ concentration on catalase activity of near-network domain variants and unmodified KatG ^N +KatG ^C for comparison..... | 83 |
| Figure 3.7 Effect of H ₂ O ₂ concentration on peroxidase activity of near-network domain variants and unmodified KatG ^N +KatG ^C for comparison..... | 85 |
| Figure 3.8 Effect of ABTS concentration on peroxidase activity of near-network domain variants and unmodified KatG ^N +KatG ^C for comparison..... | 86 |

| | |
|--|-----|
| Figure 3.9 Interactions of the effects of two single variants Y111A ^N +KatG ^C and KatG ^N +R479A ^C on catalase activity (k_{cat}) in double variant Y111A ^N +R479A ^C | 89 |
| Figure 3.10 Correlation between catalase activity k_{cat} and low-spin contribution in reactivated near-network variants (●) with KatG ^N and KatG ^N +KatG ^C as two endpoints (■) | 91 |
| Figure 3.11 Correlation between peroxidase activity k_{cat} and low-spin contribution in reactivated near-network variants (●) with KatG ^N and KatG ^N +KatG ^C as two endpoints (■): H ₂ O ₂ -dependent peroxidase activity (A) and ABTS-dependent peroxidase activity (B) | 92 |
| Figure 3.12 Correlation between H ₂ O ₂ -dependent peroxidase activity and catalase activity with respect to k_{cat}/K_M in reactivated near-network variants (●) with KatG ^N and KatG ^N +KatG ^C as two endpoints (■) | 93 |
| Figure 4.1 Effect of H ₂ O ₂ concentration on the rate of O ₂ production by KatP at pH 7.0 in the absence of PxEDs and in the presence of 0.1 mM ABTS | 102 |
| Figure 4.2 Effect of H ₂ O ₂ concentration on the rate of O ₂ production by KatP at pH 5.0 in the absence of PxEDs and in the presence of 0.1 mM ABTS | 104 |
| Figure 4.3 Effect of H ₂ O ₂ concentration on the rate of O ₂ production by KatP at pH 5.0 in the absence of PxEDs and in the presence of 0.1 mM TMB and 0.1 mM TMPD..... | 105 |
| Figure 4.4 pH profile of PxED-stimulated catalase activity (A) and unassisted catalase and peroxidase activity (B) of KatP | 106 |
| Figure 4.5 Far-UV circular dichroism spectra of KatP at low pH (4.5-3.0)..... | 109 |
| Figure 4.6 Effect of H ₂ O ₂ concentration on the rate of O ₂ production by KatP at pH 5.0 in the absence of PxEDs and in the presence of 0.1 mM NADPH..... | 110 |
| Figure 4.7 Production of ABTS ⁺ in comparison to H ₂ O ₂ consumption by KatP | 112 |
| Figure 4.8 The arginine switch and covalent adduct in KatP..... | 115 |
| Figure 4.9 Proposed mechanism accounting for the stimulation of KatP catalase activity by PxEDs | 118 |
| Figure 5.1 Divergence of catalase and peroxidase catalytic cycles in KatG | 121 |
| Figure 5.2 Construction of Δ <i>ahpCF</i> mutant..... | 126 |

| | |
|---|-----|
| Figure 5.3 Growth curves of wild-type and mutant strains in LB medium..... | 129 |
| Figure 5.4 Protein expression analyses of wild-type KatG and Y229F KatG..... | 132 |
| Figure 5.5 Effect of PxEDs on recovery of the growth of <i>katE/katG</i> double mutant complemented with wild-type <i>katG</i> (DG004) at pH 5.0 | 134 |
| Figure 5.6 Effect of PxEDs on recovery of the growth of <i>ahpCF/katE/katG</i> triple mutant complemented with wild-type <i>katG</i> (DG011) at pH 5.0 | 135 |
| Figure 5.7 Effect of PxEDs on recovery of the growth of <i>katE/katG</i> double mutant complemented with Y229F <i>katG</i> (DG005) at pH 5.0 | 137 |
| Figure 5.8 Effect of PxEDs on recovery of the growth of <i>ahpCF/katE/katG</i> triple mutant complemented with Y229F <i>katG</i> (DG012) at pH 5.0. | 138 |

List of Tables

| | |
|---|-----|
| Table 2.1 Ratios of EPR signals observed for distant-network reactivated variants along with KatG^{N} , $\text{KatG}^{\text{N}}+\text{KatG}^{\text{C}}$ and wtKatG for comparison | 51 |
| Table 2.2 Reactivation kinetic parameters of catalase activity of distant-network domain variants and unmodified $\text{KatG}^{\text{N}}+\text{KatG}^{\text{C}}$ for comparison..... | 52 |
| Table 2.3 Reactivation kinetic parameters of peroxidase activity of distant-network domain variants and unmodified $\text{KatG}^{\text{N}}+\text{KatG}^{\text{C}}$ for comparison..... | 53 |
| Table 2.4 Apparent peroxidase kinetic parameters of distant-network domain variants and unmodified $\text{KatG}^{\text{N}}+\text{KatG}^{\text{C}}$ for comparison | 55 |
| Table 2.5 Apparent catalase kinetic parameters of distant-network domain variants and unmodified $\text{KatG}^{\text{N}}+\text{KatG}^{\text{C}}$ for comparison | 56 |
| Table 3.1 Ratios of EPR signals observed for near-network reactivated variants along with KatG^{N} , $\text{KatG}^{\text{N}}+\text{KatG}^{\text{C}}$ and wtKatG for comparison | 80 |
| Table 3.2 Reactivation kinetic parameters of catalase activity of near-network domain variants and unmodified $\text{KatG}^{\text{N}}+\text{KatG}^{\text{C}}$ for comparison..... | 81 |
| Table 3.3 Reactivation kinetic parameters of peroxidase activity of near-network domain variants and unmodified $\text{KatG}^{\text{N}}+\text{KatG}^{\text{C}}$ for comparison..... | 82 |
| Table 3.4 Apparent catalase kinetic parameters of near-network domain variants and unmodified $\text{KatG}^{\text{N}}+\text{KatG}^{\text{C}}$ for comparison | 83 |
| Table 3.5 Apparent H_2O_2 -dependent peroxidase kinetic parameters of near-network domain variants and unmodified $\text{KatG}^{\text{N}}+\text{KatG}^{\text{C}}$ for comparison..... | 85 |
| Table 3.6 Apparent ABTS-dependent peroxidase kinetic parameters of near-network domain variants and unmodified $\text{KatG}^{\text{N}}+\text{KatG}^{\text{C}}$ for comparison..... | 86 |
| Table 4.1 Effect of ABTS on apparent catalase kinetic parameters of KatP at pH 7.0..... | 102 |
| Table 4.2 Effect of ABTS on apparent catalase kinetic parameters of KatP at pH 5.0..... | 104 |
| Table 4.3 Effect of TMB and TMPD on apparent catalase kinetic parameters of KatP | |

| | |
|---|-----|
| at pH 5.0 | 105 |
| Table 4.4 Effect of NADPH on apparent catalase kinetic parameters of KatP at pH 5.0 | 110 |
| Table 4.5 Comparison of peroxidase kinetic parameters of KatP with different PxEDs at pH 5.0 | 111 |
| Table 5.1 Strains and plasmids used in this study | 124 |

CHAPTER ONE LITERATURE REVIEW

1.1 The Evolution and Activation of Oxygen

The first molecule of oxygen on Earth is believed to have been generated by cyanobacteria, formerly known as blue-green algae, about three billion years ago. As a foreign moiety produced from water-splitting, molecular oxygen (O_2) is essentially unreactive due to spin restriction in its triplet ground state with most singlet organic molecules whose electrons are all paired up (1). Consequently, the activation of oxygen can be achieved either by reversing the spin of one unpaired electron to form singlet oxygen or by transfer of one electron at a time undergoing univalent reduction (2). The subsequent Great Oxidation Event occurred after emergence of cyanobacteria heralded an era with life forms bearing an aerobic metabolic plan and, at the same time, exerted enormous selection pressure on the evolution of alternative biochemical mechanisms in an oxygenic environment. Indeed, the metabolic efficiency improved dramatically. For example, the amount of ATP produced by metabolizing glucose aerobically increased by up to 19-fold. However, the benefits come at a price. Due to molecular oxygen's propensity for univalent reduction, partially reduced reactive oxygen species (ROS) are inevitably generated, posing a threat to all organisms living in aerobic habitats.

1.2 Reactive Oxygen Species and Cellular Damage

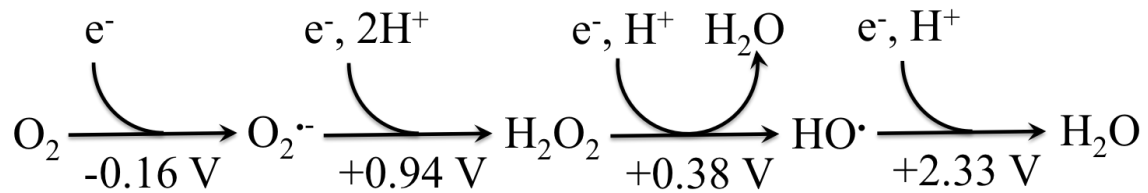
The nature of oxygen toxicity is not self-evident given the stability of molecular oxygen, and it was not until 1954 the notion that free radicals lie at the root of oxygen toxicity

was first proposed (3). The discovery suggested that oxygen poisoning occurred by mechanisms similar to X-ray radiation - by production of partially reduced reactive oxygen species (ROS). The four-electron reduction of oxygen by sequential one-electron steps first generates superoxide ($O_2^{\cdot-}$), followed by hydrogen peroxide (H_2O_2). Reduction of the peroxide O-O bond generates HO^{\cdot} and HO^- , and reduction of HO^{\cdot} generates the second equivalent of H_2O (Figure 1.1A). It is these three partially reduced oxygen species that are responsible for toxicity of O_2 and are thus relevant to the damage of critical biomolecules such as DNA, lipids and proteins (Figure 1.1B).

ROS are a major source for DNA damage (4). They can lead to the modifications of sugar and base moieties of DNA, including deoxyribose oxidation and base alterations, and result in strand breaks, removal of nucleotides and DNA-protein crosslinks (2). These changes in the nucleotides can further lead to the mismatches between the two strands causing subsequent mutations, especially G:C to T:A transversions. The DNA-protein crosslinks caused by hydroxyl radicals can severely affect normal cellular functions by blocking replication and transcription if unrepaired (5).

The primary mode of lipid damage by ROS is by way of lipid peroxidation in which lipid-derived radicals are generated. These can further react with other molecules in a chain reaction fashion aggravating the detrimental effect. The common sites that ROS attack on the phospholipids are the unsaturated carbon-carbon double bond, particularly the bis-allylic arrangement of most polyunsaturated fatty acids, as well as the ester linkage between glycerol and the fatty acid. Peroxidation of lipids by ROS can lead to chain breakage, thereby alter membrane fluidity, permeability and potentially affect membrane-bound signaling proteins as well (2).

A



B

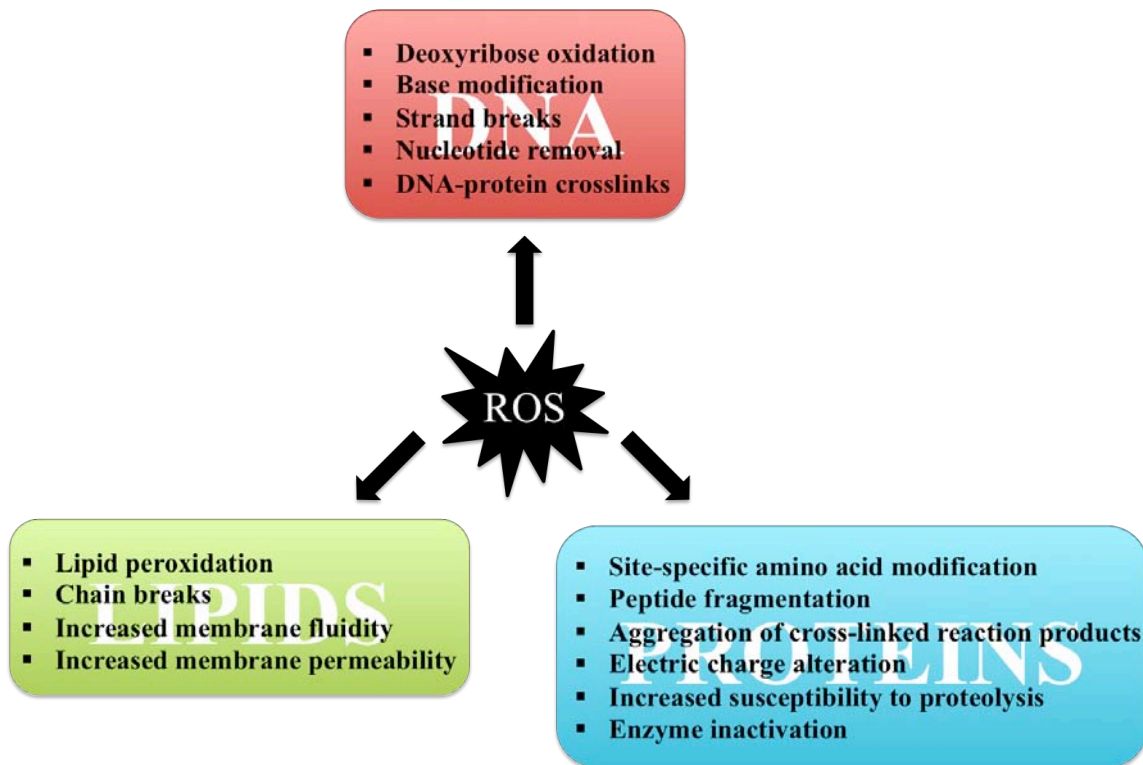


Figure 1.1. The sequential univalent reduction of oxygen (A). The standard reduction potentials are indicated for pH 7.0; the standard concentration of O_2 is designated as 1 M. Reactive oxygen species (ROS) induced oxidative damage to DNA, lipids and proteins (B).

ROS adversely affect proteins in various ways. Amino acids differ in their susceptibility to ROS attacks. Thiol groups and sulfur containing amino acids such as cysteine and methionine are very sensitive to ROS (6). Tryptophan is rapidly lost while tyrosine is cross-linked to form bi-tyrosine upon exposure to hydroxyl radicals (7). As a result, amino acid modifications, peptide fragmentations and cross-linked reaction products can further alter electric charge and promote proteolysis. It has also been shown that the iron-sulfur cluster containing proteins such as dehydratases are much sensitive to superoxide that causes an irreversible oxidation leading to enzyme inactivation (8).

1.3 Sources of Reactive Oxygen Species

ROS are formed intracellularly as unwanted (but not always) yet inevitable by-products of metabolism as well as extracellularly as desired weapons in the battleground for killing bacteria.

1.3.1 Endogenous sources

1.3.1.1 Photosynthesis

It is conceivable that cyanobacteria must be among one of the very first organisms to encounter and tackle ROS. Photosynthesis did exist before cyanobacteria and was utilized mainly by green and purple sulfur bacteria as well as heliobacteria, but only a pittance of energy could be generated by those anoxygenic photosynthetic systems. Two types of photosystems, i.e., Photosystem I (PSI) and Photosystem II (PSII), are found in the thylakoid membranes of cyanobacteria, algae and plants, and these are also the generation sites of ROS. Electron transport across the thylakoid membrane terminated by NADPH synthesis is adventitiously coupled with the formation of superoxide and hydrogen peroxide through direct photoreduction of oxygen in PSI (9, 10). In PSII, singlet oxygen

can be generated by the excitation energy transfer from triplet chlorophyll (11, 12). Additionally, the electron transport in PSII contributes to the leakage of electrons to molecular oxygen forming ROS due to incomplete oxidation of water (13). The rate of ROS production is enhanced when the absorption of light by chlorophylls exceeds the capacity for the energy utilization by photosynthesis, i.e., under conditions where photon intensity is in excess of that required for the CO₂ assimilation (14).

1.3.1.2 Aerobic respiration

As previously discussed, due to spin restriction, molecular oxygen tends to undergo univalent reductions by accepting one electron at a time. Given all the univalent electron carriers such as flavins, quinones and transition metal centers, the electron transport chain is highly likely to be the formation sites of ROS during aerobic respiration. Indeed, both superoxide and hydrogen peroxide were detected from the respiratory chains (15, 16). Specifically, it has been shown that superoxide is predominantly produced in NADH dehydrogenase (complex I) and its source has been identified as the flavin and iron-sulfur clusters in the protein (17). The cytochrome bc₁ complex (complex III) also generates superoxide, and it is believed that fully reduced ubiquinone donates one electron to cytochrome c₁ and leaves an unstable potent reductant semiquinone radical favorable for reacting with oxygen and forming superoxide (18). In *E. coli*, the non proton-pumping NADH dehydrogenase II has been shown capable of forming substantial superoxide and hydrogen peroxide and is identified as the primary site of ROS formation as opposed to the analogue of mammalian enzyme NADH dehydrogenase I (19).

1.3.1.3 Autoxidation of flavoproteins

When the prevailing hypothesis that hydrogen peroxide is primarily generated within the respiratory chain in *E. coli* was evaluated, it was surprisingly found that mutants lacking respiratory enzymes, such as NADH dehydrogenase II which *in vitro* was the most autoxidizable component of the electron transport chain, continued to form hydrogen peroxide at normal rates, suggesting that hydrogen peroxide is primarily formed by a source outside the respiratory chain (20). Later it was discovered that NadB, a flavin-dependent L-aspartate oxidase, accounted for about 25% of the endogenously generated hydrogen peroxide in *E. coli* during aerobic metabolism. Thus, it was concluded that the accidental autoxidation of non-respiratory flavoproteins are the main sources of intracellular ROS (21). Flavoproteins are abundant throughout metabolism. The reduced flavin cofactor (i.e., FMNH₂ or FADH₂) is amenable to one electron oxidation. Flavin autoxidation (Figure 1.2) occurs when oxygen reacts with the reduced dihydroflavin and through one electron transfer generates flavosemiquinone and superoxide. The generated superoxide may immediately diffuse away, but often times a second electron transfer can occur producing hydrogen peroxide (22). The titer and readiness of the autoxidizable flavoprotein determine its contribution to ROS production. It has been shown that an abundant anaerobic respiratory flavoenzyme fumarate reductase in *E. coli* reacted rapidly with oxygen as a major source of superoxide *in vivo* upon shifting into aerobic niches (23).

1.3.2 Exogenous sources

1.3.2.1 Antibiotic action

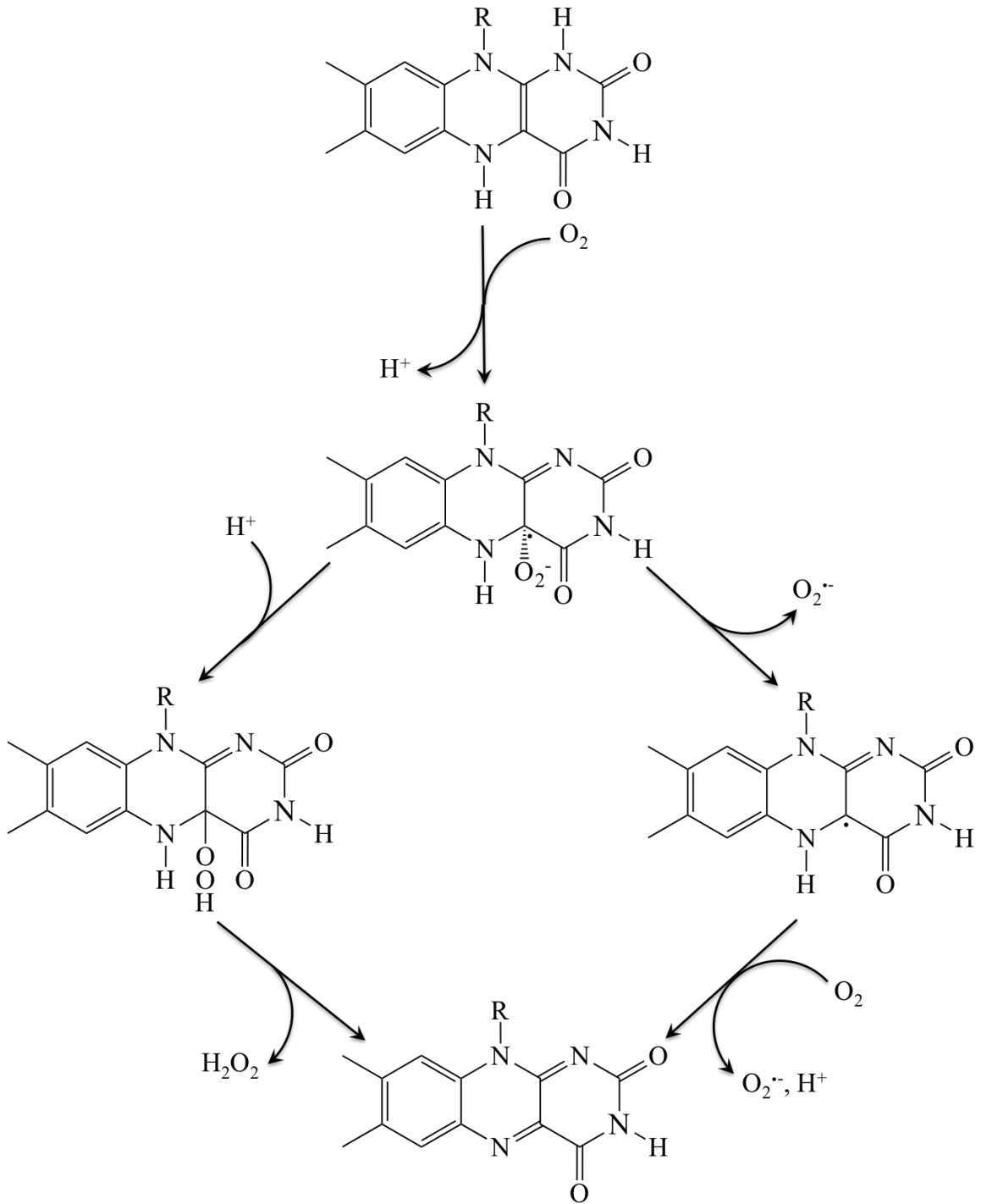


Figure 1.2. Two pathways of autoxidation of FADH₂ in flavoproteins. The left pathway predominates in most flavoenzymes studied to date.

Among all the ROS, hydroxyl radical with a reduction potential of +2.33 V is an extremely potent oxidant. It has been shown that three major classes of antibiotics, such as norfloxacin which inhibits DNA replication and repair, kanamycin which inhibits protein synthesis and ampicillin which inhibits cell-wall turnover, i.e., regardless of their specific target, all utilize a unified mechanism of killing whereby they stimulate the production of hydroxyl radicals which ultimately contribute to cell death in both Gram-negative and Gram-positive bacteria (24). It was also confirmed that respiration, citric acid cycle, a transient depletion of NADH, iron–sulfur cluster destabilization and iron misregulation all contribute to the lethal hydroxyl radical production (25). However, this antibiotic ROS paradigm was called into question recently. In 2013, two new reports independently revealed that antibiotics killed bacteria under anaerobic conditions in which ROS were not formed and there was essentially no difference in survival of bacteria treated with various antibiotics under aerobic or anaerobic conditions (26, 27), nevertheless, these studies were predicated on that ROS are the only arbiters of antibiotic induced cell death.

1.3.2.2 Oxidative burst

Oxidative burst provides one of the most rapid defenses against invading microorganisms in which ROS are the critical components of the host arsenal. It was reported in 1973 that professional phagocytes, mainly neutrophils and macrophages, utilized a membrane-bound NADPH oxidase to generate multitudes of superoxide which was then converted to hydrogen peroxide (28). The NADPH oxidase mainly expressed in phagocytes is the key source of ROS and ROS production is under tight control to prevent collateral damage to surrounding tissues (29). Upon exposure to microorganisms, the uptake of

oxygen by phagocytes is substantially increased. By using NADPH as electron donors, oxygen is reduced on the catalytic core of NADPH oxidase to produce superoxide, which can be subsequently converted into hydrogen peroxide, peroxynitrite and hypochlorous acid. These NADPH oxidase derived ROS can kill invaded microorganisms through oxidative mechanisms by oxidizing their proteins, DNA and lipids (30, 31).

1.4 Cellular Responses to Oxidative Stress

As shown above, the generation of ROS is a double-edged sword. Organisms living in an aerobic habitat have to devise strategies to contend for their adaptation and survival. On the other hand, ROS can also be harnessed as powerful weapons to combat microbial invasions for host defenses.

1.4.1 Defensive mechanisms

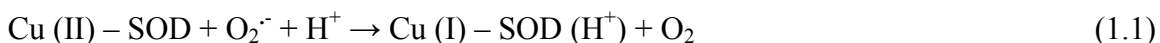
1.4.1.1 Superoxide scavengers

As previously discussed, it was first proposed in 1954 that oxygen toxicity arose from the formation of free radicals. However, this view received little attention until 1969 when Joe McCord and Irwin Fridovich discovered superoxide dismutase (SOD), the enzyme responsible for scavenging superoxide and provided the evidence that cells generate superoxide (32).

All superoxide dismutases (SODs) identified to date are metalloenzymes. As the name implies, SOD disproportionates two equivalents of $O_2^{\cdot -}$ to produce H_2O_2 and O_2 . Given that $O_2^{\cdot -}$ disproportionation is a relatively rapid reaction in the absence of SOD, it is important to point out that with SOD the reaction occurs at diffusion-controlled rates at pH 7.0. Based on amino acid sequence homology, SODs can be categorized into three groups, a feature that corresponds to the metal(s) found in the active site: (1) copper and

zinc SOD (CuZnSOD); (2) iron SOD (FeSOD), manganese SOD (MnSOD), cambialistic SOD which can bind either iron or manganese to be active; and (3) nickel SOD (NiSOD). It is interesting to point out that unlike cambialistic SOD, although FeSOD and MnSOD are closely related in terms of sequence identity, tertiary structure and can bind each other's metals, they become inactive when the native metal gets replaced by the other (33). On the other hand, the metal-specificity of cambialistic SOD can be suppressed as demonstrated by converting the enzyme to FeSOD by a single mutation located about 10 Å away from the metal center (34) suggesting structures peripheral to or distant from the active site play an essential role in enzyme functionality.

CuZnSOD is found in the cytoplasm of eukaryotes and in the periplasm of some bacteria (35). They are generally homodimers containing one copper and one zinc atom per subunit in which the copper carries out the dismutation while zinc acts a structural and facilitative role. In the resting enzyme, with one histidine bridging the two metals, Cu (II) is coordinated to four histidine residues and one solvent molecule and Zn (II) is coordinated to three histidines and one aspartate residue. The reaction cycle can be illustrated as follows:



Upon reduction of Cu (II), the bridging histidine is released from its bond to the copper and becomes protonated, concomitant with the departure of molecular oxygen; thus the active site electrostatics are overall conserved. Subsequently, when Cu (I) is re-oxidized, it recaptures its histidine and re-establishes the bridge, while the proton is transferred to another O_2^- following the release from active site in the form HO_2^- and then gets

neutralized by another proton to generate H_2O_2 (36). It is worth pointing out that in some bacteria, periplasmic CuZnSOD is expressed in the stationary phase under the control of RpoS (37) and has been implicated as an important virulence factor (38, 39).

Other than the periplasmic CuZnSOD, there are two other cytoplasmic SODs present in *E. coli*, MnSOD and FeSOD. Generally, MnSOD is found in the mitochondria of eukaryotes and some bacteria, FeSOD is found primarily in bacteria and the chloroplasts of plants, while the aforementioned cambialistic SOD is found in a wide variety of aerotolerant bacteria. This group of SODs occurs as either homotetramers or homodimers, and the active site contains a single manganese or iron atom coordinated by three histidines, one aspartate and one molecule of $\text{OH}^-/\text{H}_2\text{O}$ supported by a conserved hydrogen bond network. Although the SODs discussed so far have different protein structures and metal cofactors, they share a general “ping-pong” mechanism that requires superoxide bind to two different configurations of the same active site. As shown earlier, the electrostatic attraction of active site for incoming superoxide is maintained upon metal reduction by the coupled proton uptake, so substrate binding can still be favored allowing the return to resting state of enzyme and completion of the reaction cycle (36). Unlike the constitutively produced FeSOD, the expression of *E. coli* MnSOD is induced in response to superoxide exposure by SoxRS regulon that is also activated by redox-cycling compounds (40, 22).

NiSOD is the most recently identified SOD isolated from *Streptomyces* and cyanobacteria. The crystal structure showed the enzyme has a hexameric structure and, at the active site, the Ni (III) is coordinated to one histidine with both its imidazole and

amino group, one cysteine with both its thiolate and amide group, and another cysteine's thiolate group, with unique binding ligands compared to other SODs (41, 42).

Finally, it is also worth pointing out that another less common enzyme named superoxide reductase (SOR), found in some anaerobic bacteria and archaea, can also scavenge superoxide in which no oxygen but only hydrogen peroxide is generated (43).

1.4.1.2 Hydrogen peroxide scavengers

In contrast to superoxide scavengers, organisms express a diverse array of enzymes that are able to scavenge hydrogen peroxide, which include heme catalase, manganese catalase, catalase-peroxidase, alkyl hydroperoxide reductase, thiol peroxidase, bacterioferritin comigratory protein, glutathione peroxidase, organic hydroperoxide reductase, cytochrome *c* peroxidase, rubrerythrin and reverse rubrerythrin (44). Based on whether an exogenous electron donor is required for catalysis or turnover can be accomplished with H₂O₂ alone, these scavengers largely fall into two categories: peroxidase and catalase, respectively. The catalases include heme catalase and manganese catalase, and the peroxidases include the rest of the enzymes mentioned above, and only those with strong physiological evidences of hydrogen peroxide scavenging activity will be discussed herein.

1.4.1.2.1 Alkyl hydroperoxide reductase

Alkyl hydroperoxide reductase (AhpCF) is a two-component enzyme that consists of a thiol-based peroxidase AhpC and a flavoprotein disulfide reductase AhpF. Together, these enzymes catalyze hydrogen peroxide reduction to water at the expense of NADH as an electron donor. AhpCF was first identified in *Salmonella Typhimurium* as part of the OxyR regulon (45). Subsequent studies have shown that AhpC is a representative of a

very large and ubiquitous family of thiol-based peroxidases called peroxiredoxins with representatives in almost all living organisms. In contrast, AhpF is mainly found in bacteria (46). AhpC generally exists as dimer or a decamer in a head-to-tail manner with two conserved cysteines in each subunit, the peroxidatic cysteine C_P on one chain and the resolving cysteine C_R from near the C-terminus of the other chain by which the catalytically relevant disulfide bond can be formed (47). Peroxidation of C_P by hydrogen peroxide occurs in the fully folded active site which involves the catalytic C_P , an arginine and a threonine which stabilize the thiolate anion, and also a proline that shields the active site from water. The thiolate attacks hydrogen peroxide to generate water and a Cys-sulfenic acid at the active site which subsequently gets attacked by the resolving cysteine C_R to form an intersubunit disulfide bond and release another water molecule (48). The disulfide bond generated in AhpC is then reduced by its dedicated partner AhpF for continuing turnovers.

The *ahpF* gene is positioned proximal to *ahpC* and within the promoter of *ahpC* on the genome, therefore it is co-transcribed with *ahpC*. AhpF is a homodimer with an N-terminal domain containing redox active dithiol, an FAD-binding domain and an NADH-binding domain with redox active disulfide in the C-terminus (46). An electron is transferred within AhpF from NADH to FAD, from FAD to the C-terminal disulfide redox center, and finally to the N-terminal disulfide whose original electron being donated to AhpC (44). The hydrogen peroxide scavenging activity of AhpCF was overlooked in the initial studies due to the high concentrations of hydrogen peroxide in millimolars used in those experiments which immediately inactivated the enzyme with an apparent K_M of 1.4 μM (49). The inactivation occurs when hydrogen peroxide further

oxidizes the nascent sulfenic acid into sulfinic acid before it can condense with the resolving cysteine. However, it has been proposed that such a consequence can actually be utilized *in vivo* as a strategy in facing high hydrogen peroxide stress in that instead of exhausting NADH for futile efforts, AhpCF can then be turned off to allow the kinetically superior catalases to come into play under such circumstances (50).

1.4.1.2.2 Monofunctional heme catalases

There is a parallel between the ways in which superoxide and hydrogen peroxide are scavenged by *E. coli*. As discussed previously, for superoxide scavengers in *E. coli*, there is a constitutive FeSOD and an MnSOD that is inducible as part of the SoxRS regulon. Similarly, for hydrogen peroxide scavengers, there is a constitutive catalase (KatE) produced primarily in the stationary phase, and a KatG whose expression is inducible as part of the OxyR regulon. KatE is the monofunctional heme catalase, also referred to as the canonical catalase.

The canonical catalases are widely distributed in all domains of life. Phylogenetic analyses have revealed three clades of these enzymes. Clades I and III are referred to as small subunit catalases with about 500 amino acid residues per subunit. Clade II contains the so-called large subunit catalases with about 750 amino acid residues in each subunit (51). Interestingly, enzymes from all three clades are typically found as homotetramers. Clade I catalases are mostly found in plants and a few bacteria, while Clade II catalases are predominantly of bacterial and fungal origin utilizing heme *d* as prosthetic group instead of heme *b* like the other two clades (52). Additionally, an extra C-terminal domain of about 150 residues with a flavodoxin-like topology is found in this clade but lacks the NADPH-binding site that is present in Clade III enzymes (53). Clade III

catalases have diverse origins including bacteria, archaea, fungi, and many other eukaryotes. The NADPH-binding site found only in this clade was proposed to protect the enzyme against forming inactive intermediates by the bound NADPH (54). Regardless of origins of the heme catalase, subunits from the three clades exhibit extremely high structural similarities for about 460 conserved amino acids comprising the so called “catalase fold”.

The catalase fold in canonical catalases consists of a β -barrel domain and a α -helical domain linked by the wrapping loop containing the heme proximal ligand tyrosine. The β -barrel domain, preceded by an extended N-terminal domain and followed by the wrapping loop and the α -helical domain, is the central feature of the catalase fold. It contains eight anti-parallel β -strands along with at least six inserted α -helices. The first half of the barrel (β 1– β 4) harbors most of the heme distal side residues while for Clade III enzymes the second half (β 5– β 8) contains the NADPH binding site (55). The active site configurations (Figure 1.3A) are highly conserved among all different catalases, and several essential residues were defined for catalysis. The proximal ligand tyrosine is of great importance for heme binding and folding, and the distal histidine is responsible for hydrogen peroxide binding and heme modification by oxidation of heme *b*. The asparagine on the distal side is also well conserved. However, the replacement with either alanine or aspartate resulted in an enzyme with 10% of activity retained, suggesting the asparagine is not absolutely required but serves a facilitative role for catalysis. Similarly, mutations of the conserved serine residue that is adjacent to and interacting with the distal histidine also didn't alter the catalase activity but was proposed as essential for proper folding of the subunit (56). The main channel connecting the deeply buried active site

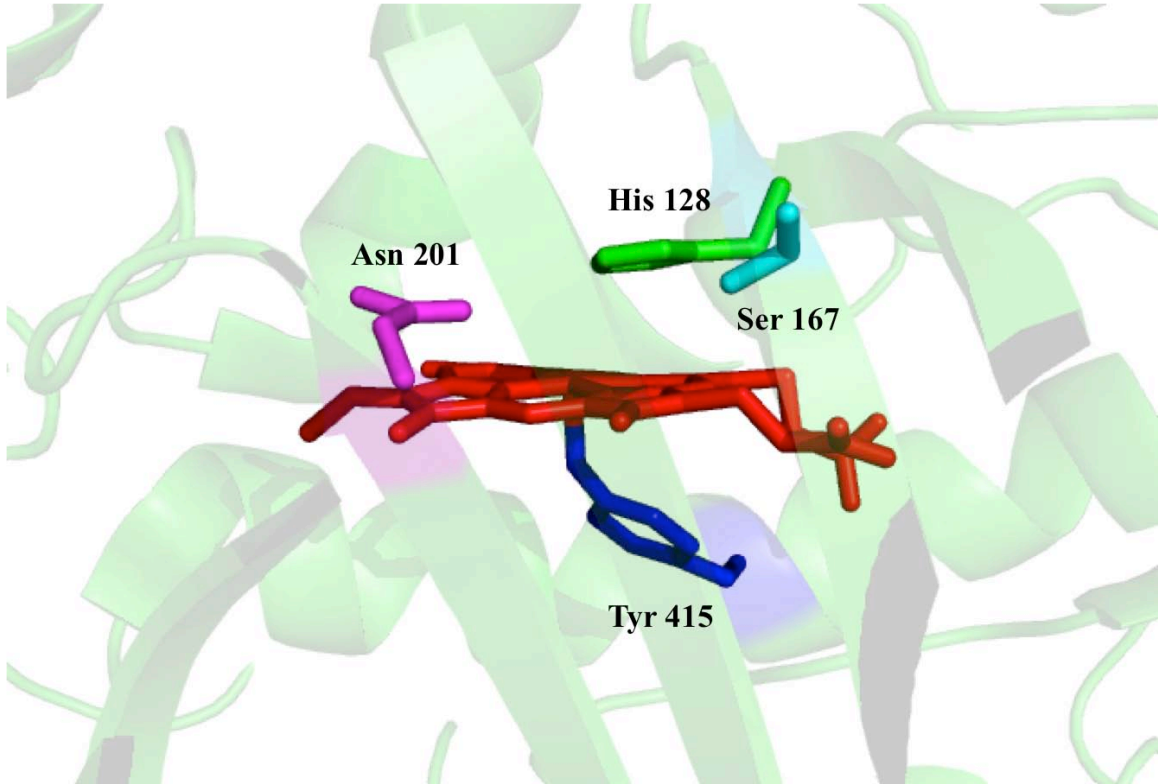
with the protein surface for substrate flow approaches the heme perpendicularly and has long been regarded as the primary access route that is long and narrow blocking the entry of molecules significantly larger than hydrogen peroxide (57). Structurally, catalases are uniquely rigid and stable enzymes especially those from Clade II, e.g., *E. coli* KatE. KatE exhibits unusual resistance to denaturation and proteolysis (58), and it was proposed this renders the stationary-phase-produced KatE an advantage given the rapid protein turnover and due to elevated protease levels in stationary phase (57).

The canonical catalases share a unified mechanism for hydrogen peroxide dismutation involving two stages (Figure 1.3B). In the first stage, one equivalent of hydrogen peroxide oxidizes the heme generating an oxyferryl porphyrin π -cation radical intermediate called compound I and releasing water. Two electrons are removed in this process, one from Fe (III) and the other from the porphyrin ring. The second stage brings the enzyme to its resting state by utilizing another equivalent of hydrogen peroxide as a reductant, releasing another water and evolving molecular oxygen. For Clade III catalases, as previously mentioned, a tightly bound NADPH is proposed to prevent the formation of an inactive species compound II due to the radical relocalization from the porphyrin to presumed oxidizable amino acids. However, the compound II formation has not yet been observed in catalases from the other two clades.

1.4.1.2.3 Bifunctional catalases

In 1979, ten years after the landmark discovery of superoxide dismutase, Irwin Fridovich and his team isolated the first catalase-peroxidase from *E. coli* and characterized it as a bifunctional catalase with a robust catalase activity and also a canonical peroxidase activity (59). The catalase-peroxidase (KatG) enzymes are mainly

A



B

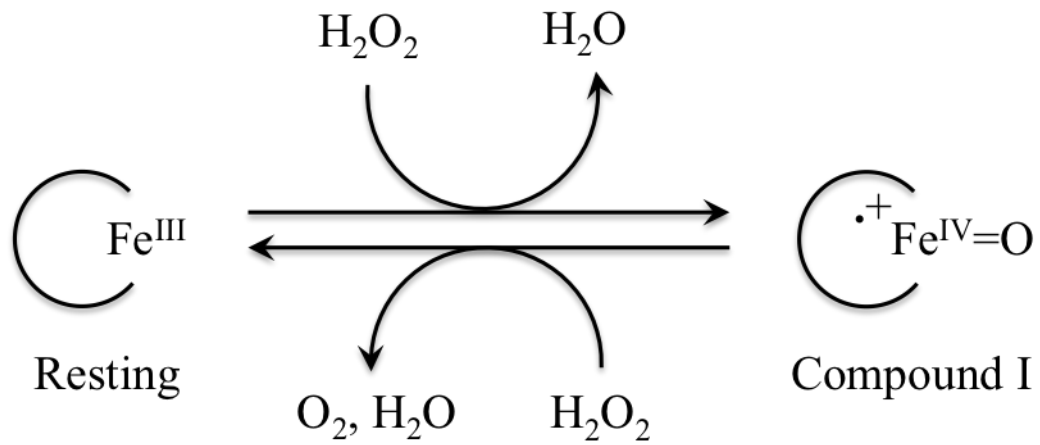


Figure 1.3. Active site of *Escherichia coli* KatE (as known as HPII) (A). Catalytic cycle of canonical catalases (B).

distributed in bacteria, a few archaea and fungi. They generally exist as homodimers with the exception of *E. coli* KatG which exists as a homotetramer. Despite the fact that KatG predominantly functions as a catalase with yet unidentified *in vivo* peroxidase substrates, phylogenetically it is related to the superfamily of plant, fungal and bacterial peroxidases, now designated as the peroxidase-catalase superfamily. Indeed, KatGs are classified as Class I of this superfamily along with cytochrome *c* peroxidases and ascorbate peroxidases. Class II includes mainly secretory fungal peroxidases such as lignin peroxidase and manganese peroxidase, and Class III is represented by secretory plant peroxidases such as horseradish peroxidase (60). Given the close structural and functional relationships between KatG and its relatives, it is important to have an examination of other heme peroxidases in the superfamily as well.

The Class II peroxidases are extracellular monomeric enzymes secreted by filamentous fungi (e.g., the white-rot fungus, *Phanerochaete chrysosporium*) responsible for lignin degradation. The representative lignin peroxidase (LiP) and manganese peroxidase (MnP) share a similar overall structure including two calcium ions tightly bound on both sides of the heme which is proposed to maintain the topology of the active site and play an important role in thermal stabilization of the enzyme (61). MnP has five disulfide bonds rather than four as observed in LiP. The additional disulfide bond is located near the C-terminus of the enzyme and it keeps the C-terminal segment away from protein body and facilitates the formation of Mn(II)-binding site (62). The heme iron is predominantly high-spin with the proximal histidine as its fifth ligand (Figure 1.4A and 1.4B). The histidine is further hydrogen bonded with a conserved aspartate that increases the anionic character of the ligand thereby stabilizing the oxidized forms of the

enzymes relative to more reduced states. The distal histidine also hydrogen bonded with an asparagine, acts as a proton acceptor for hydrogen peroxide. The arginine adjacent to the distal histidine stabilizes the negative charge developed in the cleavage of hydrogen peroxide as well as the ferryl oxygen in compound I. A unique feature in LiP has also been identified involving a posttranslational modification in which a surface tryptophan on the distal side of heme is hydroxylated and has been suggested to participate in the oxidation of veratryl alcohol via long-range electron transfer. Substitution of the tryptophan by a phenylalanine or serine completely abolished the activity with veratryl alcohol as substrates (63, 64). Interestingly, introduction of a tryptophan at the corresponding position in the wild-type MnP rendered the enzyme the ability to utilize veratryl alcohol as a substrate without reducing mediators (65).

The Class II peroxidases share a canonical peroxidase mechanism with peroxidases from the other two classes. Similar to canonical catalases, the general mechanism of peroxidase-catalyzed reaction also involves two stages (Figure 1.5). The first stage is shared by both canonical enzymes in which one equivalent of hydrogen peroxide oxidizes the heme forming compound I and releasing water with two electrons removed from the heme moiety. What distinguishes the canonical peroxidase mechanism from canonical catalase mechanism lies in the second stage. Instead of being reduced by another equivalent of hydrogen peroxide, compound I is reduced by two sequential one-electron reduction steps in peroxidases. The peroxidase substrates, or the peroxidatic electron donors (PxEDs), vary for different peroxidases. In the LiP and MnP discussed above, lignin and Mn (II) is utilized respectively. As in MnP, the product Mn (III) can in turn

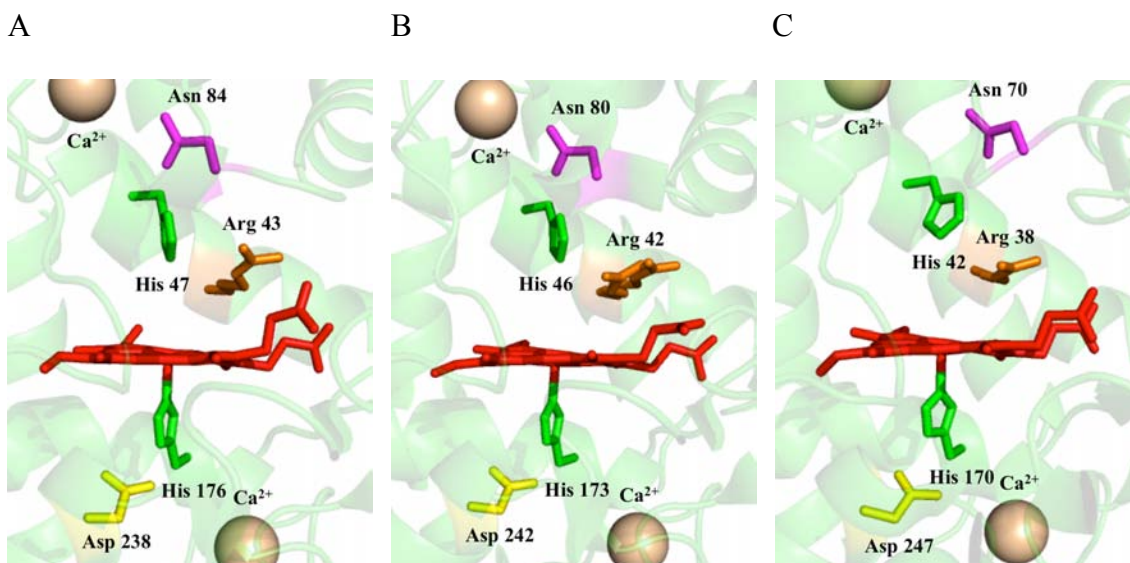


Figure 1.4. Active sites of lignin peroxidase (LiP) (A), manganese peroxidase (MnP) (B) and horseradish peroxidase (HRP) (C).

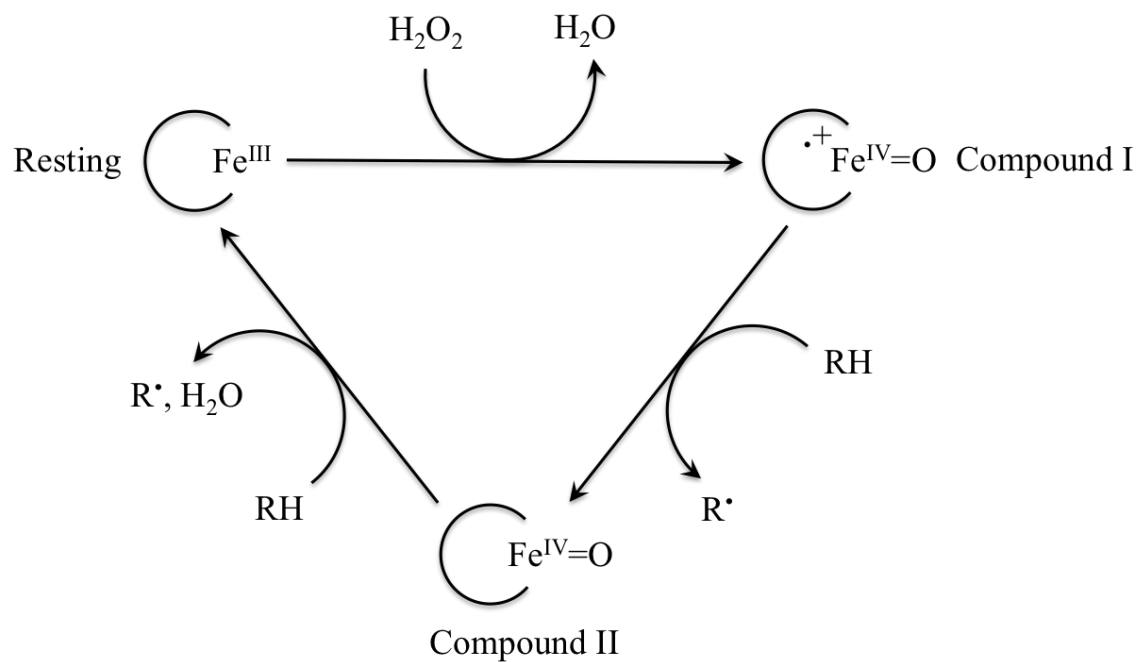


Figure 1.5. Catalytic cycle of canonical peroxidases. RH and $\text{R}\cdot$ stand for peroxidatic electron donors (PxEDs) and PxED radicals, respectively.

oxidize a variety of phenolic lignin compounds serving the physiological function of the enzyme.

The most extensively studied peroxidase, horseradish peroxidase, is a Class III representative. The specific role of HRP *in vivo* remains to be established. However, it has been observed that peroxidase activity is induced when horseradish leaves are wounded (66). Similar to lignin peroxidase and other Class II enzymes, there are four disulfide bonds and two calcium-binding sites for each HRP monomer. The proximal calcium is suggested to play more critical role in regulating the heme architecture and catalytic properties (67). The core of HRP contains highly conserved amino acid residues (Figure 1.4C), in addition to the peroxidase fold. One unique feature identified in HRP is a long interhelical loop located at the region that defines part of the substrate access channel (68). The peroxidase substrates for HRP include aromatic phenols, phenolic acids, indoles, amines and sulfonates, suggesting the primary function of HRP in plants may not be degrading hydrogen peroxide (69).

Unlike Class II and III heme peroxidases, the physiological role of Class I peroxidases appears to be the scavenging of hydrogen peroxide, and their peroxidase substrates are not as promiscuous as observed for other peroxidases. Cytochrome *c* peroxidase (CcP) and ascorbate peroxidase (APx) have adapted to utilize ferrocyanochrome *c* and ascorbate to reduce the compound I intermediate, respectively. Along with KatG, they share a highly conserved active site (Figure 1.6) with the proximal triad histidine, aspartate, tryptophan and the distal triad histidine, arginine, tryptophan located at almost identical positions. The proximal tryptophan serves as an alternative radical site in CcP although normally the porphyrin retains the π -cation radical within the

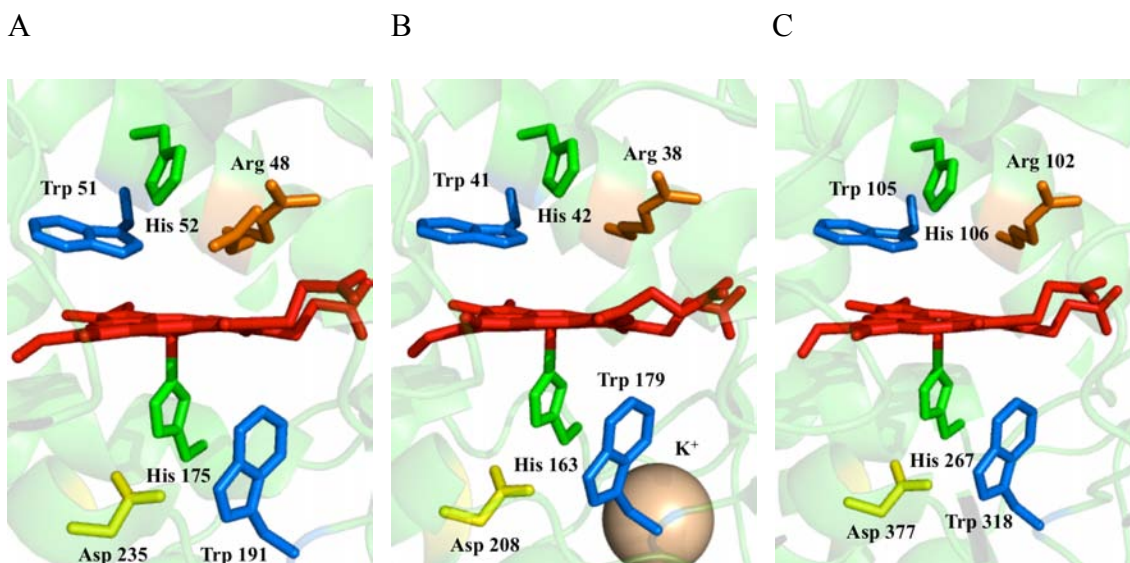
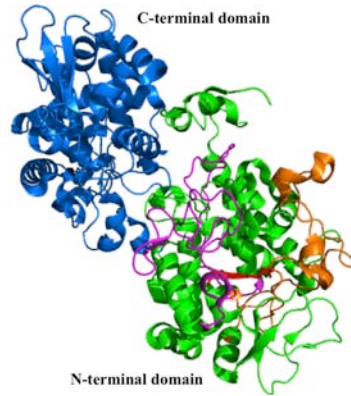


Figure 1.6. Active sites of cytochrome *c* peroxidase (CcP) (A), ascorbate peroxidase (APx) (B) and catalase-peroxidase (KatG) (C).

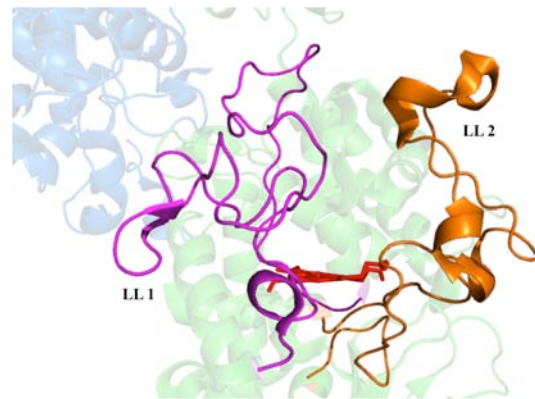
ring in compound I as observed in APx. It has been proposed that the potassium ion located about 8 Å away from the proximal tryptophan in APx would destabilize a positive charge on the tryptophan thereby making it more difficult to oxidize to form a tryptophanyl radical as in CcP (70, 71). The distal tryptophan whose position is occupied with a phenylalanine in Class II and III enzymes, on the other hand, does not appear to be essential for the peroxidase activity in CcP (72).

Among all other members of Class I peroxidases or even the entire superfamily, KatGs stand out as the only enzyme with a robust catalase activity in addition to the canonical peroxidase activity. On one hand, the catalase activity in KatGs is striking because they bear little if any structural resemblance to canonical catalases, a group of enzymes known for rapid (i.e., up to 10^6 s^{-1}) H_2O_2 disproportionation. On the other hand, this activity is striking because those enzymes which have the closest structural similarity to KatG are uniformly poor catalases (i.e., with k_{cat} of 10 s^{-1}), and in fact, are inactivated in the presence of high concentrations of H_2O_2 . Nevertheless, KatG does have several structural features that are absent from other superfamily members (Figure 1.7). As mentioned previously, KatGs are most commonly found as homodimers but occasionally as homotetramers as in *E. coli* KatG. Most other members of the superfamily are monomeric. Each KatG subunit is composed of two peroxidase-like domains. Both domains have a peroxidase fold, but only the N-terminal domain harbors the heme-containing active site. The C-terminal domain, thought to arise from a gene duplication and fusion, lacks a ligand to bind heme and the putative “active site” is occupied by several large amino acid side chains which also precludes association of the heme cofactor. Consequently, the C-terminal domain lacks heme, and as such, does not

A



B



C

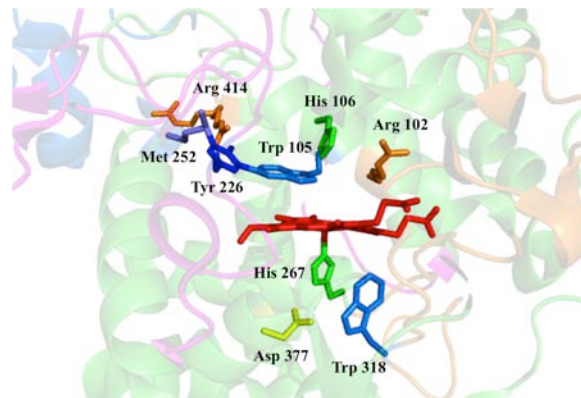


Figure 1.7. Unique structural features of KatGs: an extra C-terminal domain (A); two Large Loops (LL), i.e., LL1 and LL2 (B); Met-Tyr-Trp covalent adduct and the mobile arginine (C)

catalyze any discernable reaction (73). However, it has been shown that upon removal of the C-terminal domain, the resulting stand-alone N-terminal domain exhibits neither catalase or peroxidase activity. Spectroscopic studies revealed a shift in heme environment from predominately high-spin as in the wild-type enzyme to an exclusively hexacoordinate, low-spin state in the stand-alone N-terminal domain protein. The distal histidine was identified to be the sixth ligand suggesting the apparent role of the C-terminal domain is to maintain the correct coordination state of the heme for catalysis by preventing the association of the distal histidine to the heme iron (74). The inactivation can be reversed, however, by introduction of separately expressed and isolated C-terminal domain protein. Co-incubation of the separately generated domains results in the restructuring of the N-terminal domain active site as observed by a variety of spectroscopy methods and catalytic and peroxidatic activities (75). In addition to the C-terminal domain, two large loops (i.e., LL1 and LL2), positioned at the opposite edges of the heme have been identified as essential for catalase but not peroxidase activity of KatG. Specifically, the deletion of LL2 results in a complete loss of catalase activity while the peroxidase activity was diminished by only 50% suggesting its vital role in supporting the hydrogen-bond networks critical for the catalase reaction (76). Interestingly, LL2 contains few invariant amino acid residues, in contrast, the length of this loop is highly conserved. The catalase activity has been shown to be considerably sensitive to residue deletions of LL2 and, given the fact that the loop's apex protrudes into a hydrophobic pocket in the C-terminal domain of the other subunit, it was proposed that the length instead of residue conservation of LL2 plays a pivotal role in modulating the active site architecture and catalase activity of KatG by essential intersubunit interactions (79).

Unlike LL2, the length of LL1 varies substantially among KatGs. Nevertheless, the C-terminal end of the structure is strictly conserved among all KatGs. In particular, an invariant tyrosine participates in a Met-Tyr-Trp covalent adduct in which the tyrosine is linked to a methionine on one side and a tryptophan on the other (78). This MYW adduct is positioned on the distal side of the heme with the tryptophan roughly coplanar to and 3 Å above the heme. And substitutions of any member in the covalent adduct led to the loss of catalase activity (79). Additionally, a conserved mobile arginine 20 Å away from the active site can adopt two conformations and interact with the tyrosine residue of the covalent adduct thereby playing an essential role for the catalase activity as well (80). Interestingly, it has also been shown that elimination of the conserved tyrosine by deletions of larger portions of LL1 invariably abolished catalase activity as expected. However the peroxidase activity of the deletion variants were substantially enhanced implying the role of LL1 is to restrict the PxED entrance to the active site heme (81).

The main access channel to the distal site of the heme in KatG is similar to the one in other heme peroxidases but is longer and more constricted characterized as a pronounced funnel shape (82). The second access channel normally existed in other heme peroxidases, approximately in the heme plane, is blocked by the larger loops in KatG. However, a dramatic cleft in the side of the subunit between the two domains within the subunit has been proposed as a second entrance to the protein core. Given its elongated nature, this alternative channel entrance implies the binding site for PxEDs with an extended, possibly even polymeric character (83).

The catalase mechanism in KatGs is not immediately understood and the canonical catalase paradigm is apparently unsatisfactory based on all of the striking findings

discussed above. By the current proposed mechanism (Figure 1.8), the tyrosine residue in the covalent adduct provides the alternative radical site and the formed intermediate is known as compound I^{*}. A second equivalent of hydrogen peroxide then converts compound I^{*} to a superoxoferric/protein radical designated as compound III^{*} while releasing water. Finally, the electron transfer from the heme to the protein radical brings the enzyme to the resting state with concomitant release of oxygen (84, 85). The absence of this novel covalent adduct in canonical heme peroxidases also contributes to their incompetence in performing robust catalase activity like KatGs. Evidently, after compound I formation, shared by both catalase and peroxidase mechanisms in KatGs, catalase turnover requires oxidation of hydrogen peroxide, whereas peroxidase turnover requires oxidation of PxEDs. Thus, it has been anticipated that PxEDs should inhibit catalase turnovers. Strikingly, it has been observed that PxEDs substantially enhanced catalase activity up to 14-fold, particularly under acidic conditions normally unfavorable to catalase turnovers (86).

Given its proficient catalase activity, one can come to the conclusion that KatG plays a vital role in bacterial defenses against hydrogen peroxide. Indeed, KatG appears to be the only catalase carried by *Mycobacterium tuberculosis* (87). An additional periplasmic form of KatG was identified in several highly virulent pathogens such as *E. coli* O157:H7, *Yersinia pestis* and *Legionella pneumophila*, and has been implicated as a virulence factor (88-92).

1.4.2 Immune Responses

The preceding discussions have shown that life has evolved and elaborated sophisticated defensive mechanisms to detoxify ROS during oxidative stress. At the same

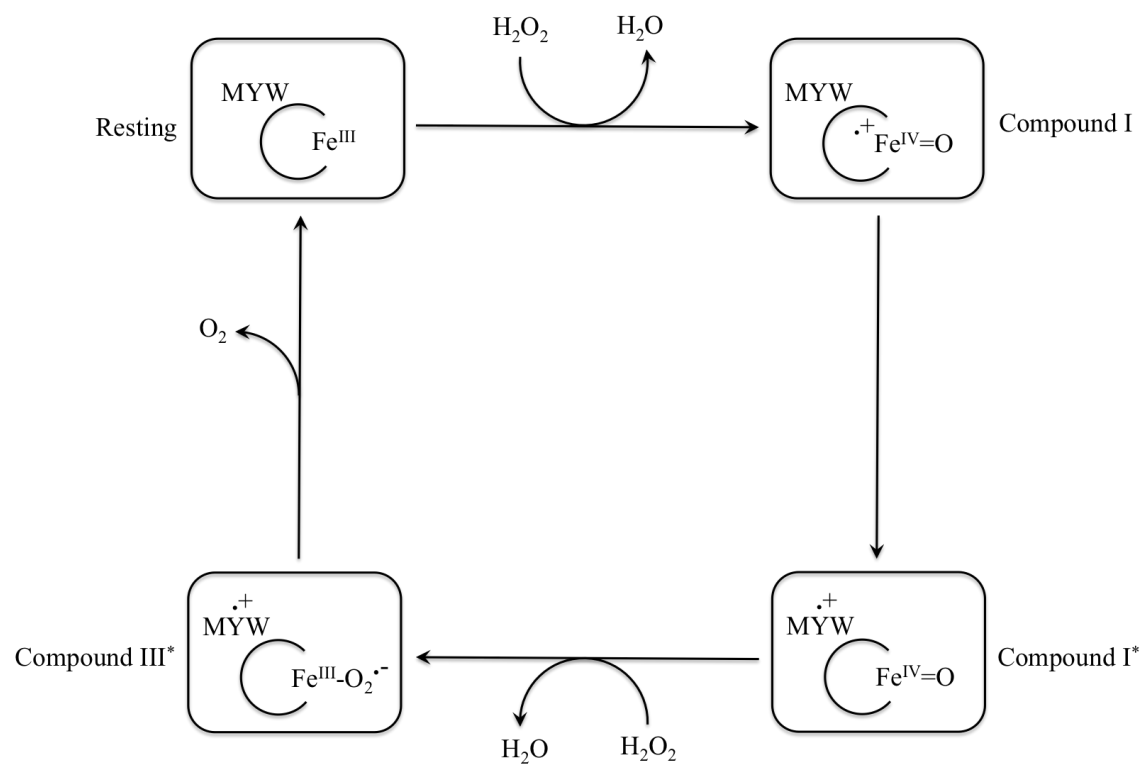


Figure 1.8. Current proposed catalytic cycle of catalase activity of KatGs.

time, ROS can be capitalized and deliberately produced as potent weapons in the host immune responses. During these processes, neutrophils and macrophages are recruited to the site of infection where they engulf, kill, and digest the microorganisms by phagocytosis. A critical component in phagocytosis by which the professional phagocytes kill the bacteria is the production of ROS by NADPH oxidase. The membrane-bound multicomponent enzyme complex NADPH oxidase transfers electron from NADPH in the cytosol across the membrane to oxygen inside the phagocyte to generate large quantities of superoxide. The short-lived superoxide is generally thought to spontaneously dismutate into hydrogen peroxide and oxygen given the low pH inside the phagocyte. However, phagocyte derived SOD may also contribute to this reaction, and the resulting hydrogen peroxide is in copious amount up to 100 mM (93, 94). It has also been shown that the microbicidal activity of these NADPH oxidase derived ROS is enhanced by myeloperoxidase, an abundant heme peroxidase in the phagocyte (95). The myeloperoxidase converts hydrogen peroxide to hypochlorous acid, a potent microbicidal agent by oxidation of chloride. Nevertheless, individuals with hereditary deficiency of myeloperoxidase generally do not exhibit increased frequency of infections, and it has been proposed that superoxide and hydrogen peroxide may be sufficient to compensate for the lack of the MPO (96). In any case, during phagocytosis, the ability to withstand hydrogen peroxide assault initiated by the host will considerably contribute to the survival of the bacterium and potentially establish an infection. Indeed, the additional KatG found in the periplasm of several highly virulent pathogens such as *E. coli* O157:H7 serotype has been implicated as a virulence determinant. Moreover, the striking discovery that PxEDs stimulate catalase activity of KatG under acidic conditions as in the

phagocyte is most likely to further contribute to bacterial defenses against hydrogen peroxide thereby contributes to pathogenesis.

CHAPTER TWO

ESSENTIAL ROLE OF DISTANT INTERDOMAIN H-BOND INTERACTIONS IN HEME ENVIRONMENT AND CATALYTIC FUNCTION OF KATGS

2.1 Introduction

The Great Oxidation Event ultimately triggered by the emergence of cyanobacteria on Earth represents a watershed in the history of life by opening up the era of oxygen retaining atmosphere and biosphere (97). Ever since then, elaborate defense mechanisms for detoxification of partially reduced, reactive oxygen species (ROS) originating from one- (i.e., $O_2^{\cdot-}$ or HO_2^{\cdot}) and two-electron reduction of O_2 (i.e., H_2O_2) has been required. Among all the available ROS scavengers, catalase-peroxidases (KatGs) have generated considerable interest as these heme-containing enzymes are capable of degrading hydrogen peroxide via two distinct mechanisms using the same active site. Both the catalase and peroxidase catalytic cycle share a common first step in which one equivalent of H_2O_2 is reduced by the ferric heme to H_2O , producing an oxyferryl porphyrin radical intermediate designated as compound I at which point these two activities diverge (Figure 2.1). In the catalase cycle, compound I is brought back to the resting state of the enzyme by oxidizing another equivalent of H_2O_2 while releasing another equivalent of H_2O and evolving O_2 . The mechanism of H_2O_2 oxidation is non-scrambling as the O-O bond remains intact (98). In contrast, the reduction of compound I by a peroxidatic mechanism is achieved by oxidizing exogenous peroxidatic electron donors (PxEDs) in two

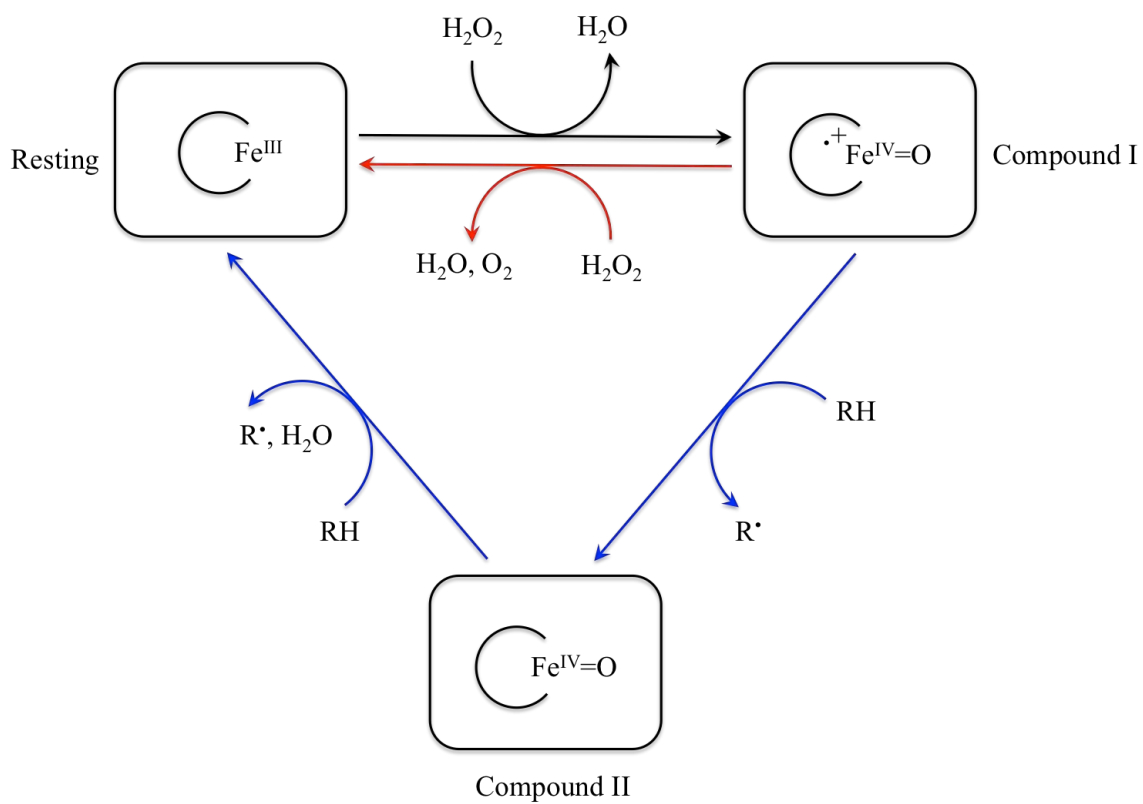


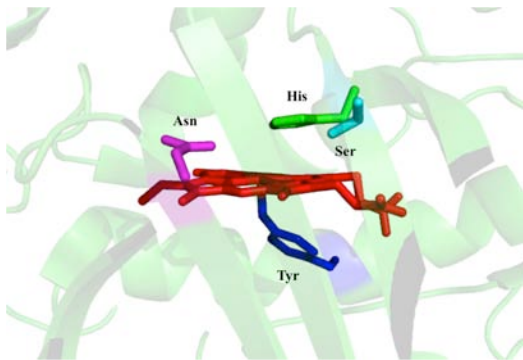
Figure 2.1. Catalytic cycles of catalase-peroxidases. RH and $\text{R}\cdot$ stand for peroxidatic electron donors (PxEDs) and PxED radicals, respectively.

sequential one-electron reduction steps, which result in formation of two equivalents of PxED radicals and release of another equivalent of H₂O.

The catalase activity of KatG enzymes is striking given the fact that they bear little if any resemblance to canonical catalases; instead, they are highly similar to Class I peroxidases from the peroxidase-catalase superfamily. The active sites of KatG and these enzymes like cytochrome *c* peroxidase and ascorbate peroxidase are essentially superimposable (Figure 2.2) (71, 83, 99, 100-103). However, other than KatGs, none of the peroxidase-catalase superfamily members exhibits appreciable catalase activity. In reconciling this stark contrast in function by two highly similar structures, it has been noted that KatGs possess several compelling structural features absent from the canonical peroxidases (83, 100-104). First of all, each KatG subunit consists of two domains rather than one. The extra C-terminal domain still retains a peroxidase fold, but its “active site” is no longer able to bind heme. It has been proposed that the two-domain KatGs arose by a gene duplication and fusion event after which the C-terminal domain likely lost its functionality (73, 105). Moreover, the N-terminal domain of KatGs contains three large loops (LL), among which two of them have been demonstrated to be essential for catalase but not peroxidase activity (76, 77, 106, 107).

The C-terminal domain of KatGs accounts for nearly half the molecular weight of the KatG subunit. It comes no closer to the active site in the N-terminal domain than 30 Å. It lacks any catalytic activity of its own, suggesting it may be a vestigial feature. On the other hand, all KatGs have a C-terminal domain. Nevertheless, its indispensable nature has been demonstrated. KatG lacking its C-terminal domain has neither catalase nor peroxidase activity. It appears that the C-terminal domain from its distant position

A



B

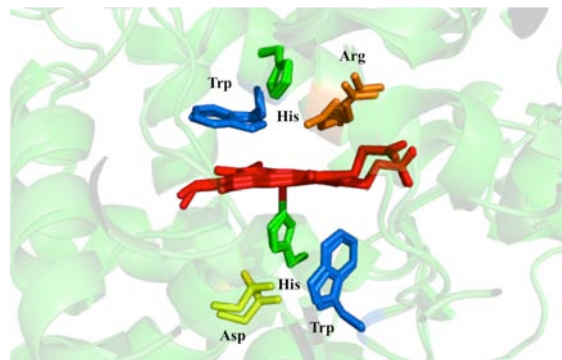


Figure 2.2. Comparison of active sites: canonical catalase (A) (PDB: 1IPH) (53), catalase-peroxidase and canonical peroxidase overlaid (B) (PDB: 1MWV and 1ZBY) (83, 99).

supports the N-terminal domain architecture by preventing the otherwise spontaneous coordination of the distal histidine (His 106 by *Escherichia coli* KatG numbering) to the heme iron (74). However, by introducing the separately expressed and isolated C-terminal domain (KatG^C), the N-terminal domain (KatG^N) can be reactivated evidenced by spectroscopic evaluation of the heme ligand environment and restored activities (75).

To investigate the mechanism by which the C-terminal domain supports the N-terminal domain active site, our focus has been placed on the interface between the two domains where highly conserved residues create two distinct hydrogen bonded networks between 20 Å and 30 Å away from the active site (Figure 2.3). At 30 Å from the active site, the distant network includes Arg 117 on the BC interhelical loop of the N-terminal domain with Asp 597 on the E' helix of the C-terminal domain. Another contact between Arg 117 and Gln 600 also appears to occur given that the same interaction can presumably be established with asparagine or aspartate as observed in KatGs from other organisms. At 20 Å from the active site, the near network involves interactions of Tyr 111 on the BC interhelical loop of the N-terminal domain with Asp 482 on the B'C' interhelical loop of the C-terminal domain which in turn interacts with adjacent Arg 479 on the same loop and will be discussed in the next chapter.

We have capitalized on the ability of KatG^C to reactivate KatG^N as a novel approach to evaluate the role of these conserved interactions, by which rates and extents of reactivation and shifts in heme environment potentially allow for valuable mechanistic insights. In particular, single variants of the stand-alone domain proteins were prepared for each of these distant H-bond network residues (R117A^N, R117D^N, D597A^C, D597R^C, Q600A^C and D597A/Q600A^C) and matched with unmodified domains and domain

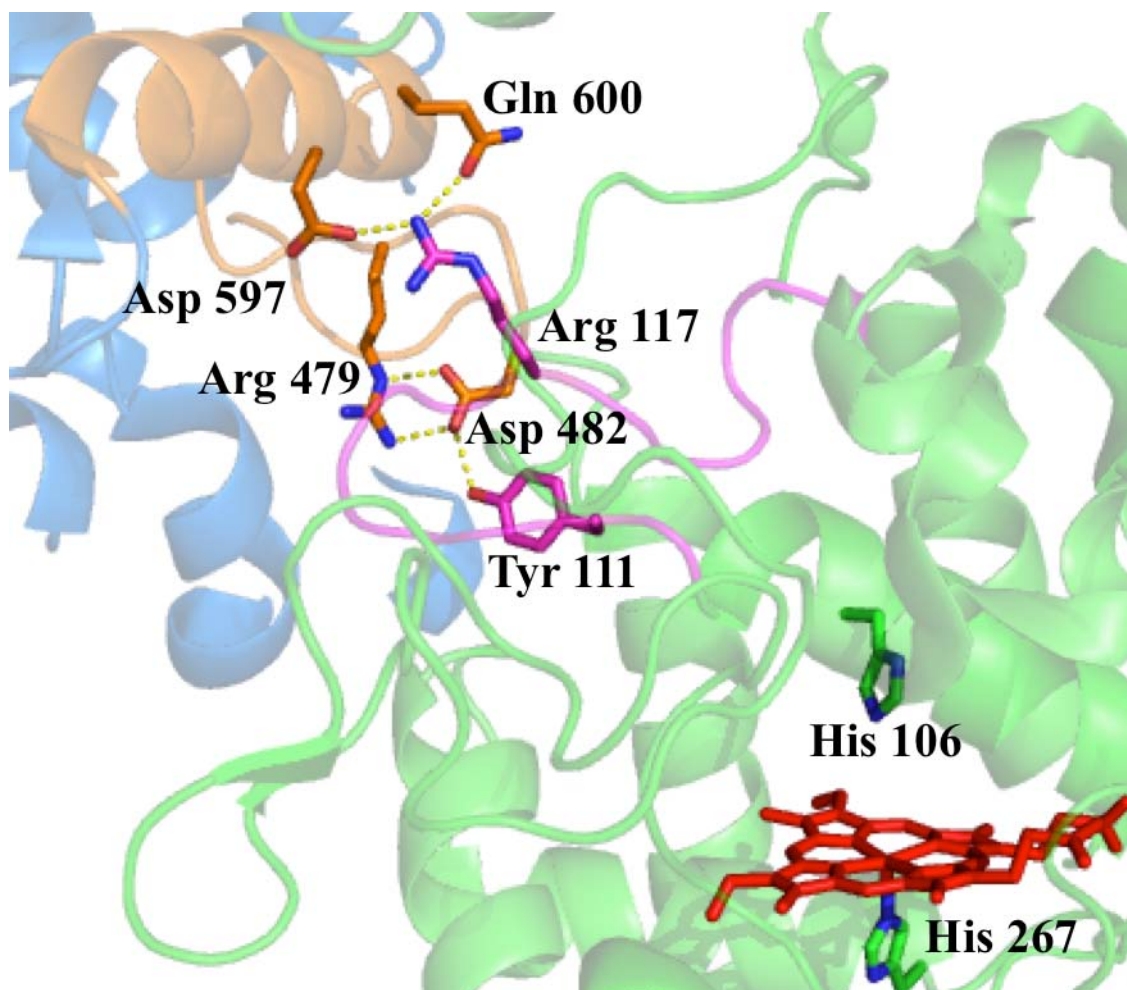


Figure 2.3. Interactions between the N-terminal domain BC interhelical loop (shown in magenta) and the C-terminal domain B'C' interhelical loop, E' helix (shown in orange) in KatG. Coordinates from the structure of *Burkholderia pseudomallei* KatG were used (PDB: 1MWV) (83). Numbering reflects *Escherichia coli* KatG sequence.

variants targeting their corresponding network partners. A series of spectroscopic analyses and kinetics studies was carried out on these stand-alone domain combinations in an effort to elucidate the part these interactions play in the function of the C-terminal domain.

2.2 Materials and Methods

2.2.1 Reagents

Hydrogen peroxide (30%), imidazole, hemin, ampicillin, chloramphenicol, sodium dithionite, phenylmethylsulfonyl fluoride (PMSF) and 2,2'-azino-bis(3-ethylbenzthiazoline-6-sulfonic acid) (ABTS) were purchased from Sigma (St. Louis, MO). Isopropyl- β -D-thiogalactopyranoside (IPTG) was obtained from GoldBio Technology (St. Louis, MO). Urea, Tris, mono- and di-basic potassium phosphate, mono- and di-basic sodium phosphate, sodium chloride, acetic acid, and sodium acetate were obtained from Fisher (Pittsburgh, PA). All oligonucleotide primers were purchased from Invitrogen (Carlsbad, CA). All *E. coli* strains [XL1-Blue and BL21-Gold(DE3)pLysS], *PfuTurbo* DNA polymerase, and T4 DNA ligase were obtained from Agilent Technologies (La Jolla, CA). All restriction enzymes were purchased from New England Biolabs (Beverly, MA). BugBuster protein extraction reagent and Benzonase Nuclease were purchased from Novagen (Madison, WI). Nickel-nitrilotriacetic acid (Ni-NTA) resin was purchased from Qiagen (Valencia, CA). Buffer exchange chromatography columns (10DG) were purchased from Bio-Rad (Hercules, CA). Amicon Ultra centrifugal filters were obtained from EMD Millipore (Billerica, MA). All buffers and media were prepared using water purified through Barnstead EASYpure II system (18.2 M Ω /cm resistivity).

2.2.2 Cloning and expression of KatG^N, KatG^C and their variants of the distant-network

Generation of a construct for the expression of KatG lacking its C-terminal domain (KatG^N) was accomplished as described elsewhere (74). The expression plasmid of stand-alone C-terminal domain of KatG (KatG^C) was produced using a deletion mutagenesis procedure developed in our laboratory (76). The plasmids of stand-alone domain variants R117A^N, R117D^N, and D597A^C were prepared using mutagenic primers [5'-GTTCAATCGATGGCGCCGGTGGCG-3' (R117A^N coding), 5'-CCCGCGCCACCGGCGCCATCGATTGAAC-3' (R117A^N non-coding), 5'-GTTCAATCGACGGAGATGGTGGCGGG-3' (R117D^N coding), 5'-CCCGCGCCACCATCTCCGTCGATTGAAC-3' (R117D^N non-coding), 5'-ACTGCTGATCGCGAAAGCACAGC-3' (D597A^C coding), and 5'-GCTGTGCTTTTCGCGATCAGCAGT-3' (D597A^C non-coding)] according to the QuikChange procedure (Agilent Technologies, La Jolla, CA). The plasmids of D597R^C, Q600A^C and D597A/Q600A^C stand-alone domain variants were generated using mutagenic primers [5'-Phos-GTAAAGCACAGCAACTGACGCTGACCGC-3' (D597R^C coding), 5'-Phos-GTATCAGCAGTGACTCGGTGGTGGAAACGTC-3' (D597R^C non-coding), 5'-Phos-GCAACTGACGCTGACCGCGCC-3' (Q600A^C coding), 5'-Phos-GCAGCTTTGTCGATCAGCAGTGACTCGG-3' (Q600A^C non-coding), 5'-Phos-GCAACTGACGCTGACCGCGCC-3' (D597A/Q600A^C coding), 5'-Phos-GCAGCTTTCGCGATCAGCAGTGACTCG-3' (D597A/Q600A^C non-coding)] according to the 'Round-the-horn procedure in which the 5' end of the two primers start at adjacent bases (108). Amplification products were then ligated using T4 DNA ligase

and used to transform *E. coli* XL1-Blue by heat shock. Plasmids from candidate colonies were screened by diagnostic restriction digests. Positive candidates were submitted for DNA sequence analysis at Davis Sequencing (Davis, CA). Verified plasmids were used to transform *E. coli* BL21-Gold(DE3)pLysS as the expression host. The expression of KatG^N, KatG^C and their variants of the distant-network was carried out as described elsewhere for another KatG (89) except that cultures were not supplemented with δ -aminolevulinic acid or ferrous ammonium sulfate.

2.2.3 Purification of KatG^N, KatG^C and their variants of the distant-network

KatG^C and all the C-terminal domain variants were expressed in a soluble state. Thus purifications were performed as described elsewhere for the wild-type KatG (76). KatG^N and all the N-terminal variants were expressed in inclusion bodies, so an alternative denaturing purification procedure was carried out. After the cells were centrifuged, the pellet was resuspended in Buffer A (50 mM NaH₂PO₄/Na₂HPO₄, 200 mM NaCl, pH 8.0) with 100 μ M PMSF, homogenized and then sonicated using Branson Sonifier 250 (Danbury, CT). After that, Benzonase Nuclease (250 U) was added to the lysate and the mixture was gently stirred for 2 hours. The cell lysate was then centrifuged. The pellet which contained the protein was resuspended in Buffer B (100 mM NaH₂PO₄, 10 mM Tris, 8 M urea), homogenized and centrifuged. The supernatant was mixed with Ni-NTA resin and gently agitated at room temperature overnight. The resin was then loaded into a column, washed with Buffer B containing 20 mM imidazole, and eluted off the column with Buffer B containing 400 mM imidazole. Urea and imidazole were finally removed by dialysis against Buffer C (50 mM KH₂PO₄/K₂HPO₄, 200 mM NaCl, pH 8.0) for 24

hours. The resulting protein was then reconstituted with 0.85 equivalents of hemin and incubated at 4 °C for at least 24 hours.

2.2.4 Domain combination and incubation

The concentrations of reconstituted KatG^N and their variants were determined using molar absorptivity calculated from pyridine hemichrome assay (109). Solutions containing both N- and C-terminal domain proteins were incubated at 4 °C for times ranging from 0 to 48 hours in the presence of 50 mM phosphate, pH 7.0, 50 mM NaCl. Following a given incubation time, aliquots were taken and activities were measured according to the assays described below.

2.2.5 UV-visible absorption spectra and activity assays

Following reconstitution, proteins were always centrifuged to remove potentially unincorporated heme and other insoluble material (e.g., precipitated protein). All spectra were recorded at 23 °C on a Shimadzu UV-1601 spectrophotometer (Columbia, MD) using a 1.0 cm quartz cell. Catalase and peroxidase activity assays were performed as described elsewhere (89). Initial rates were fit to Michaelis-Menten equation (2.1) by nonlinear regression analysis to determine apparent kinetic parameters. If substrate-dependent inhibition was evident, the fitting equation (2.2) was modified to include a substrate-dependent inhibition term K_I , a macroscopic apparent dissociation constant that reflects the ability of the substrate to act as an inhibitor.

$$\frac{v_0}{[E]_T} = \frac{k_{cat}[S]}{K_M + [S]} \quad (2.1)$$

$$\frac{v_0}{[E]_T} = \frac{k_{cat}[S]}{K_M + [S] + \frac{[S]^2}{K_I}} \quad (2.2)$$

2.2.6 Circular and magnetic circular dichroism

All circular dichroism (CD) and magnetic circular dichroism (MCD) spectra were recorded on a Jasco J-810 spectropolarimeter (Tokyo, Japan) at 23 °C. Baselineing and analysis were carried out using Jasco J-720 software. Circular dichroism spectra (250-190 nm) were obtained using 5 µM enzyme in 5 mM phosphate buffer, pH 7.0 with a 0.5 mm quartz cell. Magnetic circular dichroism spectra (680-380 nm) were obtained using 15 µM enzyme in 50 mM phosphate 50 mM NaCl buffer, pH 7.0 with a 5.0 mm quartz cell in a 1.4 Tesla magnetic cell holder. The ferrous enzyme was prepared by adding a small amount (< 10 mg) of sodium dithionite to the protein's ferric state.

2.2.7 Electron paramagnetic resonance spectroscopy

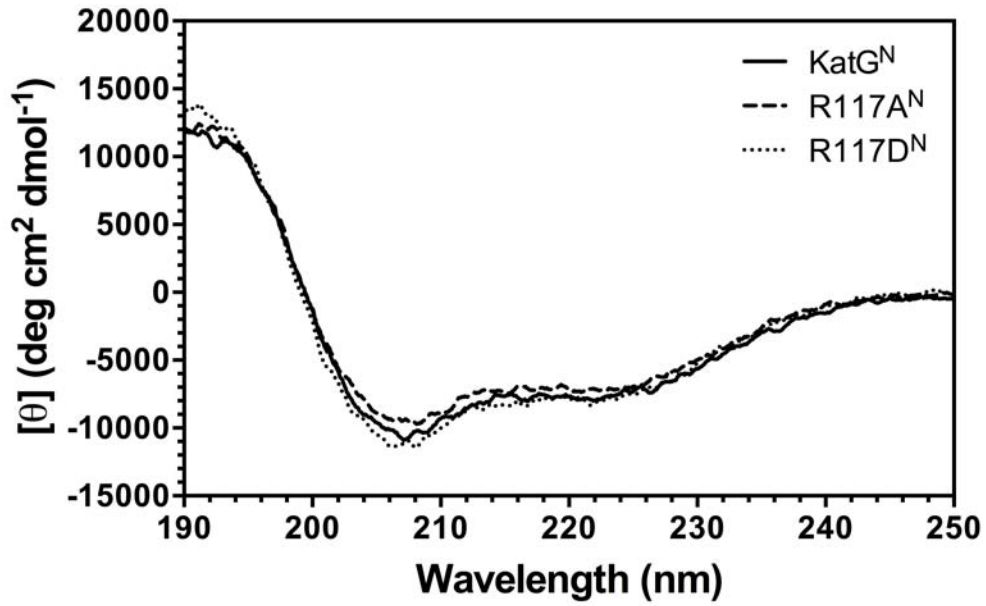
Spectra were recorded using a Bruker EMX instrument equipped with an Oxford ESR 900 cryostat and ITC temperature controller. Sample concentration was performed using Amicon Ultra-4 centrifugal devices (Billerica, MA). The settings for the spectrometer were as follows: temperature, 10 K; microwave frequency, 9.38 GHz; microwave power, 0.1 mW; modulation amplitude, 10 G; modulation frequency, 100 kHz; time constant, 655.36 ms; conversion time, 655.36 ms; and receiver gain, 1.0×10^5 . Spin quantification was carried out using the Biomolecular EPR spectroscopy software package available online (110).

2.3 Results

2.3.1 Circular dichroism and UV-visible spectroscopy

The far-UV CD spectrum is a sensitive probe for verifying protein secondary structural content. The CD spectra recorded for all KatG domain variants of the distant-network (Figure 2.4) were similar to that of unmodified KatG domains, i.e., KatG^N and KatG^C,

A



B

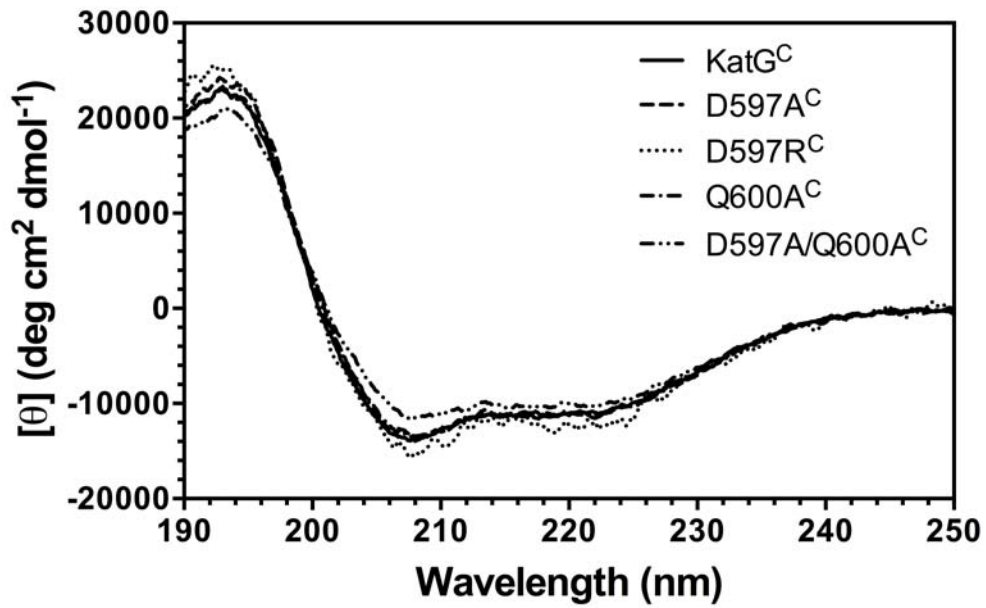


Figure 2.4. Far-UV circular dichroism spectra of KatG^N and its variants (A), KatG^C and its variants (B) in the distant-network. Spectra were recorded at 23 °C in 5 mM phosphate buffer, pH 7.0.

and showed the typical features of α -helices with the 222 and 208 nm dichroic bands suggesting mutations did not induce changes in the overall secondary structure of the proteins.

The heme absorption spectrum for the ferric form of coordination-altered inactive KatG^N is dominated by hexacoordinate low-spin heme and is characterized by a sharp Soret band at 416 nm along with prominent α and β bands at 568 and 538 nm, respectively. Conversely, the reactivated KatG^N by KatG^C is consistent with primarily hexacoordinate high-spin heme manifested by a relatively broad Soret band around 411 nm and two charge transfer (CT) bands in the neighborhood of 642 nm (CT1) and 530 nm (CT2). Substitutions made to the stand-alone N-terminal domain in the distant-network (i.e., R117A^N and R117D^N) produced spectra highly similar to unmodified KatG^N (data not shown). However, following incubation with their targeted partners of C-terminal domain protein, the Soret bands all blue shifted towards *ca.* 411 nm (Figure 2.5) as in KatG^N+KatG^C indicating a mixture of high-spin and low-spin heme species. It is worth pointing out that CT2 band appears around 506 nm in the intact wild-type KatG protein. Consequently, the presence of hexacoordinate low-spin heme is further indicated by the red shift of CT2 band into the β region indicative of simultaneous contributions from both CT2 and β band absorption.

2.3.2 Magnetic circular dichroism

Heme protein MCD allows for facile differentiation between high- and low-spin heme species, particularly when the ferrous state is evaluated. The low-spin ferrous heme Q-band shows a strong A-term signal centered around 557 nm while this feature is substantially diminished with the high-spin ferrous heme concomitant with a strong

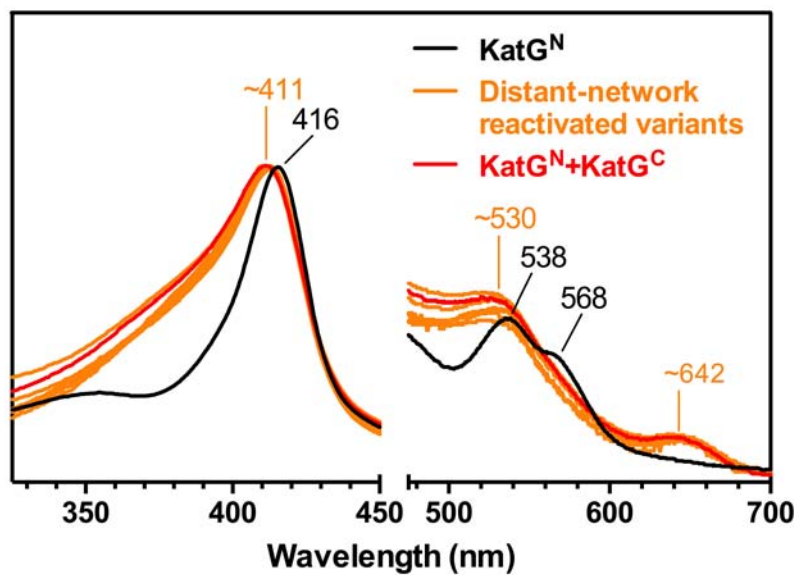


Figure 2.5. UV-visible spectral comparison of distant-network reactivated variants with inactive KatG^N and reactivated KatG^N+KatG^C in their native state. Spectra were recorded at 23 °C in 100 mM phosphate buffer, pH 7.0.

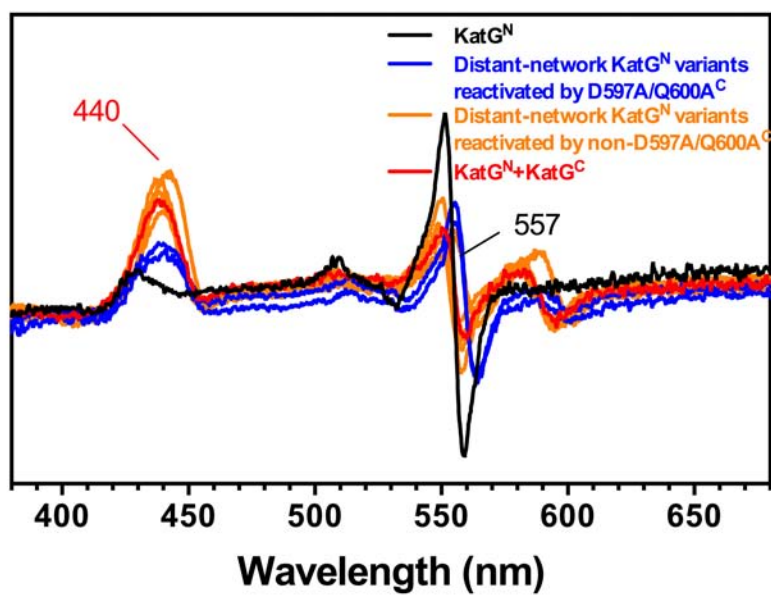


Figure 2.6. MCD spectral comparison of distant-network reactivated variants with inactive KatG^N and reactivated KatG^N+KatG^C in ferrous state of heme. Spectra were recorded at 23 °C in 50 mM phosphate, 50 mM NaCl buffer, pH 7.0.

signal near 440 nm (i.e., B-band). In agreement with UV-visible spectra data, the stand-alone N-terminal domain variants all showed identical spectra to KatG^N (data not shown) with exclusively hexacoordinate low-spin features. Nonetheless, following the incubation period, the reactivated N-terminal domain variants all demonstrated an increased contribution from high-spin as indicated by the intense B-band signal accompanied by other features in the 625-575 nm range (Figure 2.6). However, a residual A-term of the Q-band at ~557 nm suggested that an appreciable amount of low-spin heme was still present in the reactivated proteins. In variants reactivated by D597A/Q600A^C, the B-band intensity around 440 nm was noticeably lower than rest of the reactivated proteins suggesting a higher contribution from low-spin heme species in these two variants.

2.3.3 Electron paramagnetic resonance

EPR spectroscopy allows for evaluation of the ferric oxidation state and, on the basis of g-tensor anisotropy allows for distinction between high-spin populations (e.g., penta- and hexacoordinate). In KatG enzymes, at least three EPR signals are observed for native ferric state of the protein (Figure 2.7 and 2.8). These are on the basis of g-tensor anisotropy most evident near $g = 6$. At a minimum, there is a high-spin state with narrow rhombic distortion ($g_x \sim 6$, $g_y \sim 5.6$ and $g_z = 1.99$) and a high-spin state with broad rhombic distortion ($g_x \sim 6.6$, $g_y \sim 5.0$ and $g_z = 1.95$) and a rhombic low-spin signal ($g_x \sim 2.9$, $g_y \sim 2.3$ and $g_z \sim 1.5$). At first glance, except for the KatG^N+Q600A^C proteins, the reactivated distant-network domain variants all exhibited more appreciable low-spin heme species compared to the unmodified domain combination, i.e., KatG^N+KatG^C, more so in the variants reactivated by D597A/Q600A^C corroborating our MCD data. On the other hand, there was an apparent shift from narrow rhombic high-spin to broad rhombic

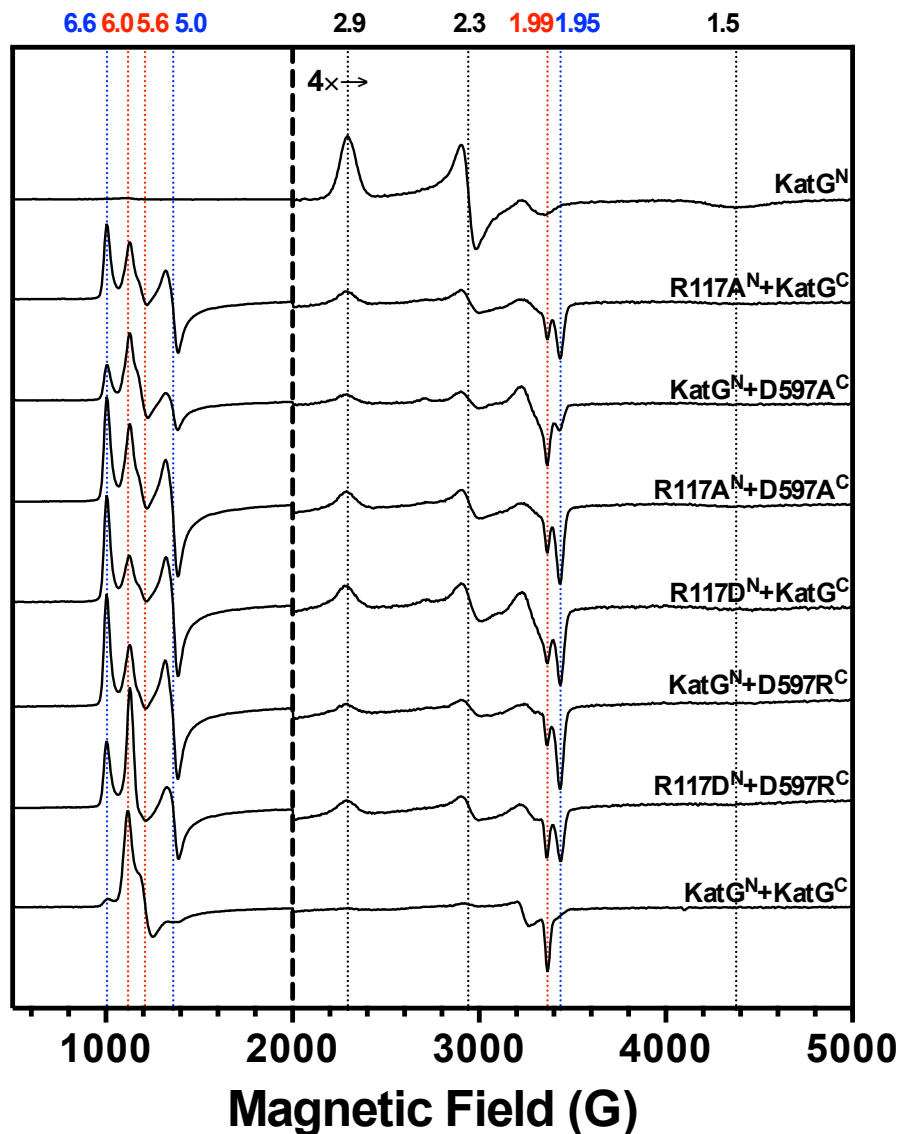


Figure 2.7. EPR spectra of distant-network reactivated variants without Q600 substitutions along with KatG^{N} and $\text{KatG}^{\text{N}}+\text{KatG}^{\text{C}}$ for comparison. Spectra were magnified by four above 2000 Gauss. The g-values corresponding to narrow rhombic high-spin signal (~ 6.0 , ~ 5.6 and 1.99) and broad rhombic high-spin signal (~ 6.6 , ~ 5.0 and 1.95) observed in KatGs are shown as those of the hexacoordinate low-spin signal (~ 2.9 , ~ 2.3 and ~ 1.5).

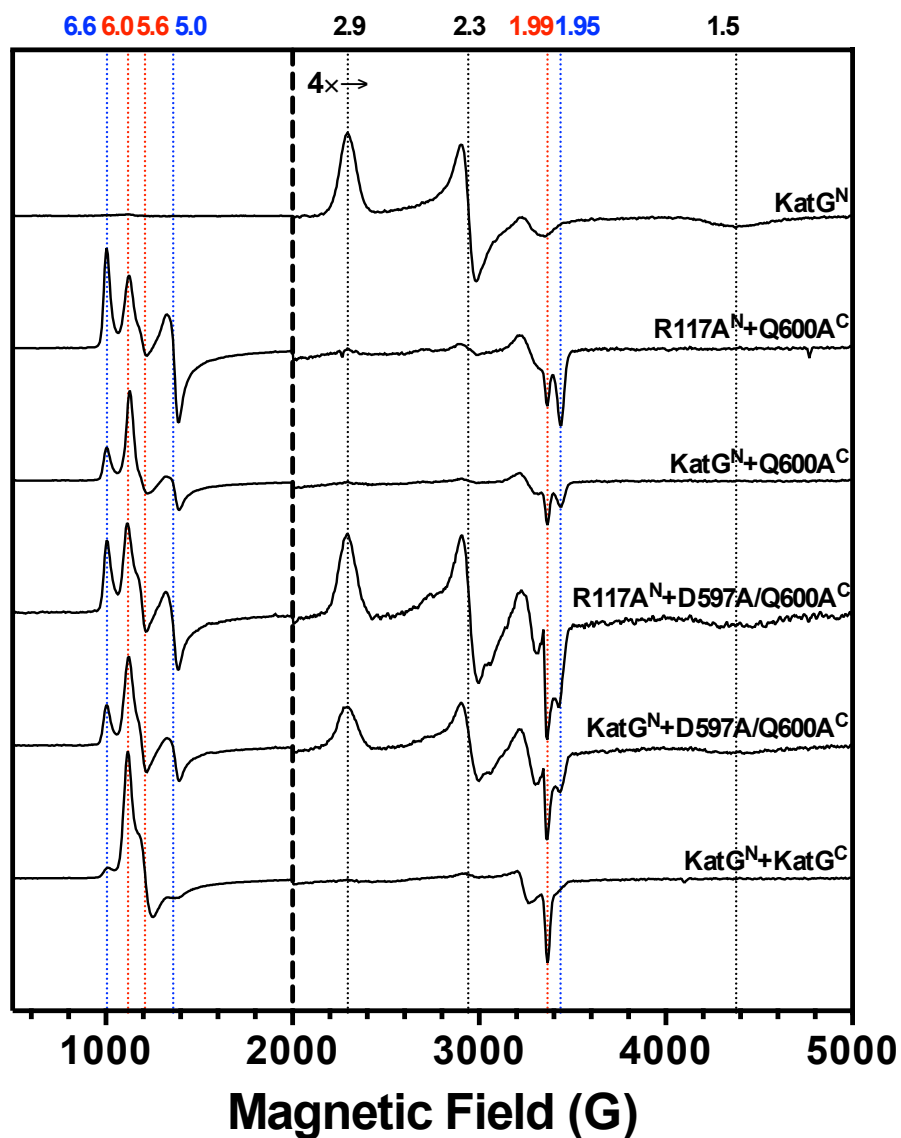


Figure 2.8. EPR spectra of distant-network reactivated variants with Q600 substitutions along with KatG^{N} and $\text{KatG}^{\text{N}}+\text{KatG}^{\text{C}}$ for comparison. Spectra were magnified by four above 2000 Gauss. The g-values corresponding to narrow rhombic high-spin signal (~ 6.0 , ~ 5.6 and 1.99) and broad rhombic high-spin signal (~ 6.6 , ~ 5.0 and 1.95) observed in KatGs are shown as those of the hexacoordinate low-spin signal (~ 2.9 , ~ 2.3 and ~ 1.5).

high-spin component in all the domain variants. Quantification of the relative contributions of each heme species to the ferric state was accomplished by EPR spectral simulations and signal integrations. Simulations were carried out by accounting for two rhombic high-spin species (BRHS: $g_x = 6.64$, $g_y = 4.95$ and $g_z = 1.95$; NRHS: $g_x = 5.99$, $g_y = 5.60$ and $g_z = 1.99$) and one rhombic low-spin species (LS: $g_x = 2.92$, $g_y = 2.28$ and $g_z = 1.53$) (111-113). As clearly demonstrated in Table 2.1, the alanine single substitution for Q600 as in KatG^N+Q600A^C did not produce more low-spin species compared to unmodified domain proteins. However, the mutation resulted in equal amount of broad rhombic and narrow rhombic high-spin species as opposed to predominantly narrow rhombic high-spin species observed in the unmodified domain proteins. The rest of domain variants showed even more pronounced contribution from the broad rhombic high-spin species, in some cases approaching 90%. The D597A/Q600A^C double variant generated the most abundant low-spin species with about 40% hexacoordinate low-spin component whereas other domain variants were still dominated by high-spin species with less than 15% contribution observed from low-spin state.

2.3.4 Reactivation and steady-state kinetics

In order to evaluate the effect of interdomain residue substitutions on the active site recovery, the return of activity (catalase and peroxidase) was monitored as a function of N- and C-terminal domain co-incubation time, from which the rate and amplitude of reactivation were obtained. As shown in Table 2.2 and 2.3, except for variants reactivated by D597A/Q600A^C, the observed rates for reactivation were not substantially diminished compared to unmodified domain proteins and a parallel return of catalase and peroxidase activities was also observed. By increasing the amount of incubated C-terminal domain

Table 2.1. Ratios of EPR signals observed for distant-network reactivated variants along with KatG^N and KatG^N+KatG^C for comparison.

| Protein | | % contribution | | |
|--------------------|------------------------------|-----------------------------------|---------------------------------------|------------------|
| N-terminal Domain | C-terminal Domain | HS ^a : LS ^b | NRHS ^c : BRHS ^d | NRHS : BRHS : LS |
| KatG ^N | KatG ^C | 96 : 4 | 82 : 18 | 78 : 18 : 4 |
| R117A ^N | KatG ^C | 88 : 12 | 19 : 81 | 16 : 72 : 12 |
| KatG ^N | D597A ^C | 90 : 10 | 41 : 59 | 37 : 53 : 10 |
| R117A ^N | D597A ^C | 88 : 12 | 18 : 82 | 16 : 72 : 12 |
| R117D ^N | KatG ^C | 87 : 13 | 11 : 89 | 9 : 78 : 13 |
| KatG ^N | D597R ^C | 92 : 8 | 14 : 86 | 13 : 79 : 8 |
| R117D ^N | D597R ^C | 86 : 14 | 37 : 63 | 31 : 54 : 14 |
| R117A ^N | Q600A ^C | 93 : 7 | 18 : 82 | 17 : 76 : 7 |
| KatG ^N | Q600A ^C | 95 : 5 | 49 : 51 | 46 : 49 : 5 |
| R117A ^N | D597A/ Q600A ^C | 56 : 44 | 30 : 70 | 17 : 39 : 44 |
| KatG ^N | D597A/ Q600A ^C | 62 : 38 | 44 : 56 | 27 : 35 : 38 |
| KatG ^N | | 0 : 100 | 0 : 0 | 0 : 0 : 100 |

^a High-spin; HS = NRHS + BRHS.

^b Low-spin ($g_x = 2.92$, $g_y = 2.28$ and $g_z = 1.53$).

^c Narrow rhombic high-spin ($g_x = 5.99$, $g_y = 5.60$ and $g_z = 1.99$).

^d Broad rhombic high-spin ($g_x = 6.64$, $g_y = 4.95$ and $g_z = 1.95$).

Table 2.2. Reactivation kinetic parameters of catalase activity of distant-network domain variants and unmodified KatG^N+KatG^C for comparison.

| Protein | | Reactivation of Catalase Activity ^a | | | | Relative to KatG ^N + KatG ^C (1:1) | | | |
|--------------------|------------------------------|---|----------|---|----------|---|------|--------------------|------|
| | | Rate Constant (10 ⁻⁵ s ⁻¹) | | Amplitude {v ₀ /[E] _T (s ⁻¹)} | | Relative Rate Constant | | Relative Amplitude | |
| N-terminal Domain | C-terminal Domain | 1:1 | 1:10 | 1:1 | 1:10 | 1:1 | 1:10 | 1:1 | 1:10 |
| KatG ^N | KatG ^C | 4.5±0.1 | 34.8±3.4 | 4270±40 | 4540±60 | 1.0 | 7.7 | 1.0 | 1.1 |
| R117A ^N | KatG ^C | 5.8±0.5 | 13.4±2.2 | 1750±40 | 2160±70 | 1.3 | 3.0 | 0.4 | 0.5 |
| KatG ^N | D597A ^C | 5.0±0.3 | 25.0±3.7 | 3450±60 | 3910±90 | 1.1 | 5.6 | 0.8 | 0.9 |
| R117A ^N | D597A ^C | 4.6±0.3 | 12.6±2.0 | 1630±30 | 2040±70 | 1.0 | 2.8 | 0.4 | 0.5 |
| R117D ^N | KatG ^C | 2.9±0.3 | 10.9±1.1 | 1390±50 | 1200±20 | 0.6 | 2.4 | 0.3 | 0.3 |
| KatG ^N | D597R ^C | 8.7±1.2 | 39.3±6.2 | 2020±70 | 2300±40 | 1.9 | 8.7 | 0.5 | 0.5 |
| R117D ^N | D597R ^C | 10.4±1.7 | 28.6±5.3 | 830±30 | 1140±20 | 2.3 | 6.4 | 0.2 | 0.3 |
| R117A ^N | Q600A ^C | 2.8±0.1 | 8.3±1.3 | 2800±40 | 3600±130 | 0.6 | 1.8 | 0.7 | 0.8 |
| KatG ^N | Q600A ^C | 3.6±0.2 | 11.6±2.1 | 3470±50 | 4070±150 | 0.8 | 2.6 | 0.8 | 1.0 |
| R117A ^N | D597A/ Q600A ^C | 1.6±0.1 | 5.3±0.6 | 1320±40 | 2230±70 | 0.4 | 1.2 | 0.3 | 0.5 |
| KatG ^N | D597A/ Q600A ^C | 1.9±0.1 | 6.9±0.8 | 1270±30 | 2050±70 | 0.4 | 1.5 | 0.3 | 0.5 |

^a Assays included 20 nM KatG^N+KatG^C, 30 nM for all other domain variants in 100 mM phosphate buffer, pH 7.0 at 5.0 mM H₂O₂ concentration, 23 °C.

Table 2.3. Reactivation kinetic parameters of peroxidase activity of distant-network domain variants and unmodified KatG^N+KatG^C for comparison.

| Protein | | Reactivation of Peroxidase Activity ^a | | | | Relative to KatG ^N + KatG ^C (1:1) | | | |
|--------------------|------------------------------|---|----------|---|----------|---|------|--------------------|------|
| | | Rate Constant (10 ⁻⁵ s ⁻¹) | | Amplitude {v ₀ /[E] _T (s ⁻¹)} | | Relative Rate Constant | | Relative Amplitude | |
| N-terminal Domain | C-terminal Domain | 1:1 | 1:10 | 1:1 | 1:10 | 1:1 | 1:10 | 1:1 | 1:10 |
| KatG ^N | KatG ^C | 4.4±0.3 | 21.6±3.3 | 10.6±0.2 | 13.7±0.3 | 1.0 | 4.9 | 1.0 | 1.3 |
| R117A ^N | KatG ^C | 4.7±0.2 | 10.8±1.5 | 10.3±0.2 | 12.3±0.4 | 1.1 | 2.5 | 1.0 | 1.2 |
| KatG ^N | D597A ^C | 4.1±0.3 | 14.1±1.7 | 10.2±0.2 | 13.5±0.3 | 0.9 | 3.2 | 1.0 | 1.3 |
| R117A ^N | D597A ^C | 3.3±0.2 | 8.6±1.3 | 7.7±0.1 | 10.0±0.4 | 0.8 | 2.0 | 0.7 | 0.9 |
| R117D ^N | KatG ^C | 2.1±0.2 | 5.4±0.4 | 8.8±0.3 | 9.6±0.2 | 0.5 | 1.2 | 0.8 | 0.9 |
| KatG ^N | D597R ^C | 7.4±0.8 | 29.1±3.6 | 35.9±1.0 | 42.3±0.6 | 1.7 | 6.6 | 3.4 | 4.0 |
| R117D ^N | D597R ^C | 8.9±1.1 | 31.8±4.5 | 13.0±0.4 | 17.8±0.3 | 2.0 | 7.2 | 1.2 | 1.7 |
| R117A ^N | Q600A ^C | 3.4±0.3 | 12.9±1.4 | 12.5±0.3 | 16.7±0.4 | 0.8 | 2.9 | 1.2 | 1.6 |
| KatG ^N | Q600A ^C | 4.7±0.3 | 14.8±1.7 | 12.7±0.3 | 17.8±0.4 | 1.1 | 3.4 | 1.2 | 1.7 |
| R117A ^N | D597A/ Q600A ^C | 1.3±0.1 | 4.4±0.5 | 6.7±0.3 | 12.4±0.5 | 0.3 | 1.0 | 0.6 | 1.2 |
| KatG ^N | D597A/ Q600A ^C | 1.7±0.1 | 5.8±0.7 | 11.4±0.3 | 20.1±0.7 | 0.4 | 1.3 | 1.1 | 1.9 |

^a Assays included 20 nM KatG^N+KatG^C, 30 nM for all other domain variants in 50 mM acetate buffer, pH 5.0 at 1.0 mM H₂O₂, 0.1 mM ABTS concentration, 23 °C.

proteins to ten-fold of N-terminal, it was evident that the reactivation rates were all enhanced across the board while the amplitudes remained largely unaffected (Table 2.2 and 2.3).

The extent of reactivation of each domain variant in the distant-network was also evaluated by determining steady-state kinetic parameters of the recovered activities following 48 hour incubations of equimolar concentration of the stand-alone domains. The peroxidase activity was largely unaffected among all the variants compared to the unmodified domain proteins (Table 2.4); however, the catalase activity was diminished to various degrees (Figure 2.9 and Table 2.5). Surprisingly, the most detrimental effect on catalase activity occurred on the R117D^N+D597R^C proteins with less than 20% catalase activity retained in which the polarity of the two residues were reversed by mutations albeit variants reactivated by D597A/Q600A^C bearing most low-spin species. It was also shown that single substitution of R117 and D597 with aspartate and arginine, respectively, resulted in catalase compromised proteins comparable to that of double variant R117A^N+D597A^C, in all three cases about 70% of catalase activity was abolished compared to unmodified domain proteins.

2.4 Discussion

An important consequence of gene duplication in evolution is the emergence of a novel function (87, 114). In catalase-peroxidases, gene duplication coupled with fusion, produces a C-terminal domain that has no active site of its own but has a profound impact on the catalytic abilities of its N-terminal domain. Indeed, the C-terminal domain still retains a peroxidase-like overall fold but appears to be vestigial given the fact it doesn't bind any heme or catalyze any discernable reactions on its own (105). Nevertheless, in

Table 2.4. Apparent peroxidase^a kinetic parameters of distant-network domain variants and unmodified KatG^N+KatG^C for comparison.

| Protein | | H ₂ O ₂ -dependent Peroxidase Cycle Parameters | | | |
|--------------------|--------------------------|--|--|---|--|
| N-terminal Domain | C-terminal Domain | k _{cat} (s ⁻¹) | K _M (mM H ₂ O ₂) | k _{cat} /K _M (10 ⁵ M ⁻¹ s ⁻¹) | K _I (mM H ₂ O ₂) |
| KatG ^N | KatG ^C | 26.1±0.7 | 0.14±0.01 | 1.8 | 17.4±2.0 |
| R117A ^N | KatG ^C | 34.6±2.2 | 0.16±0.02 | 2.1 | 3.1±0.5 |
| KatG ^N | D597A ^C | 22.2±0.7 | 0.18±0.02 | 1.2 | 16.8±2.1 |
| R117A ^N | D597A ^C | 18.5±0.7 | 0.13±0.01 | 1.5 | 3.4±0.4 |
| R117D ^N | KatG ^C | 23.4±1.4 | 0.19±0.03 | 1.2 | 3.9±0.6 |
| KatG ^N | D597R ^C | 45.9±1.5 | 0.28±0.02 | 1.6 | 5.0±0.4 |
| R117D ^N | D597R ^C | 61.0±4.2 | 0.40±0.05 | 1.5 | 2.2±0.3 |
| R117A ^N | Q600A ^C | 36.3±1.8 | 0.17±0.02 | 2.1 | 4.5±0.6 |
| KatG ^N | Q600A ^C | 38.7±1.3 | 0.25±0.02 | 1.5 | 16.4±2.2 |
| R117A ^N | D597A/Q600A ^C | 15.9±0.8 | 0.12±0.02 | 1.3 | 2.8±0.3 |
| KatG ^N | D597A/Q600A ^C | 27.2±1.4 | 0.17±0.02 | 1.6 | 3.1±0.4 |

| Protein | | ABTS-dependent Peroxidase Cycle Parameters | | | |
|--------------------|--------------------------|--|--------------------------|---|--------------------------|
| N-terminal Domain | C-terminal Domain | k _{cat} (s ⁻¹) | K _M (mM ABTS) | k _{cat} /K _M (10 ⁵ M ⁻¹ s ⁻¹) | K _I (mM ABTS) |
| KatG ^N | KatG ^C | 28.0±0.7 | 0.093±0.009 | 3 | N/D ^b |
| R117A ^N | KatG ^C | 27.1±0.6 | 0.089±0.007 | 3 | N/D |
| KatG ^N | D597A ^C | 21.7±0.5 | 0.094±0.009 | 2.3 | N/D |
| R117A ^N | D597A ^C | 17.6±0.8 | 0.13±0.02 | 1.4 | 18.6±10.0 |
| R117D ^N | KatG ^C | 22.6±1.0 | 0.11±0.01 | 2.1 | 4.3±0.7 |
| KatG ^N | D597R ^C | 41.2±0.9 | 0.042±0.002 | 9.9 | 2.2±0.2 |
| R117D ^N | D597R ^C | 46.6±2.4 | 0.14±0.01 | 3.3 | 2.7±0.4 |
| R117A ^N | Q600A ^C | 33.9±0.5 | 0.12±0.01 | 2.9 | N/D |
| KatG ^N | Q600A ^C | 33.2±0.4 | 0.086±0.005 | 3.9 | N/D |
| R117A ^N | D597A/Q600A ^C | 15.1±0.5 | 0.12±0.01 | 1.3 | 3.9±0.5 |
| KatG ^N | D597A/Q600A ^C | 27.7±0.9 | 0.13±0.01 | 2.1 | 1.9±0.2 |

^a Assays included 20 nM KatG^N+KatG^C, 30 nM for all other domain variants in 50 mM acetate buffer, pH 5.0 at 0.5 mM ABTS and 1.0 mM H₂O₂ concentration, respectively, 23 °C.

^b N/D – not detected within substrate concentration range evaluated.

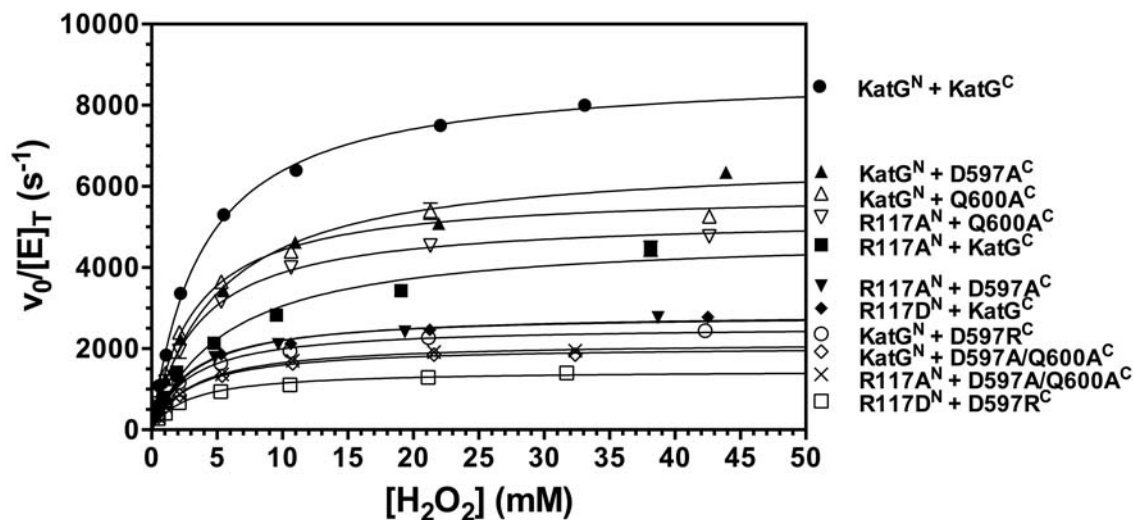


Figure 2.9. Effect of H₂O₂ concentration on catalase activity of distant-network domain variants and unmodified KatG^N+KatG^C for comparison.

Table 2.5. Apparent catalase^a kinetic parameters of distant-network domain variants and unmodified KatG^N+KatG^C for comparison.

| Protein | | Catalase Cycle Parameters | | |
|--------------------|--------------------------|-------------------------------------|--|---|
| N-terminal Domain | C-terminal Domain | k _{cat} (s ⁻¹) | K _M (mM H ₂ O ₂) | k _{cat} /K _M (10 ⁶ M ⁻¹ s ⁻¹) |
| KatG ^N | KatG ^C | 8840±80 | 3.8±0.1 | 2.3 |
| R117A ^N | KatG ^C | 4800±180 | 5.8±0.7 | 0.83 |
| KatG ^N | D597A ^C | 6700±150 | 5.0±0.4 | 1.3 |
| R117A ^N | D597A ^C | 2850±50 | 2.9±0.2 | 0.97 |
| R117D ^N | KatG ^C | 2880±40 | 3.1±0.2 | 0.93 |
| KatG ^N | D597R ^C | 2560±40 | 2.8±0.2 | 0.90 |
| R117D ^N | D597R ^C | 1470±20 | 2.7±0.1 | 0.54 |
| R117A ^N | Q600A ^C | 5250±50 | 3.6±0.1 | 1.5 |
| KatG ^N | Q600A ^C | 5900±100 | 3.3±0.2 | 1.8 |
| R117A ^N | D597A/Q600A ^C | 2170±10 | 3.1±0.1 | 0.69 |
| KatG ^N | D597A/Q600A ^C | 2070±20 | 3.0±0.1 | 0.70 |

^a Assays included 20 nM KatG^N+KatG^C, 30 nM for all other domain variants in 100 mM phosphate buffer, pH 7.0, 23 °C.

the absence of the C-terminal domain, the active site harboring N-terminal domain lost both activities due to the coordination of the distal histidine to the heme iron as a strong field ligand shifting the active site to a hexacoordinate low-spin state (74). Therefore, the apparent role of C-terminal domain is directing the correct configuration of the active site of the N-terminal domain. Interestingly, a similar function is addressed by calcium ions among related Class II peroxidases (61).

The interface between the two domains of KatGs provides an excellent site to investigate the mechanisms by which the C-terminal domain facilitates the active site configuration. Just as in Class II peroxidases, the shift of heme iron coordination and loss of activity are reversible upon re-introduction of calcium, we have demonstrated the same consequences for structure and activity that are observed in KatGs (75). As such, we produced stand-alone domain variants targeting the H-bond partners at the interface as a novel approach to evaluate the interdomain interactions. All the C-terminal domain proteins were obtained in soluble forms, in stark contrast, none of the N-terminal proteins including unmodified KatG^N was able to be expressed in soluble forms. Thus, the resulting inclusion bodies needed to be refolded signifying the essential role of C-terminal domain in KatG structural stability. The secondary structure content verified by CD spectroscopy suggested no apparent misfolding across all the domain variants including the N-terminal proteins purified from inclusion bodies.

Both UV-visible and MCD spectroscopy unequivocally demonstrated the presence of low-spin species in reactivated domain variants suggesting the substitution made at the domain interface resulted in an inability of the C-terminal domain to fully address the N-terminal domain's active site configuration. It is further evidenced in EPR spectroscopy

and simulations that substitution of both D597 and Q600 on C-terminal domain generated noticeable amount of low-spin species in the variants reactivated by D597A/Q600A^C. Although it is not invariant, the intended H-bond interaction between the two domains by virtue of its carbonyl oxygen from Q600 side chain is conserved with an asparagine in *Mycobacterium tuberculosis* KatG, and an aspartate in *Haloarcula marismortui* KatG. The latter is not too surprising given the solvent-exposed position of the residue as well as the high salt living environment of the organism. Moreover, as shown previously, a greater contribution of broad rhombic high-spin species was observed in all domain variants, in which the position of the sixth ligand of the heme iron became unoccupied as opposed to the weakly bound water as the sixth ligand in the narrow rhombic high-spin species. The shift from narrow to broad rhombic high-spin state was especially remarkable when R117 was substituted, resulting in nearly 90% contribution from broad rhombic high-spin heme species as opposed to predominantly narrow rhombic state in unmodified domain proteins, suggesting this interdomain arginine plays an essential role in modulating the coordination of active site heme iron.

Our reactivation kinetics results suggested the reactivation process generally followed one-phase exponential association mechanism (data not shown), and single substitution to C-terminal domain residues did not impair the observed reactivation rates compared to unmodified domain proteins. During the reactivation process, several conformational changes are likely to occur, including opening of the heme iron coordination sphere, re-establishment of interactions not only within the N-terminal domain but also between the two domains. Therefore, it is likely that by disruption of intrasubunit interactions, some of the conformational changes are prevented from taking

place. Indeed, substitution of D597 with arginine as in $\text{KatG}^{\text{N}}+\text{D597R}^{\text{C}}$ and $\text{R117D}^{\text{N}}+\text{D597R}^{\text{C}}$ variants, allowed the proteins to recover at a relatively faster rate, however, the resulting proteins were also much less active. That is, the amplitude of reactivation was diminished. The rates of reactivation were decreased by 60-70% when both D597 and Q600 were substituted with alanine suggesting that the conformation of the C-terminal domain in this local region might be compromised in $\text{D597A/Q600A}^{\text{C}}$ protein compared to unmodified KatG^{C} and other C-terminal domain variants which resulted a slower reactivation rate (Table 2.2 and 2.3). Increasing the amount of C-terminal domain enhanced the rates of reactivation by at least 3-fold for all the reactivation proteins, and this can be understood by the fact that KatG generally exists as dimer or tetramer, therefore, both intra- (as in this study) and inter-subunit interactions are likely to be involved in the reactivation process.

The extents of reactivation revealed by steady-state kinetics varied among the distant-network domain variants. Substitutions to these residues had little influence on peroxidase activity. The most compromised catalase activity was observed in $\text{R117D}^{\text{N}}+\text{D597R}^{\text{C}}$ variant in which the polarity was reversed by switching the two residues. Although the interaction would presumably be retained, the resulting proteins lost more than 80% catalase activity compared to the unmodified domains. Moreover, the single variant proteins $\text{R117D}^{\text{N}}+\text{KatG}^{\text{C}}$ and $\text{KatG}^{\text{N}}+\text{D597R}^{\text{C}}$ exhibited equally detrimental effect even comparable to that of double alanine substitution proteins $\text{R117A}^{\text{N}}+\text{D597A}^{\text{C}}$. Examination of the spin distributions revealed that except for the variants bearing the C-terminal double substitution D597A/Q600A , all other variants all had similar contribution about 10% from low-spin species with one another.

As clearly demonstrated in Figure 2.10, the loss of catalase activity in terms of k_{cat} has no significant correlation with observed low-spin contribution in the variants. Furthermore, none of the reactivated domain variants follows the linear relationship established between KatG^{N} and unmodified $\text{KatG}^{\text{N}}+\text{KatG}^{\text{C}}$ suggesting the loss of catalase activity observed in these variants has little dependence on low-spin contribution. It can also be seen from the graph that $\text{R117A}^{\text{N}}+\text{D597A}^{\text{C}}$, $\text{R117D}^{\text{N}}+\text{KatG}^{\text{C}}$, $\text{KatG}^{\text{N}}+\text{D597R}^{\text{C}}$ and $\text{R117D}^{\text{N}}+\text{D597R}^{\text{C}}$ variants appear to have the least dependence on low-spin contribution. No significant correlation between peroxidase activity and low-spin contribution is found in the reactivated variants (Figure 2.11), and the least dependence is revealed in $\text{R117D}^{\text{N}}+\text{D597R}^{\text{C}}$ variant which has the most peroxidase activity compared to other variants with similar low-spin contribution. When the two activities are compared against one another with respect to apparent second-order rate constant $k_{\text{cat}}/K_{\text{M}}$ (Figure 2.12), although no significant correlation can be obtained, it is clear that catalase activity is affected to a greater extent than peroxidase activity implying the mechanisms underlying loss of catalase activity are unique to catalase but not applicable to peroxidase activity.

The diminished catalase activity in the distant-network variants is not unexpected. However, what is striking is that the impaired catalase activity observed in these reactivated domain variants, by and large, is not due to the formation of hexacoordinate low-spin species. Interestingly, the substitutions generated on the conserved I'-helix of C-terminal domain which contacts N-terminal domain through intersubunit interactions have shown a strong correlation between decreased catalase activity and hexacoordinate

low-spin species contribution. Indeed, double substitution to the conserved I'-helix residues resulted in a C-terminal domain protein that was no longer able to reactivate N-

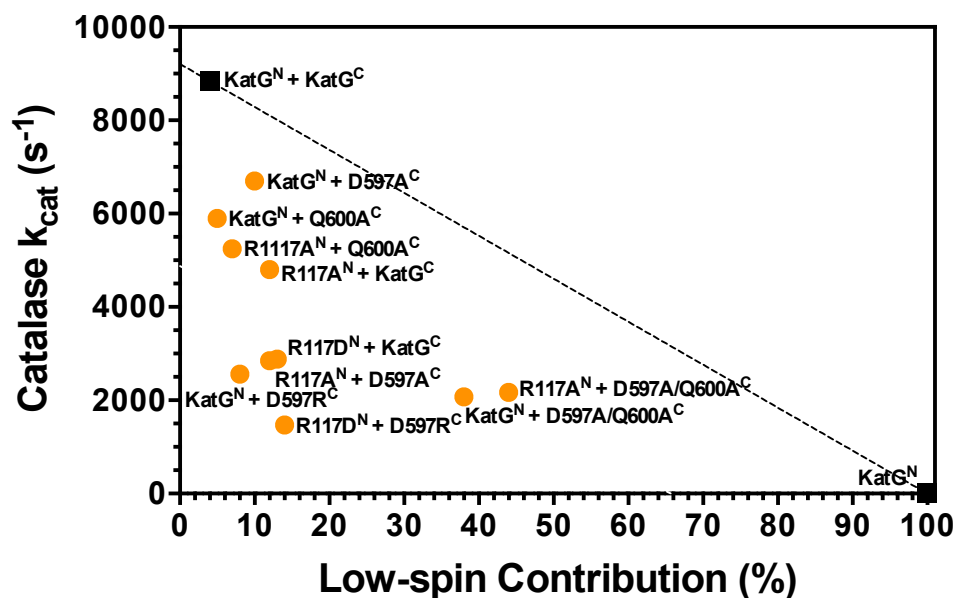
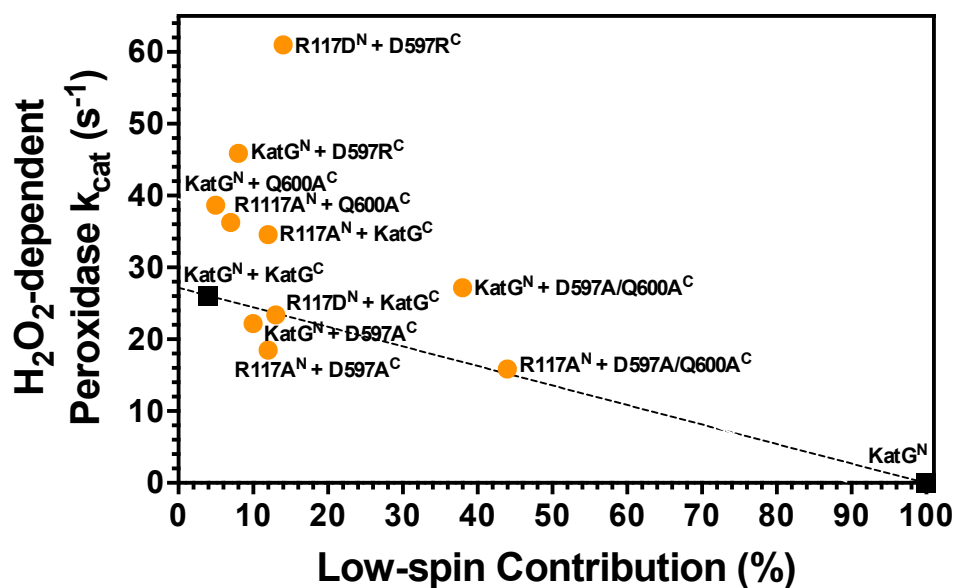


Figure 2.10. Correlation between catalase activity k_{cat} and low-spin contribution in reactivated distant-network variants (●) with KatG^N and KatG^N+KatG^C as two endpoints (■).

A



B

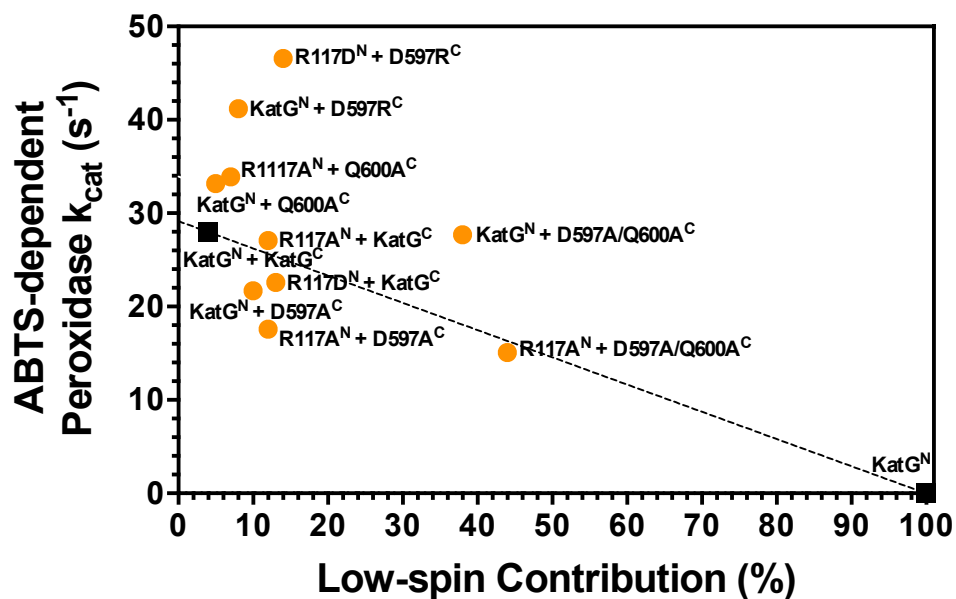


Figure 2.11. Correlation between peroxidase activity k_{cat} and low-spin contribution in reactivated distant-network variants (●) with KatG^N and KatG^N+KatG^C as two endpoints

(■): H₂O₂-dependent peroxidase activity (A) and ABTS-dependent peroxidase activity (B).

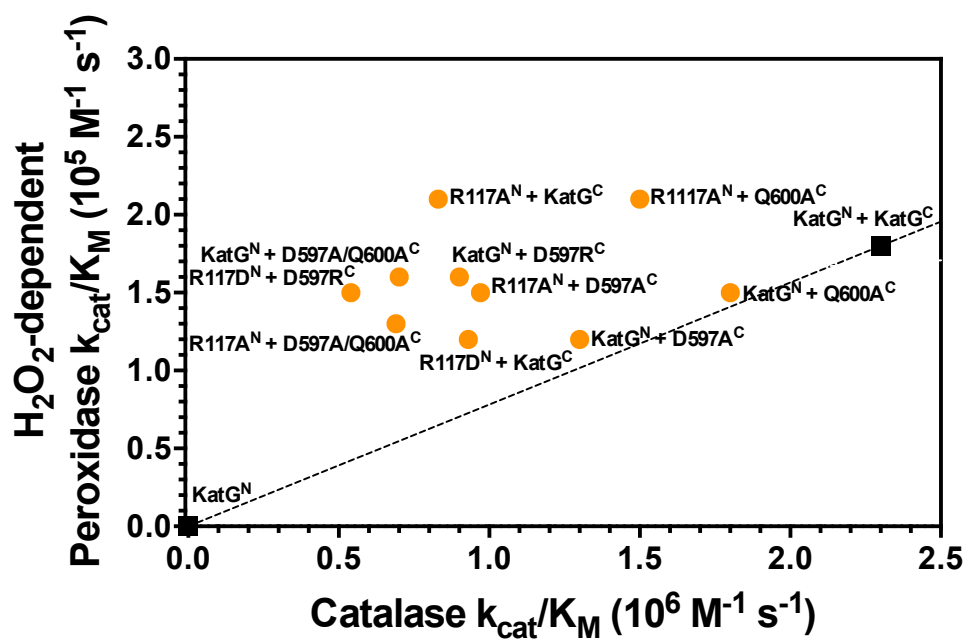


Figure 2.12. Correlation between H₂O₂-dependent peroxidase activity and catalase activity with respect to k_{cat}/K_M in reactivated distant-network variants (●) with KatG^N and KatG^N+KatG^C as two endpoints (■).

terminal domain (154). At any rate, the formation of Met-Tyr-Trp covalent adduct that is indispensable for catalase turnover in KatG is unlikely to be impaired by substitutions of distant-network residues, because the inability of formation of the covalent adduct would abolish catalase activity and result in a substantially elevated apparent K_M for H_2O_2 , while none of the reactivated distant-network variants behaved as such (80). On the other hand, the mobile arginine, as known as the arginine switch that interacts with the covalent adduct which in turn modulates catalase activity by adopting two different conformations is likely to be influenced by substitutions of the conserved charged residues due to the alteration of local pK_a . At the same time, it is evident that such an influence is limited by proximity of the distant-network residues to the arginine switch by the fact none of substitutions replicates the effect of substituting the arginine with residues other than lysine (80).

Although the mechanisms by which the distant-network residues affect catalase activity is not clearly understood, our data presented here suggest that these residues play an essential role in catalase turnover in KatG. It has been demonstrated that Arg 117 maintains the coordination sphere of heme iron for the active site architecture and the conserved H-bond interaction imparted between Arg 117 and Asp 597 is essential for catalase activity for KatG enzymes.

CHAPTER THREE
INTEGRAL ROLE OF INTERDOMAIN INTERACTIONS 20 Å FROM ACTIVE
SITE IN HEME ENVIRONMENT AND CATALYTIC FUNCTION OF KATGS

3.1 Introduction

Catalase-peroxidases (KatGs) are heme-dependent enzymes mainly found in bacteria and lower eukaryotes such as fungi that are capable of scavenging hydrogen peroxide (H_2O_2) via both catalase and peroxidase pathways. The robust catalase activity in KatGs, even overwhelming when compared to their peroxidase activity, is both striking and baffling given the fact KatGs bear virtually no resemblance to canonical catalases and none of their structurally- and evolutionarily-related relatives in the entire peroxidase-catalase superfamily exhibits appreciable catalase activity (115, 116, 120, 121). Instead of having a single domain like almost all other members of the superfamily, KatG has two peroxidase-like domains in each subunit. The N-terminal domain harbors the active site with heme deeply buried at its core while the C-terminal domain does not bind heme or catalyze any disenable reactions on its own. It is proposed that the C-terminal domain originated by gene duplication after which its peroxidase function was lost. Susumu Ohno pointed out in his monograph “Evolution by Gene Duplication” that as a general matter, duplicated domains are preserved to take care of the ancestral function. Consistent

with this principle, removal of the vestigial and seemingly redundant C-terminal domain resulted in a stand-alone N-terminal domain with neither peroxidase nor catalase activity (122). Subsequent studies revealed that the energetically favorable coordination of active site distal histidine to the heme iron shifted the populations of heme species from predominately high-spin to exclusively hexacoordinate low-spin state accounting for the loss of all enzymatic activities (74).

Interestingly, a similar effect was reported in related Class II peroxidases such as manganese peroxidase in which the loss of calcium ions on the distal side of the heme led to the inactivation of the enzyme (61). It was demonstrated that there was also a shift in the spin-state of heme iron to predominately low-spin concomitant with the loss of calcium, however, the activity could be restored upon re-introduction of calcium, suggesting the inactivation was reversible. Similarly, the separately expressed and isolated C-terminal domain was able to reactivate the stand-alone N-terminal domain. The reactivated enzyme was revealed by re-established heme environment and restored catalase and peroxidase activities, suggesting the duplicated C-terminal domain directs the active site configuration of N-terminal domain by preventing the otherwise spontaneous coordination of distal histidine to the heme iron. Ohno's theory seemed plausible, however it is not immediately understood why such a large structure as C-terminal domain is needed in KatGs to complete a task that is simply fulfilled by calcium ions in closely related heme peroxidases.

To elucidate the mechanisms by which the C-terminal domain regulates KatG active site structure and function, we altered the intrasubunit interface between the two domains particularly with respect to two highly conserved H-bond networks. By distance from the

active site, they appear to be 30 Å and 20 Å from the heme iron. As such, we have designated them the distant-network and near-network, respectively. As discussed in Chapter Two, the distant-network involves Arg 117 on the BC interhelical loop from N-terminal domain which forms H-bonds with both Asp 597 and Gln 600 on the E' helix of C-terminal domain. It was clearly demonstrated that Arg 117 modulated the coordination sphere of active site heme iron and both Arg 117 and Asp 597 are essential for catalase turnovers in KatG by their intended interaction. The near-network residue from the N-terminal domain side Tyr 111 is also located on the B'C' interhelical loop as Arg 117, but appears 10 Å closer to the active site. Tyr 111 interacts with Asp 482, which is on the B'C' interhelical loop of C-terminal domain, Asp 482 in turn forms H-bonds with adjacent Arg 479 on the same loop from C-terminal domain (Figure 3.1). As demonstrated with the reactivated distant-network variants, substitutions of the conserved residues diminished catalase activity to different extents, but the impaired catalase activity was not due to the low-spin contribution. To further evaluate such a striking effect, for the near-network we produced alanine substitution for all the three residues in stand-alone domain protein (Y111A^N, D482A^C and R479A^C) and combined with both unmodified and modified partners. With the same approach, the reactivation processes were monitored, and the reactivated domain proteins were characterized by spectroscopic analyses and kinetics studies. Taken together, the near-network residues between the domain interface were demonstrated to play an integral role in both catalase and peroxidase activities in KatG.

Materials and Methods

3.2.1 Reagents

Hydrogen peroxide (30%), imidazole, hemin, sodium dithionite, ampicillin, chloramphenicol, phenylmethylsulfonyl fluoride (PMSF) and 2,2'-azino-bis(3-ethylbenzthiazoline-6-sulfonic acid) (ABTS) were purchased from Sigma (St. Louis,

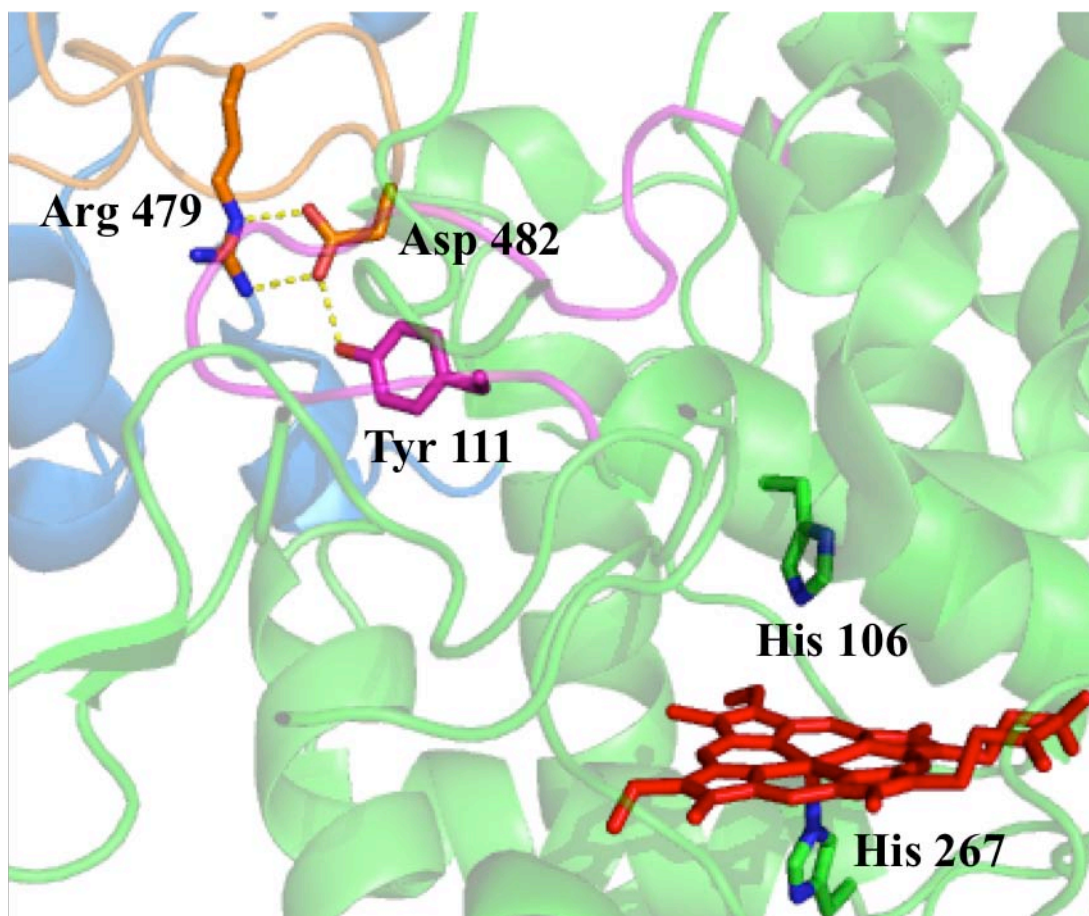


Figure 3.1. Near-network Interactions between the N-terminal domain BC interhelical loop (shown in magenta) and the C-terminal domain B'C' interhelical loop (shown in orange) in KatG. Coordinates from the structure of *Burkholderia pseudomallei* KatG were used (PDB: 1MWV) (83). Numbering reflects *Escherichia coli* KatG sequence.

MO). Isopropyl- β -D-thiogalactopyranoside (IPTG) was obtained from GoldBio Technology (St. Louis, MO). Tris, mono- and di-basic potassium phosphate, mono- and di-basic sodium phosphate, sodium chloride, acetic acid, sodium acetate and urea were obtained from Fisher (Pittsburgh, PA). All oligonucleotide primers were purchased from Invitrogen (Carlsbad, CA). All *E. coli* strains [XL1-Blue and BL21-Gold(DE3)pLysS], *PfuTurbo* DNA polymerase, and T4 DNA ligase were obtained from Agilent Technologies (La Jolla, CA). All restriction enzymes were purchased from New England Biolabs (Beverly, MA). BugBuster protein extraction reagent and Benzonase Nuclease were purchased from Novagen (Madison, WI). Nickel-nitrilotriacetic acid (Ni-NTA) resin was purchased from Qiagen (Valencia, CA). Buffer exchange chromatography columns (10DG) were obtained from Bio-Rad (Hercules, CA). Amicon Ultra centrifugal filters were obtained from EMD Millipore (Billerica, MA). All buffers and media were prepared using water purified through Barnstead EASYpure II system (18.2 M Ω /cm resistivity).

3.2.2 Cloning and expression of KatG^N, KatG^C and their variants of the near-network

Generation of a construct for the expression of KatG lacking its C-terminal domain (KatG^N) was achieved as previously described (74). The expression vector of stand-alone C-terminal domain of KatG (KatG^C) was produced using a deletion mutagenesis procedure developed in our laboratory (76). The plasmids of stand-alone domain variants Y111A^N, D482A^C, and R479A^C were generated using mutagenic primers [5'-Phos-

CGCGCTCAATCGATGGACGCGGTGG-3' (Y111A^N coding), 5'-Phos-
 CAGTCCCCGCGCCGTGCCAG-3' (Y111A^N non-coding), 5'-Phos-
 GCGCCAAACGCGGTGGTGCC-3' (D482A^C coding), 5'-Phos-
 CACCACGGAAGGTAGAAGCAGATGCCAG-3' (D482A^C non-coding), 5'-Phos-
 CCGGCGGCGACAAACGCGG-3' (R479A^C coding), 5'-Phos-
 CGAAGGTAGAAGCAGATGCCAGGCCAC-3' (R479A^C non-coding)] according to
 the 'Round-the-horn procedure in which the 5' end of the two primers start at adjacent
 bases (108). The PCR products were then ligated using T4 DNA ligase and used to
 transform *E. coli* XL1-Blue by heat shock. Plasmids from candidate colonies were
 screened by diagnostic restriction digests. Positive candidates were submitted for DNA
 sequence analysis at Davis Sequencing (Davis, CA). Verified plasmids were used to
 transform *E. coli* BL21-Gold(DE3)pLysS as the expression host. The expression of
 KatG^N, KatG^C and their variants of the near-network was carried out as previously
 described for another KatG (89) except that cultures were not supplemented with δ -
 aminolevulinic acid or ferrous ammonium sulfate.

3.2.3 Purification of KatG^N, KatG^C and their variants of the near-network

KatG^C and all the C-terminal domain variants were expressed in a soluble form. Thus,
 purifications were performed as previously described for the wild-type KatG (76). KatG^N
 and Y111A^N domain variants were expressed in inclusion bodies, so an alternative
 denaturing purification procedure was carried out. After the cells were centrifuged, the
 pellet was resuspended in Buffer A (50 mM NaH₂PO₄/Na₂HPO₄, 200 mM NaCl, pH 8.0)
 with 100 μ M PMSF, homogenized and then sonicated using Branson Sonifier 250
 (Danbury, CT). After that, Benzonase Nuclease (250 U) was added to the lysate and the

mixture was gently stirred for 2 hours. The cell lysate was then centrifuged. The pellet which contained the protein was resuspended in Buffer B (100 mM NaH₂PO₄, 10 mM Tris, 8 M urea), homogenized and centrifuged. The supernatant was mixed with Ni-NTA resin and gently agitated at room temperature overnight. The resin was then loaded into a column, washed with Buffer B containing 20 mM imidazole, and eluted off the column with Buffer B containing 400 mM imidazole. Urea and imidazole were finally removed by dialysis against Buffer C (50 mM KH₂PO₄/K₂HPO₄, 200 mM NaCl, pH 8.0) for 24 hours. The resulting protein was then reconstituted with 0.85 equivalents of hemin and incubated at 4 °C for at least 24 hours.

3.2.4 Domain combination and incubation

The concentrations of reconstituted KatG^N and their variants were determined using molar absorptivity calculated from pyridine hemichrome assay (109). Solutions containing both N- and C-terminal domain proteins were incubated at 4 °C for times ranging from 0 to 48 hours in the presence of 50 mM phosphate, pH 7.0, 50 mM NaCl. Following a given incubation time, aliquots were taken and activities were measured according to the assays described below.

3.2.5 UV-visible absorption spectra and activity assays

Following reconstitution, proteins were always centrifuged to remove potentially unincorporated heme and other insoluble material (e.g., precipitated protein). All spectra were recorded at 23 °C on a Shimadzu UV-1601 spectrophotometer (Columbia, MD) using a 1.0 cm quartz cell. Catalase and peroxidase activity assays were performed as described elsewhere (89). Initial rates were fit to Michaelis-Menten equation (2.1) by nonlinear regression analysis to determine apparent kinetic parameters. If substrate-

dependent inhibition was evident, the fitting equation (2.2) was modified to include a substrate-dependent inhibition term K_I , a macroscopic apparent dissociation constant that reflects the ability of the substrate to act as an inhibitor.

$$\frac{v_0}{[E]_T} = \frac{k_{cat}[S]}{K_M + [S]} \quad (2.1)$$

$$\frac{v_0}{[E]_T} = \frac{k_{cat}[S]}{K_M + [S] + \frac{[S]^2}{K_I}} \quad (2.2)$$

3.2.6 Circular and magnetic circular dichroism

All circular dichroism (CD) and magnetic circular dichroism (MCD) spectra were recorded on a Jasco J-810 spectropolarimeter (Tokyo, Japan) at 23 °C. Baseline and analysis were carried out using Jasco J-720 software. Circular dichroism spectra (250-190 nm) were obtained using 5 μ M enzyme in 5 mM phosphate buffer, pH 7.0 with a 0.5 mm quartz cell. Magnetic circular dichroism spectra (680-380 nm) were obtained using 15 μ M enzyme in 50 mM phosphate 50 mM NaCl buffer, pH 7.0 with a 5.0 mm quartz cell in a 1.4 Tesla magnetic cell holder. The ferrous enzyme was prepared by adding a small amount (< 10 mg) of sodium dithionite to the protein's ferric state.

3.2.7 Electron paramagnetic resonance spectroscopy

Spectra were recorded using a Bruker EMX instrument equipped with an Oxford ESR 900 cryostat and ITC temperature controller. Sample concentration was performed using Amicon Ultra-4 centrifugal devices (Billerica, MA). The settings for the spectrometer were as follows: temperature, 10 K; microwave frequency, 9.38 GHz; microwave power, 0.1 mW; modulation amplitude, 10 G; modulation frequency, 100 kHz; time constant, 655.36 ms; conversion time, 655.36 ms; and receiver gain, 1.0×10^5 . Spin quantification

was carried out using the Biomolecular EPR spectroscopy software package available online (110).

3.3 Results

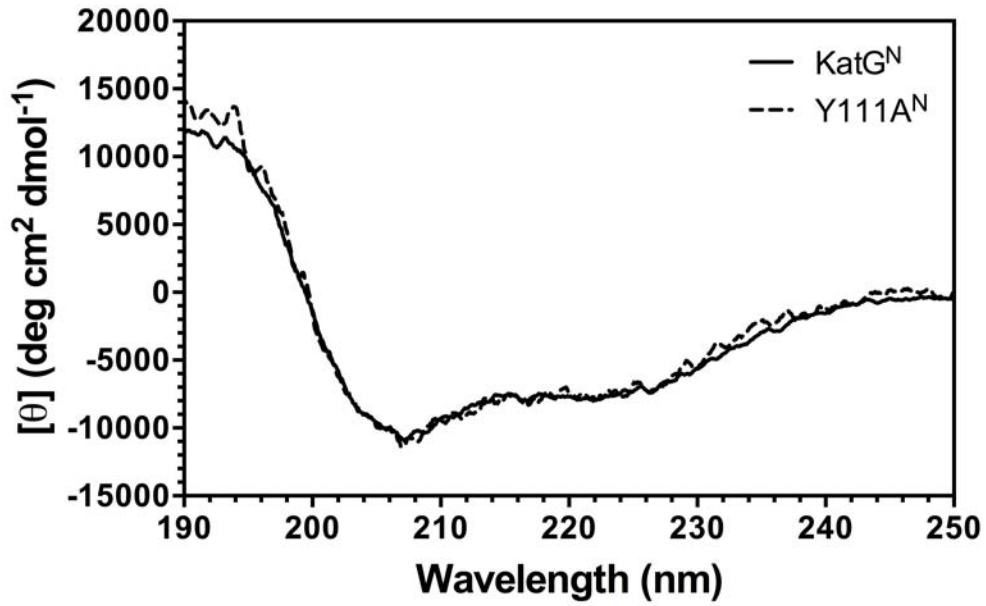
3.3.1 Circular dichroism and UV-visible spectroscopy

Consistent with our previous observations of distant-network domain proteins, the CD spectra recorded for Y111A^N, D482A^C and R479A^C in the near-network (Figure 3.2) resembled the corresponding spectra of unmodified KatG^N and KatG^C revealed by α -helical features at 222 and 208 nm confirming substitutions did not alter the secondary structural content of the domain variants.

Like the stand-alone N-terminal domain variants of distant-network, the near-network variant Y111A^N replicated the effect of the unmodified KatG^N, showing heme overwhelmingly in a hexacoordinate low-spin state. The Soret band λ_{\max} is at 416 nm with α and β bands absorption maxima at 568 and 538 nm, respectively. In contrast, reactivated KatG^N by KatG^C is characterized by a broad Soret band with a λ_{\max} at 411 nm and two charge transfer (CT) bands around 642 nm (CT1) and 530 nm (CT2). Following combination and incubation of the domain proteins, blue shifted Soret bands were all observed in the neighborhood of 412 nm for all variant combinations targeting the near H-bond network (Figure 3.3). This was suggestive of a mixed population of both high- and low-spin heme species. Moreover, co-incubation of separated domains did not return intensities of the CT1 band observed in intact wild-type KatG. Likewise, red shifted CT2 bands around 530 nm were also detected, all indicative of remaining contributions from hexacoordinate low-spin heme.

3.3.2 Magnetic circular dichroism

A



B

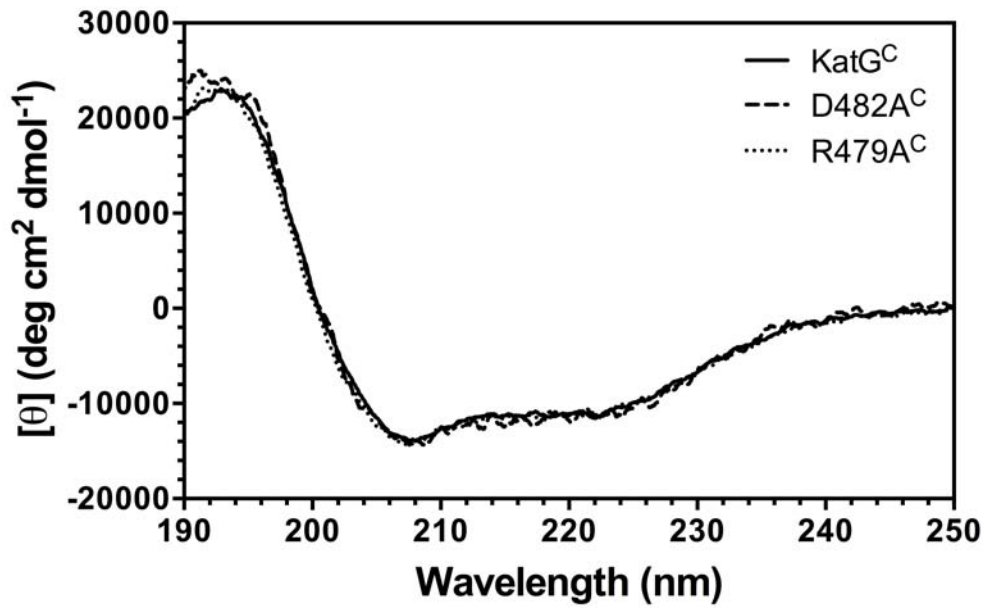


Figure 3.2. Far-UV circular dichroism spectra of KatG^N and Y111A^N (A), KatG^C and its variants (B) in the near-network. Spectra were recorded at 23 °C in 5 mM phosphate buffer, pH 7.0.

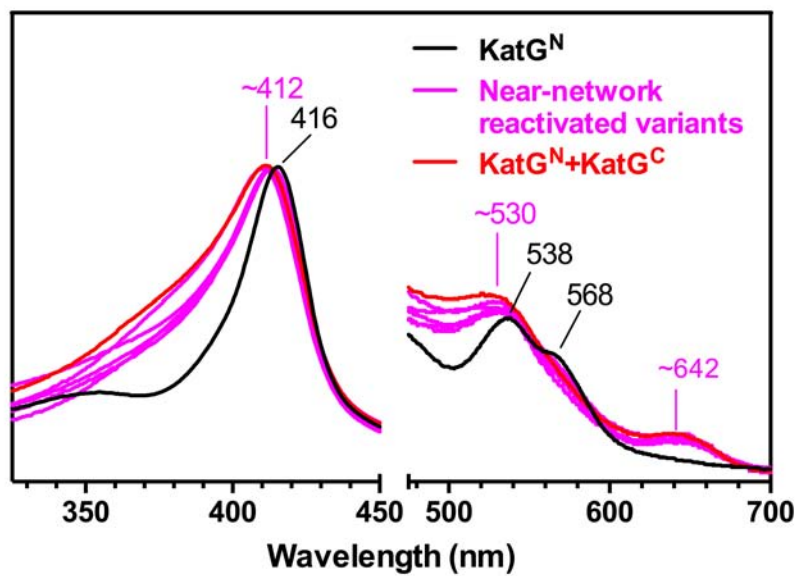


Figure 3.3. UV-visible spectral comparison of near-network reactivated variants with inactive KatG^N and unmodified KatG^N+KatG^C in their native state. Spectra were recorded at 23 °C in 100 mM phosphate buffer, pH 7.0.

As discussed in Chapter Two, the high- and low-spin species of KatG are better distinguished by MCD spectroscopy, particularly when evaluating the ferrous oxidation state. Again, Y111A^N exhibited similar features as KatG^N and all the distant-network N-terminal domain variants with an intense signal centered around 557 nm, a feature diagnostic for low-spin heme. Consistent with UV-visible spectroscopy results, following the incubation period of both N- and C-terminal proteins, the reactivated near-network domain variants all indicated a substantial increase in contribution from high-spin heme, manifested by the increased intensity of the B-type feature around 440 nm. Other features of high-spin ferrous heme including a doublet of bands in the 625-575 nm range were more prominent following stand-alone domain co-incubation along with a significant decrease of the Q-band signal around 557 nm (Figure 3.4). Nevertheless, contributions from hexacoordinate low-spin heme persisted in the reactivated near-network variants.

3.3.3 Electron paramagnetic resonance

The spin and coordination state of near-network variants following domain co-incubation was further evaluated by EPR spectroscopy. As mentioned in Chapter Two, three EPR signals are generally detected in the ferric state of the KatG proteins on the basis of their different g-values (Figure 3.5), a narrow rhombic high-spin signal ($g_x \sim 6.0$, $g_y \sim 5.6$ and $g_z = 1.99$), a broad rhombic high-spin signal ($g_x \sim 6.6$, $g_y \sim 5.0$ and $g_z = 1.95$) and a hexacoordinate low-spin signal ($g_x \sim 2.9$, $g_y \sim 2.3$ and $g_z \sim 1.5$). In the near-network domain variants, the low-spin signal became generally more apparent than that of distant-network proteins even with single substitution as in KatG^N+R479A^C variant. The coordination shift of heme iron from narrow rhombic to broad rhombic high-spin was also observed in near-network variants. To quantify the relative contributions of each

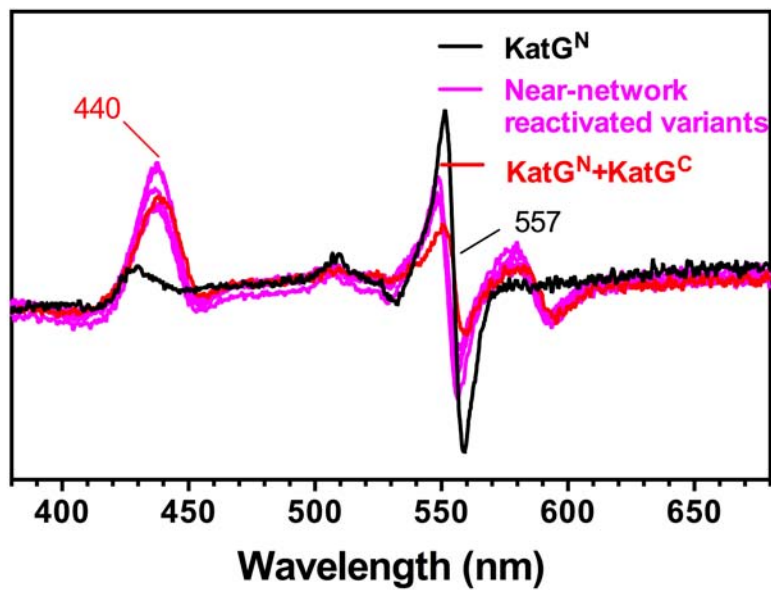


Figure 3.4. MCD spectral comparison of near-network reactivated variants with inactive KatG^N and reactivated KatG^N+KatG^C in ferrous state of heme. Spectra were recorded at 23 °C in 50 mM phosphate, 50 mM NaCl buffer, pH 7.0.

heme species, EPR simulations were performed accounting for both broad and narrow rhombic high-spin species (BRHS: $g_x = 6.64$, $g_y = 4.95$ and $g_z = 1.95$; NRHS: $g_x = 5.99$, $g_y = 5.60$ and $g_z = 1.99$) and one rhombic low-spin species (LS: $g_x = 2.92$, $g_y = 2.28$ and $g_z = 1.53$). Simulation and spin-integration suggested a 10% contribution from low-spin heme following co-incubation of Y111A^N and KatG^C. All other variant combinations generated a low-spin population of ~30% (Table 3.1). A shift in distribution of high-spin species was also detected particularly when both N- and C-terminal domains were variants or when R479A^C represented KatG^C.

3.3.4 Reactivation and steady-state kinetics

The reactivation process was monitored for 48 hours for each near-network domain variant combination. As demonstrated in Table 3.2 and 3.3, rates of reactivation varied across all combinations by no more than a factor of 4. For each domain combination, the rates of reactivation monitored by peroxidase and catalase activity were highly similar. Increasing the relative concentration of the C-terminal domain partner increased the reactivation rate to a similar extent. However, the amplitudes (i.e., the extent of reactivation) was unaffected by C-terminal domain concentration.

Steady-state kinetic parameters for catalase and peroxidase activity for each domain combination were obtained following their 48-hour co-incubation. The Y111A^N+KatG^C pairing showed the smallest low-spin contribution (10%); however, the k_{cat} for its catalase activity was only about 30% of that observed for the unmodified domain combination (Figure 3.6 and Table 3.4). Single substitution of R479 also markedly diminished the catalase k_{cat} by over 60% while for the KatG^N+D482A^C domain combination only about 40% reduction was observed given their similar low-spin

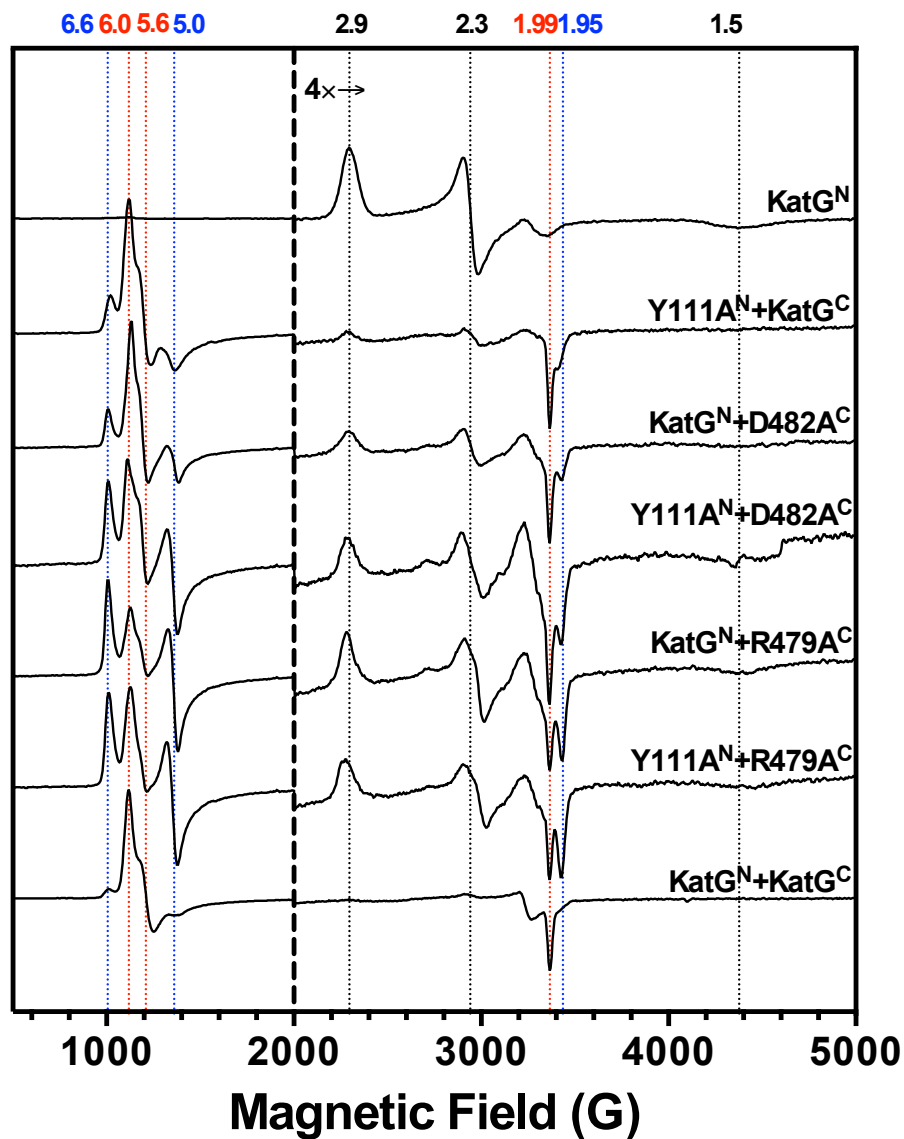


Figure 3.5. EPR spectra of near-network reactivated variants along with KatG^{N} , and $\text{KatG}^{\text{N}}+\text{KatG}^{\text{C}}$ for comparison. Spectra were magnified by four above 2000 Gauss. The g -values corresponding to narrow rhombic high-spin signal (~ 6.0 , ~ 5.6 and 1.99) and broad rhombic high-spin signal (~ 6.6 , ~ 5.0 and 1.95) observed in KatGs are shown as those of the hexacoordinate low-spin signal (~ 2.9 , ~ 2.3 and ~ 1.5).

Table 3.1. Ratios of EPR signals observed for near-network reactivated variants along with KatG^N and KatG^N+KatG^C for comparison.

| Protein | | % contribution | | |
|--------------------|--------------------|-----------------------------------|---------------------------------------|------------------|
| N-terminal Domain | C-terminal Domain | HS ^a : LS ^b | NRHS ^c : BRHS ^d | NRHS : BRHS : LS |
| KatG ^N | KatG ^C | 96 : 4 | 82 : 18 | 78 : 18 : 4 |
| Y111A ^N | KatG ^C | 90 : 10 | 55 : 45 | 49 : 41 : 10 |
| KatG ^N | D482A ^C | 73 : 27 | 54 : 46 | 39 : 34 : 27 |
| Y111A ^N | D482A ^C | 69 : 31 | 28 : 72 | 19 : 50 : 31 |
| KatG ^N | R479A ^C | 69 : 31 | 18 : 82 | 12 : 57 : 31 |
| Y111A ^N | R479A ^C | 75 : 25 | 28 : 72 | 21 : 54 : 25 |
| KatG ^N | | 0 : 100 | 0 : 0 | 0 : 0 : 100 |

^a High-spin; HS = NRHS + BRHS.

^b Low-spin ($g_x = 2.92$, $g_y = 2.28$ and $g_z = 1.53$).

^c Narrow rhombic high-spin ($g_x = 5.99$, $g_y = 5.60$ and $g_z = 1.99$).

^d Broad rhombic high-spin ($g_x = 6.64$, $g_y = 4.95$ and $g_z = 1.95$).

Table 3.2. Reactivation kinetic parameters of catalase activity of near-network domain variants and unmodified KatG^N+KatG^C for comparison.

| Protein | | Reactivation of Catalase Activity ^a | | | | Relative to KatG ^N + KatG ^C (1:1) | | | |
|--------------------|--------------------|---|----------|---|----------|---|------|--------------------|------|
| | | Rate Constant (10 ⁻⁵ s ⁻¹) | | Amplitude {v ₀ /[E] _T (s ⁻¹)} | | Relative Rate Constant | | Relative Amplitude | |
| N-terminal Domain | C-terminal Domain | 1:1 | 1:10 | 1:1 | 1:10 | 1:1 | 1:10 | 1:1 | 1:10 |
| KatG ^N | KatG ^C | 4.5±0.1 | 34.8±3.4 | 4270±40 | 4540±60 | 1.0 | 7.7 | 1.0 | 1.1 |
| Y111A ^N | KatG ^C | 5.1±0.3 | 17.1±2.7 | 1800±40 | 1880±50 | 1.1 | 3.8 | 0.4 | 0.4 |
| KatG ^N | D482A ^C | 3.8±0.3 | 14.3±2.2 | 3480±80 | 3530±110 | 0.8 | 3.2 | 0.8 | 0.8 |
| Y111A ^N | D482A ^C | 2.8±0.3 | 7.7±0.8 | 1300±50 | 1310±30 | 0.6 | 1.7 | 0.3 | 0.3 |
| KatG ^N | R479A ^C | 9.1±1.7 | 26.4±5.1 | 1920±80 | 1940±60 | 2.0 | 5.9 | 0.4 | 0.5 |
| Y111A ^N | R479A ^C | 9.0±0.9 | 17.5±2.5 | 48±1 | 59±2 | 2.0 | 3.9 | 0.01 | 0.01 |

^a Assays included 20 nM KatG^N+KatG^C, 30 nM for all other domain variants in 100 mM phosphate buffer, pH 7.0 at 5.0 mM H₂O₂ concentration, 23 °C.

Table 3.3. Reactivation kinetic parameters of peroxidase activity of near-network domain variants and unmodified KatG^N+KatG^C for comparison.

| Protein | | Reactivation of Peroxidase Activity ^a | | | | Relative to KatG ^N + KatG ^C (1:1) | | | |
|--------------------|--------------------|---|----------|---|-----------|---|------|--------------------|------|
| | | Rate Constant (10 ⁻⁵ s ⁻¹) | | Amplitude {v ₀ /[E] _T (s ⁻¹)} | | Relative Rate Constant | | Relative Amplitude | |
| N-terminal Domain | C-terminal Domain | 1:1 | 1:10 | 1:1 | 1:10 | 1:1 | 1:10 | 1:1 | 1:10 |
| KatG ^N | KatG ^C | 4.4±0.3 | 21.6±3.3 | 10.6±0.2 | 13.7±0.3 | 1.0 | 4.9 | 1.0 | 1.3 |
| Y111A ^N | KatG ^C | 4.3±0.2 | 13.2±2.3 | 18.1±0.3 | 17.1±0.6 | 1.0 | 3.0 | 1.7 | 1.6 |
| KatG ^N | D482A ^C | 3.1±0.2 | 10.4±1.7 | 6.7±0.2 | 7.0±0.3 | 0.7 | 2.4 | 0.6 | 0.7 |
| Y111A ^N | D482A ^C | 5.9±0.4 | 16.0±1.8 | 1.65±0.03 | 1.74±0.04 | 1.3 | 3.6 | 0.2 | 0.2 |
| KatG ^N | R479A ^C | 8.1±1.4 | 26.5±5.8 | 3.3±0.1 | 3.0±0.1 | 1.8 | 6.0 | 0.3 | 0.3 |
| Y111A ^N | R479A ^C | 11.8±1.6 | 21.5±4.0 | 2.64±0.08 | 2.65±0.08 | 2.7 | 4.9 | 0.2 | 0.3 |

^a Assays included 20 nM KatG^N+KatG^C, 30 nM for all other domain variants in 50 mM acetate buffer, pH 5.0 at 1.0 mM H₂O₂, 0.1 mM ABTS concentration, 23 °C.

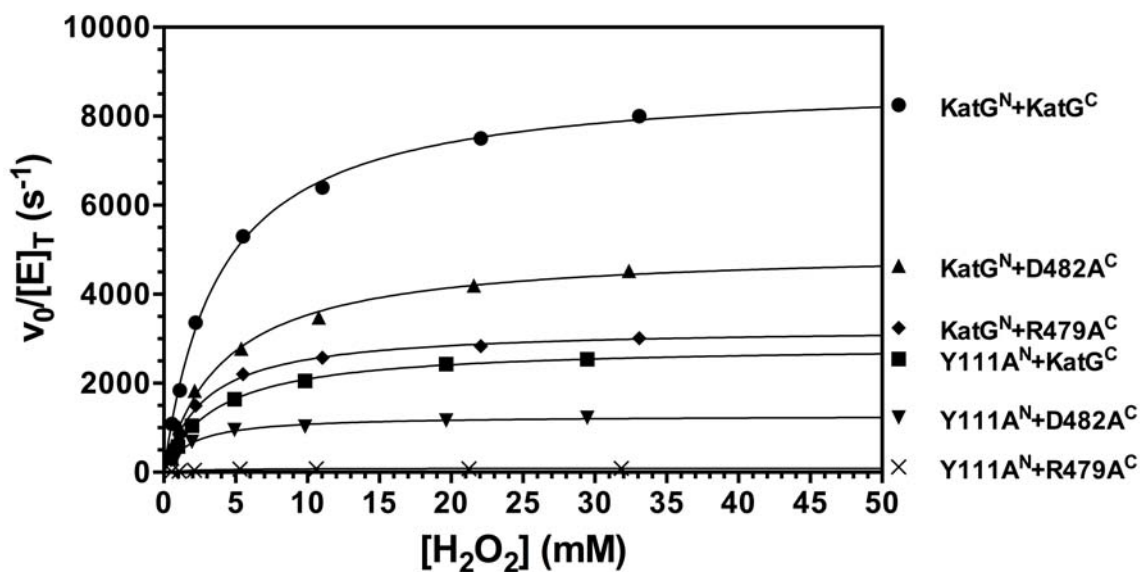


Figure 3.6. Effect of H₂O₂ concentration on catalase activity of near-network domain variants and unmodified KatG^N+KatG^C for comparison.

Table 3.4. Apparent catalase^a kinetic parameters of near-network domain variants and unmodified KatG^N+KatG^C for comparison.

| Protein | | Catalase Cycle Parameters | | |
|--------------------|--------------------|------------------------------|---|--|
| N-terminal Domain | C-terminal Domain | k_{cat} (s ⁻¹) | K_M (mM H ₂ O ₂) | k_{cat}/K_M (10 ⁶ M ⁻¹ s ⁻¹) |
| KatG ^N | KatG ^C | 8840±80 | 3.8±0.1 | 2.3 |
| Y111A ^N | KatG ^C | 2860±20 | 3.6±0.1 | 0.79 |
| KatG ^N | D482A ^C | 5020±60 | 4.2±0.2 | 1.2 |
| Y111A ^N | D482A ^C | 1280±20 | 1.8±0.1 | 0.70 |
| KatG ^N | R479A ^C | 3250±30 | 2.8±0.1 | 1.1 |
| Y111A ^N | R479A ^C | 93±2 | 2.4±0.2 | 0.038 |

^a Assays included 20 nM KatG^N+KatG^C, 30 nM for all other domain variants in 100 mM phosphate buffer, pH 7.0, 23 °C.

contributions. The alanine double substitutions were highly disruptive to catalase activity. Indeed, the Y111A^N+D482A^C variant diminished catalase k_{cat} by nearly 90% and more strikingly, a k_{cat} of only about 1% was retained with Y111A^N+R479A^C pairing in comparison to the unmodified domains. Except Y111A^N+KatG^C, peroxidase activity was reduced relative to KatG^N+KatG^C. Indeed, for all but Y111A^N+KatG^C and Y111A^N+R479A^C, peroxidase activity was diminished to an even greater extent than catalase activity (Figure 3.7, 3.8 and Table 3.5, 3.6).

3.4 Discussion

The C-terminal domain, a result of gene duplication, is an intriguing structural component in KatG enzymes given the fact it has lost its functionality and thus appears to be vestigial. Nevertheless, in the absence of this bulky and seemingly extraneous C-terminal domain, the remaining N-terminal domain alone loses all activity signifying the integral role of C-terminal domain in KatG functionality (73, 74). That this domain is a conserved feature of all KatG's further supports its indispensable nature. It has been proposed that the C-terminal domain may serve as a platform for folding of the N-terminal domain (105). Previous studies in our laboratory suggest one role of the C-terminal domain is to prevent the otherwise favorable coordination of the distal histidine to the heme iron. The result of such an event in an N-terminal domain is exclusively hexacoordinate low-spin heme species and no observable activity (74). Re-introduction of a separately expressed C-terminal domain restores active site structure and activity (75). This domain restructuring process depends, at least in part, on a series of intersubunit interactions between N- and C-terminal domains (154). At first glance, the analogous function is achieved in other members of the superfamily. For example,

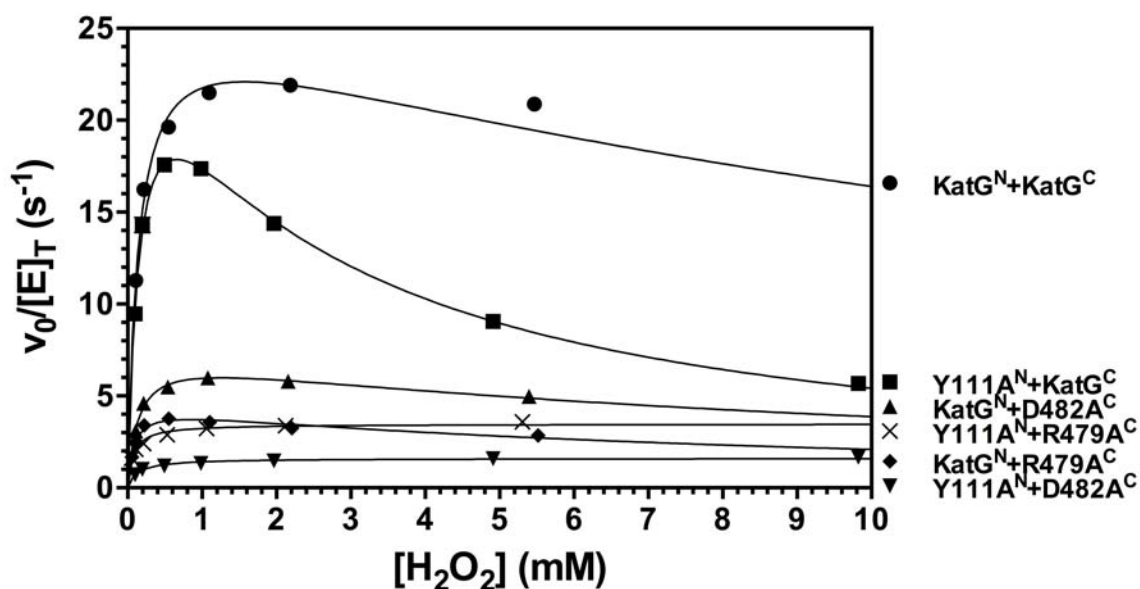


Figure 3.7. Effect of H_2O_2 concentration on peroxidase activity of near-network domain variants and unmodified $\text{KatG}^{\text{N}}+\text{KatG}^{\text{C}}$ for comparison.

Table 3.5. Apparent H_2O_2 -dependent peroxidase^a kinetic parameters of near-network domain variants and unmodified $\text{KatG}^{\text{N}}+\text{KatG}^{\text{C}}$ for comparison.

| Protein | | H_2O_2 -dependent Peroxidase Cycle Parameters | | | |
|---------------------------|---------------------------|---|---|--|---|
| N-terminal Domain | C-terminal Domain | k_{cat} (s^{-1}) | K_{M} (mM H_2O_2) | $k_{\text{cat}}/K_{\text{M}}$ ($10^5 \text{ M}^{-1} \text{ s}^{-1}$) | K_{I} (mM H_2O_2) |
| KatG^{N} | KatG^{C} | 26.1 ± 0.7 | 0.14 ± 0.01 | 1.8 | 17.4 ± 2.0 |
| Y111A^{N} | KatG^{C} | 27.3 ± 0.7 | 0.17 ± 0.01 | 1.6 | 2.5 ± 0.1 |
| KatG^{N} | D482A^{C} | 7.29 ± 0.11 | 0.14 ± 0.01 | 0.53 | 11.5 ± 0.6 |
| Y111A^{N} | D482A^{C} | 1.60 ± 0.03 | 0.14 ± 0.01 | 0.12 | N/D ^b |
| KatG^{N} | R479A^{C} | 4.41 ± 0.13 | 0.079 ± 0.008 | 0.55 | 9.1 ± 1.3 |
| Y111A^{N} | R479A^{C} | 3.47 ± 0.05 | 0.073 ± 0.006 | 0.47 | N/D |

^a Assays included 20 nM $\text{KatG}^{\text{N}}+\text{KatG}^{\text{C}}$, 30 nM for all other domain variants in 50 mM acetate buffer, pH 5.0 at 0.5 mM ABTS for $\text{KatG}^{\text{N}}+\text{KatG}^{\text{C}}$, 0.1 mM ABTS concentration for all other domain variants, 23 °C.

^b N/D – not detected within substrate concentration range evaluated.

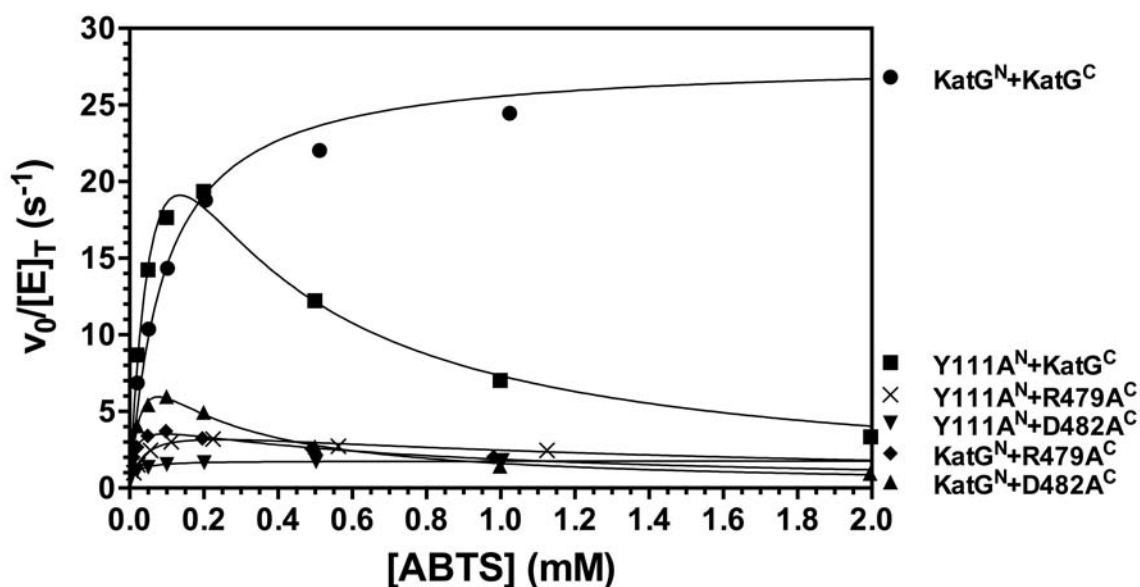


Figure 3.8. Effect of ABTS concentration on peroxidase activity of near-network domain variants and unmodified KatG^N+KatG^C for comparison.

Table 3.6. Apparent ABTS-dependent peroxidase^a kinetic parameters of near-network domain variants and unmodified KatG^N+KatG^C for comparison.

| Protein | | ABTS-dependent Peroxidase Cycle Parameters | | | |
|--------------------|--------------------|--|-----------------|--|------------------|
| N-terminal Domain | C-terminal Domain | k_{cat} (s ⁻¹) | K_M (mM ABTS) | k_{cat}/K_M (10 ⁵ M ⁻¹ s ⁻¹) | K_I (mM ABTS) |
| KatG ^N | KatG ^C | 28.0±0.7 | 0.093±0.009 | 3.0 | N/D ^b |
| Y111A ^N | KatG ^C | 46.1±4.9 | 0.096±0.016 | 4.8 | 0.19±0.03 |
| KatG ^N | D482A ^C | 11.7±0.8 | 0.037±0.005 | 3.1 | 0.16±0.02 |
| Y111A ^N | D482A ^C | 1.77±0.02 | 0.014±0.001 | 1.3 | N/D |
| KatG ^N | R479A ^C | 4.45±0.11 | 0.012±0.001 | 3.7 | 0.75±0.06 |
| Y111A ^N | R479A ^C | 4.10±0.13 | 0.036±0.003 | 1.1 | 1.6±0.2 |

^a Assays included 20 nM KatG^N+KatG^C, 30 nM for all other domain variants in 50 mM acetate buffer, pH 5.0 at 1.0 mM H₂O₂ concentration, 23 °C.

^b N/D – not detected within substrate concentration range evaluated.

manganese peroxidase contains two calcium ions, one of which is necessary to maintain the coordination sphere of heme iron. The loss of this calcium either by chelation or mutagenesis results in an enzyme with no activity and a hexacoordinate low-spin heme (61). Our data showed that substitution of near-network residues in KatG produced appreciable amount of low-spin species, with 15% more low-spin contribution compared to distant-network variants when C-terminal residue in the near-network was substituted, supporting our initial characterization of the role of C-terminal domain.

However, the translation from the spectroscopic features to enzyme kinetic data was remarkable given previous results with intersubunit interactions between the N- and C-terminal domain, and even the distant-network residues discussed in Chapter Two (154). The loss of catalase activity in single variants $Y111A^N+KatG^C$ and $KatG^N+R479A^C$ rivaled that of double variant $R117A^N+D597A^C$ despite the fact $Y111A^N+KatG^C$ exhibited the least low-spin component. Moreover, substitutions of both Tyr 111 and Asp 482 not only produced about 20% more low-spin heme species compared to substitution of Tyr 111 alone but also substantially diminished catalase activity by nearly 90% suggesting Tyr 111 and Asp 482 play a key role in catalase turnover in KatGs. More strikingly, substitutions of both Arg 479 and Tyr 111 with alanine resulted in a 99% loss of catalase k_{cat} . The double variant $Y111A^N+R479A^C$ can be further evaluated by inverse analysis which provides more simple and intuitive understandings (Figure 3.9) (123). In the inverse analysis, the double variant rather than the wild-type enzyme is used as the reference point. As such, in the case of $Y111A^N+R479A^C$, take the above double variant as reference, restoring only Arg 479 to the double variant (as in the $Y111A^N+KatG^C$ single variant) enhances k_{cat} by 31-fold when compared to the double variant which

directly measures the intrinsic, noncooperative contribution of Arg 479 to k_{cat} given Tyr 111 is absent. Restoring only Tyr 111 to the double variant (as in the single variant KatG^N+R479A^C) enhances k_{cat} by 35-fold which directly measures the noncooperative contribution of Tyr 111 to k_{cat} in the absence of Arg 479. Restoring both Arg 479 and Tyr 111 to the double variant (as in the unmodified domain proteins KatG^N+KatG^C) enhances k_{cat} by 95-fold, which is about 12-fold less than the product of the enhancing effects of the two single variants (1100-fold). Hence, a factor of 12 has disappeared with the double substitutions suggesting anticooperativity imparted by the two alanine residues. And such a synergistic effect as analyzed in Y111A^N+R479A^C variant resulted in a catalase activity loss that competes with effect of removing the entire C-terminal domain, suggestive of the indispensable roles of Arg 479 and Tyr 111 in catalase activity.

The KatG peroxidase activity generally receives less attention because the measured k_{cat} is about 100-fold below KatG catalase activity and 10-fold lower in catalytic efficiency with respect to H₂O₂ (125). Moreover, it is the catalase activity that is more adversely affected by substitutions. Conversely, the peroxidase activity is generally either uninfluenced or even enhanced (81). In this study we report that peroxidase activity was substantially diminished due to the substitution of non-active site residues. As clearly demonstrated, substitutions of C-terminal domain residues Asp 482 and Arg 479 in reactivated domain proteins all impaired peroxidase activity. In the case of Y111A^N+D482A^C, only 6% peroxidase activity was retained along with 15-fold decrease of apparent second-order rate constant with respect to H₂O₂ and the same apparent K_M . On the other hand, the ABTS-dependent peroxidase activity exhibited a similar k_{cat} .

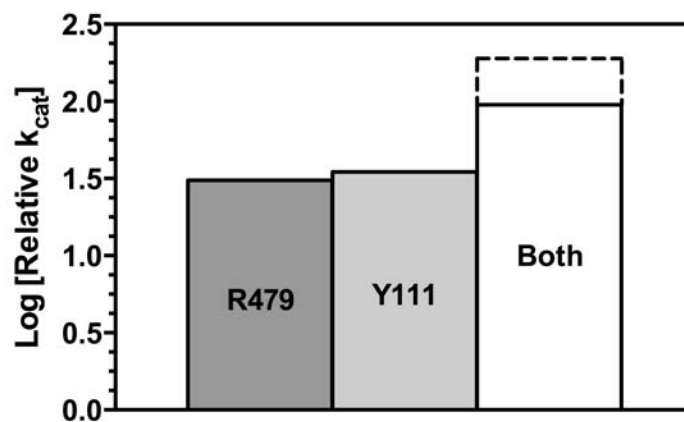


Figure 3.9. Interactions of the effects of two single variants $Y111A^N+KatG^C$ and $KatG^N+R479A^C$ on catalase activity (k_{cat}) in double variant $Y111A^N+R479A^C$. Each bar is labeled indicating the residue(s) being restored to the double variant. The dotted bar indicates the product of the effects of restoring the two residues individually, the expected result from simple additivity.

However, the apparent K_M with respect to ABTS was also notably decreased, resulting in a comparable apparent second-order rate constant to that of unmodified domain proteins.

Similar to reactivated domain variants of the distant-network, no significant correlation between catalase activity and low-spin contribution is found in near-network proteins. As shown in Figure 3.10, with all the data points below the line established by $KatG^N$ and $KatG^N+KatG^C$, four domain variants with comparable low-spin contributions exhibited catalase activity ranging from the highest to lowest observed in the near-network. The peroxidase k_{cat} , with respect to both H_2O_2 and ABTS, also shows no significant correlation with low-spin contribution (Figure 3.11). When the correlation between peroxidase and catalase k_{cat}/K_M with respect to the mutual substrate H_2O_2 is examined, it reveals that substitutions of near-network residues impair the peroxidase k_{cat}/K_M to a similar extent with catalase k_{cat}/K_M , if not more (Figure 3.12). In particular, single substitutions of Asp 482 and Arg 479 to the C-terminal domain protein share a similar effect on k_{cat}/K_M for both activities. As shown earlier, a higher low-spin contribution is generally observed in near-network variants, but like the distant-network proteins, the low-spin contribution again cannot account for the loss of catalase activity observed.

Given the much closer proximity of near-network residues to the arginine switch (Arg 414 in *E. coli* KatG numbering) in KatG, at an average of 5 Å distance from the R conformation of the mobile arginine, Tyr 111, Asp 482 and Arg 479 are likely to be responsible for maintaining the local pK_a . Any substitution of these residues would therefore potentially affect the distribution of the two conformations of Arg 414. The loss

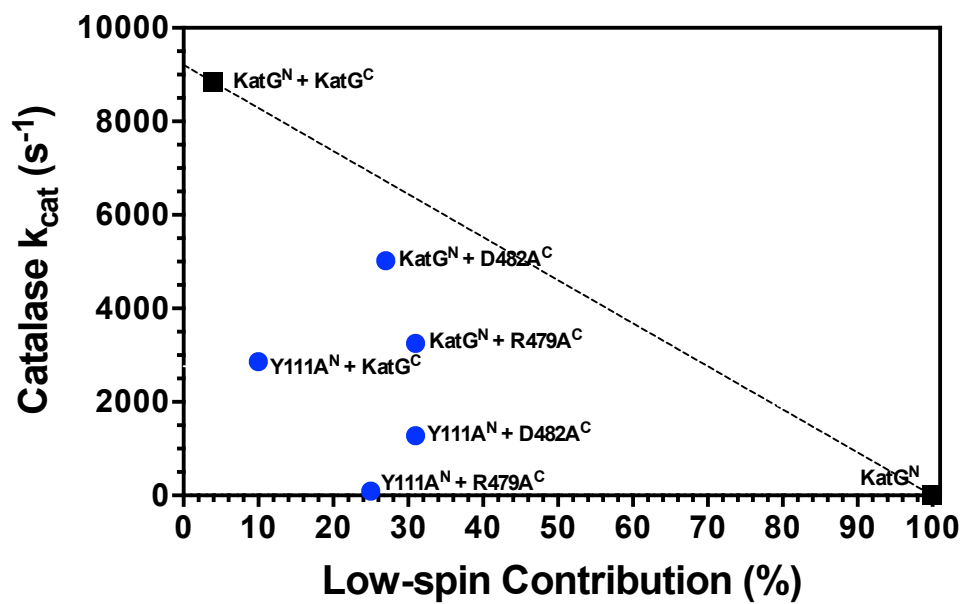
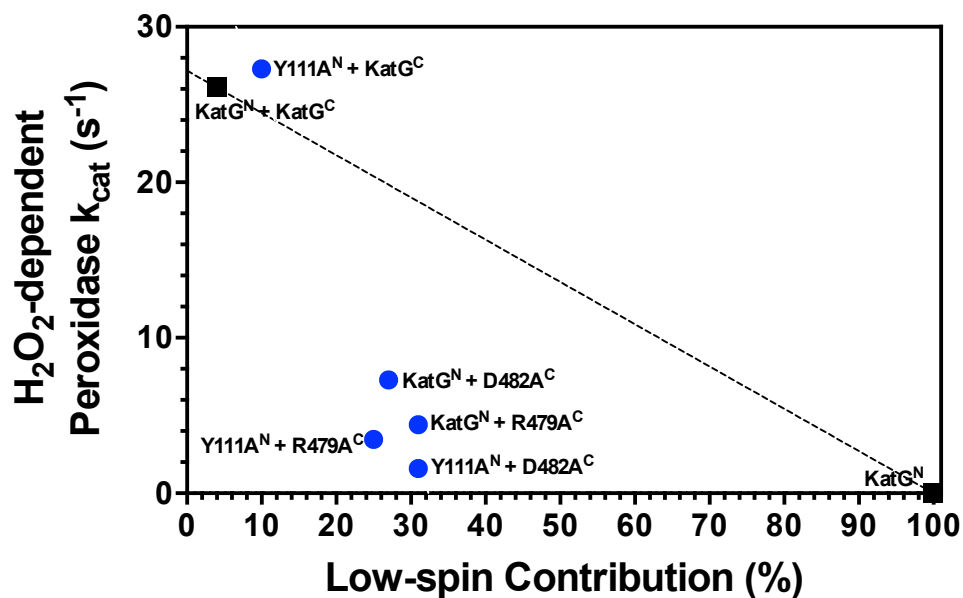


Figure 3.10. Correlation between catalase activity k_{cat} and low-spin contribution in reactivated near-network variants (●) with KatG^N and KatG^N+KatG^C as two endpoints (■).

A



B

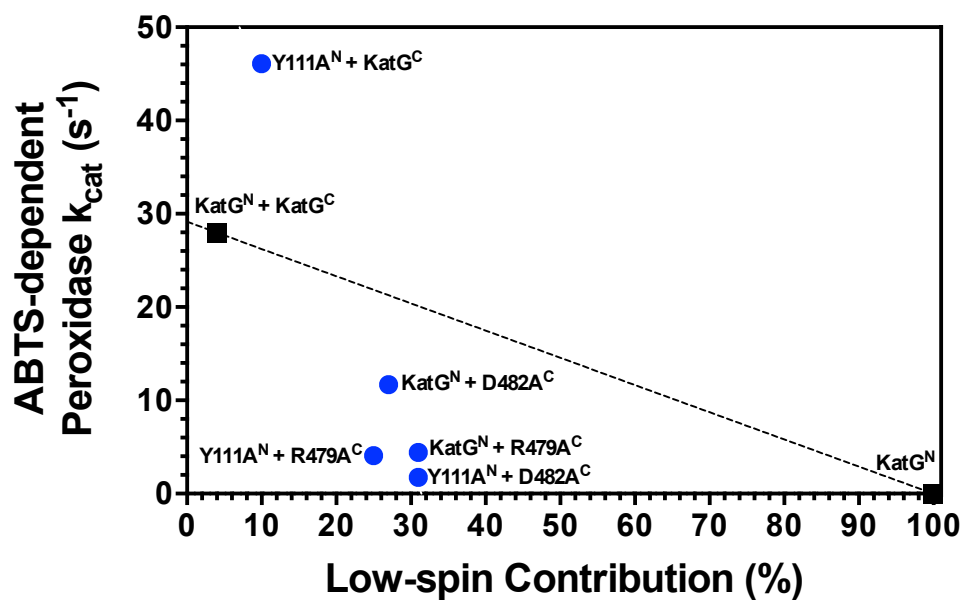


Figure 3.11. Correlation between peroxidase activity k_{cat} and low-spin contribution in reactivated near-network variants (●) with KatG^N and KatG^N+KatG^C as two endpoints (■): H₂O₂-dependent peroxidase activity (A) and ABTS-dependent peroxidase activity (B).

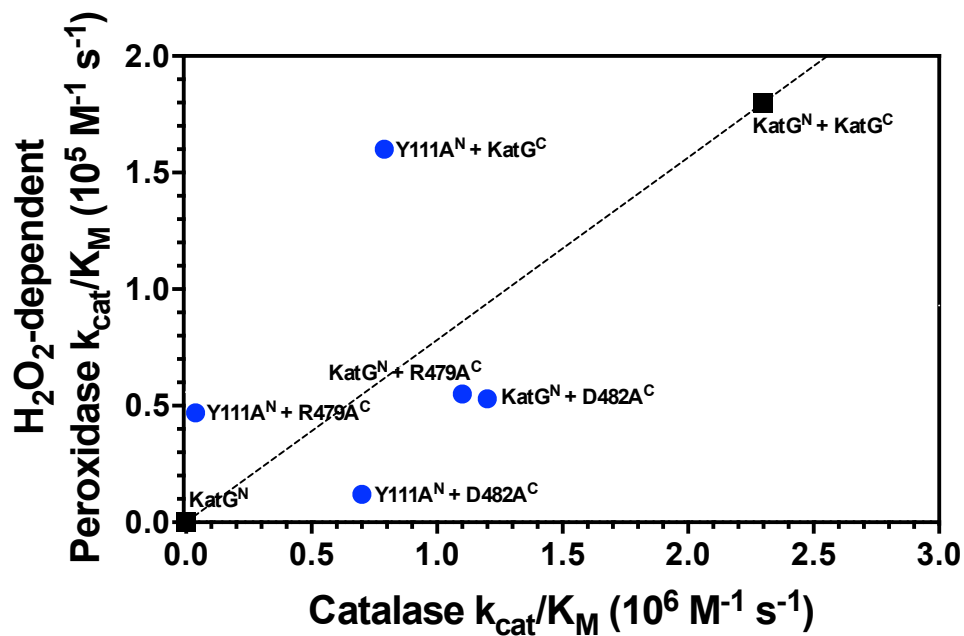


Figure 3.12. Correlation between H₂O₂-dependent peroxidase activity and catalase activity with respect to k_{cat}/K_M in reactivated near-network variants (●) with KatG^N and KatG^N+KatG^C as two endpoints (■).

of peroxidase activity in the near-network to an extent that rivals the impaired catalase activity is not well understood. At any rate, it is clear that while H_2O_2 -dependent peroxidase k_{cat}/K_M is substantially diminished, ABTS-dependent peroxidase k_{cat}/K_M is largely unaffected suggesting substrate binding of ABTS is not likely to be influenced.

In summary, by characterizing near-network residues involved in the conserved interdomain H-bond interactions, we suggest that the role of C-terminal in KatGs is multifaceted, it not only directs the configuration of active site necessary for both activities by virtue of preventing the formation of hexacoordinate low-spin species, but also facilitates catalase and peroxidase functions by low-spin-independent mechanisms which remain to be elucidated. In addition, the unusual loss of peroxidase activity points toward another imperative yet poorly defined aspect of KatGs, the peroxidatic electron donors in KatGs, and will be further discussed in the next chapter.

CHAPTER FOUR
EFFECT OF PEROXIDATIC ELECTRON DONORS ON THE
CATALASE ACTIVITY OF PATHOGEN-DERIVED PERIPLASMIC
CATALASE-PEROXIDASE

4.1 Introduction

The cellular location of *Escherichia coli* catalase-peroxidase (KatG) has been established to be in the cytoplasm. However, an additional copy of catalase-peroxidase has also been identified in the periplasm of the enterohemorrhagic serotype *E. coli* O157:H7, which is encoded by the large plasmid pO157 thus given the name KatP (88, 127). It has been demonstrated that during exponential growth, KatP scavenged more H₂O₂ than canonical catalase KatE, and KatP was also induced by H₂O₂ in biofilm cells (147, 155). As with *E. coli* O157:H7, a periplasmic catalase-peroxidase is also found in other pathogenic bacteria such as *Yersinia pestis* and *Legionella pneumophila* and proposed to be a virulence factor (88, 90-92). Therefore elucidating the potential role of periplasmic catalase-peroxidases would shed light on the mechanisms by which these enzymes contribute to bacterial virulence.

As demonstrated in previous chapters, the catalase activity of *E. coli* KatG dominates over its peroxidase activity. Indeed, a comparative study of KatGs from seven different organisms suggest that the catalase k_{cat} is generally two orders of magnitude higher than that of the peroxidase, and when it comes to k_{cat}/K_M with respect to H₂O₂, the efficiency of catalase activity is at least 10-fold higher (115). Adding to this, the physiological peroxidatic electron donor (PxED) of KatG has been speculated about ever

since the first discovery of *E. coli* KatG but has never been identified (59). It raises the question: What role does KatG peroxidase activity play in the H₂O₂-scavenging function of the enzyme? Both activities consume H₂O₂, and while a PxED is not required for *catalatic* turnover, most conceptions of the KatG catalytic mechanism imply that PxEDs should inhibit catalase activity. So, how do these two activities interrelate and what is the impact of this interplay *in vivo*?

Based on the currently proposed catalytic mechanisms of KatGs (Figure 2.1), the formation of the potent oxidant historically known as Compound I is shared by both catalatic and peroxidatic cycles as the first step, i.e., the half reaction of H₂O₂ reduction to H₂O is the same for both pathways. However, returning the intermediate Compound I to the resting enzyme can be pursued in two distinct routes. On the one hand, Compound I can be reduced catalatically by another equivalent of H₂O₂ with the hallmark evolution of oxygen. On the other hand, Compound I can be reduced peroxidatically by two equivalents of exogenous PxED while yielding the corresponding PxED radical as a consequence. The divergence of the two activities is obvious under this paradigm, to complete each cycle either another H₂O₂ or exogenous PxED has to be oxidized, presumably competing for Compound I. The antagonism was indeed observed in initial studies of *E. coli* KatG in which the catalase activity was inhibited by one of the commonly used PxED *o*-dianisidine at pH 7.5 (59).

It is also noteworthy that the two activities of KatGs function at different pH optima, it has been consistently observed that catalase activity is optimal near neutral pH (6.5-7.0), but peroxidase activity is optimal under much more acidic conditions (i.e., pH 4.5-5.0) (89, 128, 129). Moreover, the peroxidase activity requires much lower

concentrations of H₂O₂ to reach maximum output while a robust catalase activity increases according to a much higher apparent K_M. The copious H₂O₂ and acidic pH conditions are reminiscent of oxidative burst which occurs inside a phagocyte during host-pathogen interactions. Considering the dominance of catalase over peroxidase activity in KatGs and also the acidic conditions under which pathogenic bacteria face the oxidative burst in host immune responses, such pH preferences for bacterial defenses against H₂O₂ would presumably be detrimental for those highly virulent pathogens such as *E. coli* O157:H7.

Therefore, in this work we investigated on the pH-dependent catalase and peroxidase activity from the periplasmic catalase-peroxidase (KatP) from *E. coli* O157:H7 and demonstrated that peroxidatic electron donors (PxEDs) greatly enhanced the catalase activity especially under acidic conditions that are normally not optimal for catalatic turnover thereby broadening the pH range of catalase function to facilitate disarming of the deleterious H₂O₂.

4.2 Materials and Methods

4.2.1 Reagents

Hydrogen peroxide (30%), δ -aminolevulinic acid, ferrous ammonium sulfate, imidazole, sodium dithionite, ampicillin, chloramphenicol, NADPH, phenylmethylsulfonyl fluoride (PMSF), 2,2'-azino-bis(3-ethylbenzthiazoline-6-sulfonic acid) (ABTS), 3,3',5,5'-tetramethylbenzidine dihydrochloride hydrate (TMB), *N,N,N',N'*-tetramethyl-*p*-phenylenediamine dihydrochloride (TMPD) and citrate acid monohydrate were purchased from Sigma (St. Louis, MO). LB broth, Miller (Luria-Bertani) was obtained from BD Biosciences (San Jose, CA). Isopropyl- β -D-thiogalactopyranoside (IPTG) was

obtained from GoldBio Technology (St. Louis, MO). Tris, mono- and di-basic potassium phosphate, mono- and di-basic sodium phosphate, sodium chloride, acetic acid, sodium acetate and urea were obtained from Fisher (Pittsburgh, PA). All oligonucleotide primers were purchased from Invitrogen (Carlsbad, CA). All *E. coli* strains [XL1-Blue and BL21-Gold(DE3)pLysS], *PfuTurbo* DNA polymerase, and T4 DNA ligase were obtained from Agilent Technologies (La Jolla, CA). All restriction enzymes were purchased from New England Biolabs (Beverly, MA). BugBuster protein extraction reagent and Benzonase Nuclease were purchased from Novagen (Madison, WI). Nickel-nitrilotriacetic acid (Ni-NTA) resin was purchased from Qiagen (Valencia, CA). Buffer exchange chromatography columns (10DG) were obtained from Bio-Rad (Hercules, CA). Amicon Ultra centrifugal filters were obtained from EMD Millipore (Billerica, MA). All buffers and media were prepared using water purified through Barnstead EASYpure II system (18.2 M Ω /cm resistivity).

4.2.2 Cloning and expression of KatP

Generation of a construct for the expression of KatP from *E. coli* O157:H7 was achieved as previously described (89). The expression of KatP was carried out in LB broth supplemented with ampicillin (100 μ g/mL) and chloramphenicol (34 μ g/mL). Cells were grown at 37 °C to mid-log phase with optical density at 600 nm (OD₆₀₀) of 0.4 to 0.5 and expression of KatP was induced by addition of IPTG (1 mM). At the time of induction, δ -aminolevulinic acid (0.5 mM) and ferrous ammonium sulfate (0.5 mM) were also supplemented in the cultures. Cells continued to grow for four hours and then were harvested by centrifugation. The cell pellets were stored at -80 °C until purification.

4.2.3 Purification of KatP

The cell pellets were resuspended in BugBuster reagent supplemented with PMSF and then homogenized with a Dounce homogenizer followed by addition of Benzonase Nuclease and incubation of the mixture at 23 °C for two hours with gentle stirring. The cell lysate was then centrifuged and the supernatant was loaded onto a Ni-NTA column by circulating the solution through the column bed at 1 mL/min for overnight. The column was washed with 50 mM Tris, pH 8.0, followed by Buffer A (50 mM phosphate, 200 mM NaCl, pH 7.0). Subsequent washes were carried out using Buffer A supplemented with 2 mM, 20 mM, and 50 mM imidazole. The protein was finally eluted off the column with Buffer A supplemented with 200 mM imidazole and concentrated by ultrafiltration, the excess imidazole still present in the concentrated protein was then removed using buffer exchange chromatography columns (10DG) with Buffer B (50 mM phosphate, 50 mM NaCl, pH 7.0).

4.2.4 UV-visible absorption spectra and activity assays

All spectra were recorded at 23 °C on a Shimadzu UV-1601 spectrophotometer (Columbia, MD) with a cell path length of 1.0 cm. Catalase and peroxidase activity assays were performed as previously described (89). For peroxidase activity assay, similarly with ABTS, oxidation of TMB as the PxED to its radical ($\text{TMB}^{\cdot+}$) was monitored spectrophotometrically ($\epsilon_{652} = 39 \text{ mM}^{-1} \text{ cm}^{-1}$) (130). Initial rates were fit to Michaelis-Menten equation by nonlinear regression analysis to determine apparent kinetic parameters.

4.2.5 Catalase activity assay by O₂ production

To avoid the interference from intense absorption of PxEDs on a spectrophotometer, catalase activity was also monitored polarigraphically for O₂ production using a

Hansatech Clark-type oxygen electrode (Norfolk, UK). Calibration was achieved using N₂ saturated solution to establish a zero O₂ level within the reaction chamber prior to experimental measurements. All reactions were carried out at 23 °C with 5 nM enzymes in either 50 mM citrate or 50 mM acetate or 100 mM phosphate buffer at the corresponding pH. Data collection was initiated with the buffer, enzyme, and PxED (when present) in the reaction chamber for 15 seconds to establish a baseline, followed by injection of H₂O₂ to monitor O₂ production. In cases where two different responses of catalase activity to H₂O₂ concentrations were observed, the fitting equation was modified to include a linear phase component in addition to the hyperbolic phase as previously described (86):

$$\frac{v_0}{[E]_T} = \frac{k_{\text{cat}}[S]}{K_M + [S]} + k_{\text{app}}[S] \quad (4.1)$$

where k_{cat} and K_M are the apparent kinetic parameters that best fit the hyperbolic component at low H₂O₂ concentrations, and k_{app} is the slope of the linear component at high H₂O₂ concentrations.

4.2.6 Comparison of PxED radical production and H₂O₂ consumption

Reactions containing 20 nM enzymes, 0.1 mM ABTS, and varying concentrations of H₂O₂ were allowed to proceed to completion and could be verified by the observation that adding more enzymes or ABTS did not produce more ABTS radicals but adding more H₂O₂ did. The absorbance of ABTS radicals produced in each reaction was then recorded at 417 nm ($\epsilon_{417} = 34.7 \text{ mM}^{-1} \text{ cm}^{-1}$), the concentration was calculated and compared against the concentration of H₂O₂ consumed for each reaction (131).

4.2.7 Circular dichroism

All circular dichroism (CD) spectra were recorded on a Jasco J-810 spectropolarimeter (Tokyo, Japan) at 23 °C. Baseline and analysis were carried out using Jasco J-720 software. Circular dichroism spectra (250-190 nm) were obtained in a 0.5 mm quartz cell using 5 μM enzyme in either 5 mM phosphate (pH 7.0) or 5 mM citrate buffer for each corresponding pH.

4.3 Results

4.3.1 Peroxidatic electron donor enhances the catalytic turnover of KatP at neutral pH.

Catalase activity can be determined by monitoring either the consumption of H₂O₂ spectrophotometrically (240 nm) or the production of O₂ polarigraphically. Because of the intense UV absorption of most PxEDs, the latter is especially useful for assessing catalase activity when PxEDs are present. The apparent K_M of *E. coli* KatG for H₂O₂ is about 4 mM at pH 7.0 (129). Consistent with previous observation from our laboratory, KatP showed a much higher apparent K_M for H₂O₂, ~20 mM (Figure 4.1 and Table 4.1). When one of the most commonly used PxEDs, ABTS, was included in the assay at pH 7.0, the catalase activity was stimulated (Figure 4.1 and Table 4.1). This is in contrast to the inhibition effect observed for *o*-dianisidine (59). A two-component kinetic behavior was observed in ABTS-assisted catalase activity with respect to H₂O₂ concentrations. At lower H₂O₂ concentrations, i.e., below 1.0 mM, a hyperbolic component represented a much more sensitive response to H₂O₂ concentrations, indicating an apparent K_M decreased by more than 30-fold compared to the unassisted catalase activity. The linear component which appeared to operate at high H₂O₂ concentrations, albeit relatively slow

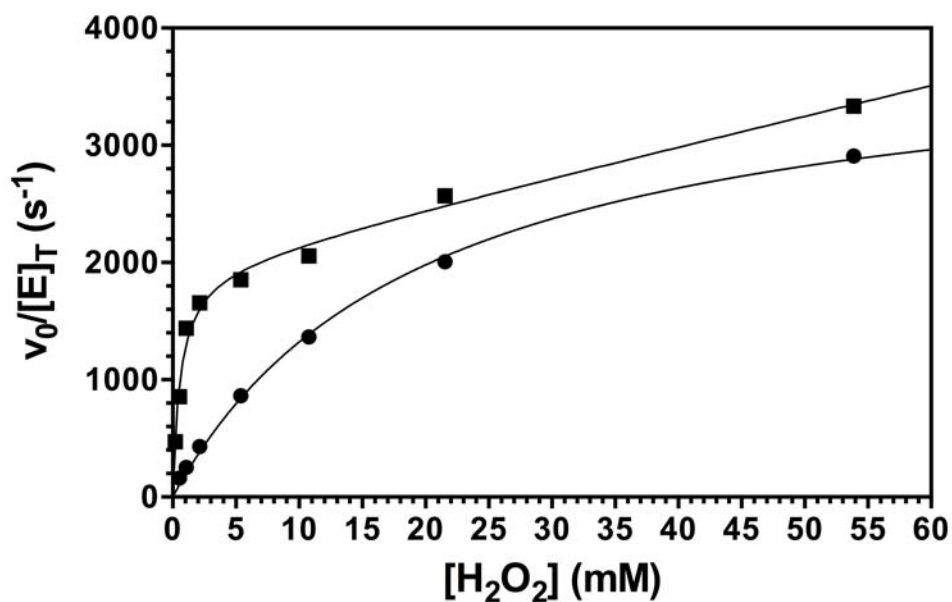


Figure 4.1. Effect of H₂O₂ concentration on the rate of O₂ production by KatP at pH 7.0 in the absence of PxEDs (●) and in the presence of 0.1 mM ABTS (■).

Table 4.1. Effect of ABTS on apparent catalase^a kinetic parameters of KatP at pH 7.0.

| PxEDs | Catalase Kinetic Parameters | | | |
|-------|-------------------------------------|--|---|---|
| | Component 1 | | | Component 2 |
| | k _{cat} (s ⁻¹) | K _M (mM H ₂ O ₂) | k _{cat} /K _M (10 ⁵ M ⁻¹ s ⁻¹) | k _{app} (10 ⁵ M ⁻¹ s ⁻¹) |
| None | 3940±70 | 19.8±0.8 | 2.0 | - |
| ABTS | 1980±70 | 0.60±0.07 | 33 | 0.26 |

^a Assays included 5 nM KatP, 0.1 mM PxEDs when present, in 100 mM phosphate buffer, pH 7.0, 23 °C.

in terms of apparent second-order rate constant, still resulted in a greater catalase activity in the presence of ABTS at all H₂O₂ concentrations evaluated. The observation that ABTS stimulated KatP catalase activity at pH 7.0 is striking given that this is the only example of catalase stimulation by peroxidatic electron donors at neutral pH to date.

4.3.2 PxED stimulation of KatP catalase activity at acidic pH.

The PxED effect on the catalytic turnover was even more striking at pH 5.0, where unassisted catalase activity is much less efficient. In the presence of 0.1 mM ABTS, the apparent k_{cat} for catalase activity increased 10-fold. A decrease in apparent K_M was also observed such that the apparent second-order rate constant (i.e., k_{cat}/K_M) was increased by about 20-fold compared to the unassisted catalase activity at pH 5.0 (Figure 4.2 and Table 4.2). Indeed, in terms of catalytic efficiency, the ABTS-stimulated catalase activity observed at pH 5.0 even outpaced the catalase activity at pH 7.0 by a factor of 14.

The effect of other PxEDs such TMB and TMPD on catalase activity of KatP at pH 5.0 were also evaluated (Figure 4.3 and Table 4.3). TMB was able to facilitate more efficient catalytic turnover, increasing k_{cat}/K_M about 20-fold. Though two-component kinetic response to H₂O₂ concentrations was once again observed in TMPD-assisted catalase activity, an enhancement of k_{cat}/K_M of about 13-fold was recorded.

4.3.3 Effect of pH on PxED-assisted catalase activity of KatP.

To further evaluate the effect of pH on PxED dependent stimulation, we monitored catalase activity from pH 8.0 to pH 3.0 in the absence and presence of PxEDs, ABTS, TMB and TMPD (Figure 4.4A). All three PxEDs were able to enhance catalase activity below pH 6.0 and the stimulatory effect by TMB persisted even at pH 3.0. On the other hand, the unassisted catalase activity of KatP functioned poorly below pH 6.0. Indeed,

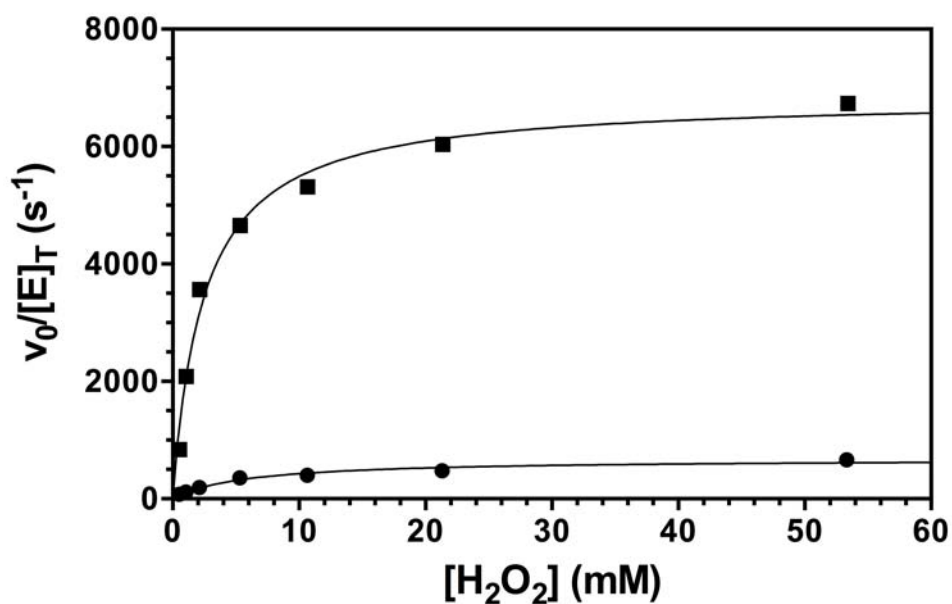


Figure 4.2. Effect of H₂O₂ concentration on the rate of O₂ production by KatP at pH 5.0 in the absence of PxEDs (●) and in the presence of 0.1 mM ABTS (■).

Table 4.2. Effect of ABTS on apparent catalase^a kinetic parameters of KatP at pH 5.0.

| PxEDs | Catalase Kinetic Parameters | | |
|-------|-------------------------------------|--|---|
| | k _{cat} (s ⁻¹) | K _M (mM H ₂ O ₂) | k _{cat} /K _M (10 ⁵ M ⁻¹ s ⁻¹) |
| None | 680±30 | 5.9±0.7 | 1.2 |
| ABTS | 6840±130 | 2.5±0.2 | 28 |

^a Assays included 5 nM KatP, 0.1 mM PxEDs when present, in 50 mM acetate buffer, pH 5.0, 23 °C.

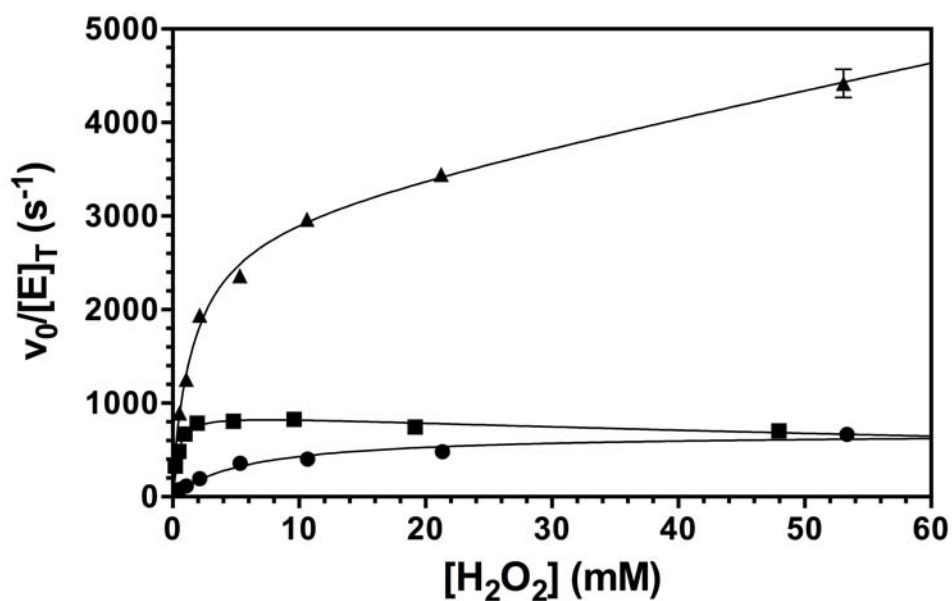


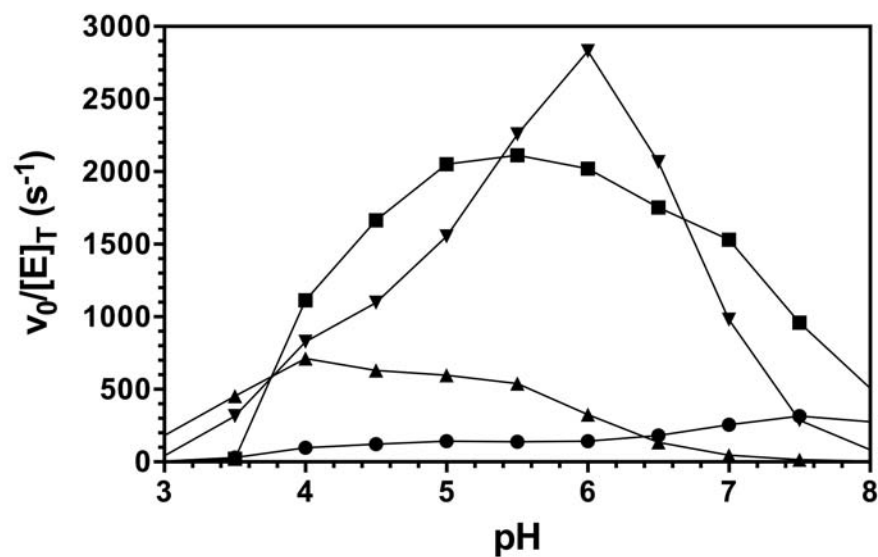
Figure 4.3. Effect of H_2O_2 concentration on the rate of O_2 production by KatP at pH 5.0 in the absence of PxEDs (●) and in the presence of 0.1 mM TMB (■) and 0.1 mM TMPD (▲).

Table 4.3. Effect of TMB and TMPD on apparent catalase^a kinetic parameters of KatP at pH 5.0.

| PxEDs | Catalase Kinetic Parameters | | | |
|-------|--------------------------------------|---|--|---|
| | Component 1 | | | Component 2 |
| | k_{cat} (s^{-1}) | K_{M} (mM H_2O_2) | $k_{\text{cat}}/K_{\text{M}}$ ($10^5 \text{ M}^{-1} \text{ s}^{-1}$) | k_{app} ($10^5 \text{ M}^{-1} \text{ s}^{-1}$) |
| None | 680±30 | 5.9±0.7 | 1.2 | - |
| TMB | 900±20 | 0.35±0.03 | 26 | - |
| TMPD | 2820±160 | 1.7±0.5 | 16 | 0.28 |

^a Assays included 5 nM KatP, 0.1 mM PxEDs when present, in 50 mM acetate buffer, pH 5.0, 23 °C.

A



B

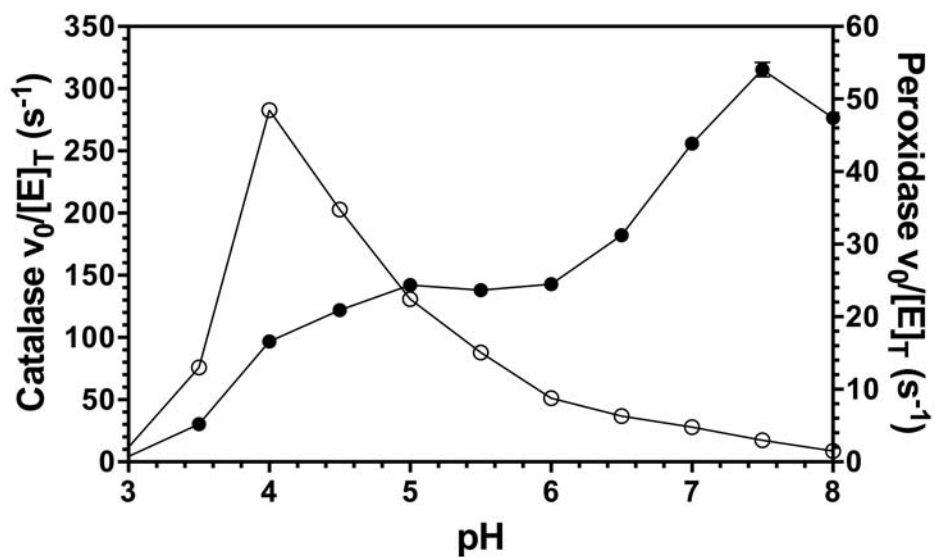


Figure 4.4. pH profile of PxED-stimulated catalase activity (A) and unassisted catalase and peroxidase activity (B) of KatP. Catalase activity was evaluated with 1.0 mM H₂O₂ by O₂ production in the absence of PxEDs (●) and in the presence of 0.1 mM ABTS (■), 0.1 mM TMB (▲) and 0.1 mM TMPD (▼). Peroxidase activity was evaluated with 1.0 mM H₂O₂ and 0.1 mM ABTS (○).

acidic conditions are optimal for the peroxidase over catalase for this bifunctional enzyme (Figure 4.4B). Our results suggested that PxEDs not only overcame the disadvantage for catalase function at acidic conditions by broadening the pH range, but also enhanced the catalytic turnover to the extent that it rivaled and even considerably surpassed unassisted catalytic performance at its ideal conditions (i.e., pH 7.0). On the other hand, the PxEDs were not equivalent in their ability to stimulate catalase activity, for example, TMB appeared to stimulate catalase activity to a lesser extent and also exhibited an inhibitory effect above pH 6.0.

For intracellular *E. coli* KatG, it is known that catalytic activity decreases below pH 3.7 due to unfolding of the protein (129). To determine if the decrease in KatP activity at low pH was due to the same, we used far UV-CD to monitor the secondary structure content of the enzyme across a pH range from 4.5 to 3.0 (Figure 4.5). CD spectra remained unchanged to pH 3.2. There was a slight decrease in intensity at 190 nm observed at pH 3.0. The data suggest that KatP, a catalase-peroxidase produced by an acid tolerant organism (*E. coli* O157:H7) has substantially greater stability with respect to low pH than the cytosolic enzyme common to all *E. coli* (156).

4.3.4 NADPH marginally assisted catalase activity of KatP at pH 5.0.

The physiological PxED for the catalase-peroxidase enzyme remains to be established. Given the PxED-dependent stimulatory effect on catalase activity, we evaluated the ability of NADPH to stimulate KatP catalase activity. In spite of its low reduction potential, the stimulatory effect was considerably less than other artificial PxEDs (Figure 4.6 and Table 4.4) It is also noteworthy that NADPH did not appear to be an effective

substrate for peroxidase activity of KatP with an apparent k_{cat} of 1 s^{-1} which is much lower than other commonly used PxEDs (Table 4.5).

4.3.5 Production of ABTS radical is minimal and even negligible compared to the production of O_2 even at peroxidase optimal condition.

We quantified the $\text{ABTS}^{\cdot+}$ generated during assisted catalytic turnover of KatP as a function of H_2O_2 concentration (Figure 4.7). As mentioned, the depletion of H_2O_2 for each reaction was verified by the fact H_2O_2 is the only factor that governs additional $\text{ABTS}^{\cdot+}$ production. At most, $40 \mu\text{M}$ $\text{ABTS}^{\cdot+}$ was generated, but nearly 11 mM H_2O_2 was consumed over the course of the same reaction. Thus, only 0.004 equivalents of $\text{ABTS}^{\cdot+}$ was generated for every equivalent of H_2O_2 consumed, far off the canonical PxED radical/ H_2O_2 stoichiometry of 2:1. Interestingly, the ratio increased substantially, particularly at the lower concentrations of H_2O_2 . This has been a pattern observed with PxED catalase stimulation in *Mycobacterium tuberculosis* KatG, especially for variants targeting the arginine switch (86, 133).

4.4 Discussion

The PxED-assisted catalase activity of KatP from *E. coli* O157:H7 is striking and might provide insight into the mechanisms by which KatP contributes to the virulence of this successful bacterial pathogen, and by extension, possibly even other highly virulent pathogens bearing the periplasmic catalase-peroxidase such as *Yersinia pestis* (KatY) and *Legionella pneumophila* (KatA). Indeed, it has been revealed that KatP share a higher sequence similarity with KatA and KatY than it does with cytoplasmic catalase-peroxidase (87, 132). At first glance, a much higher apparent K_M of 20 mM of H_2O_2 observed for KatP at pH 7.0 seems a disadvantage for *E. coli* O157:H7 to cope with H_2O_2

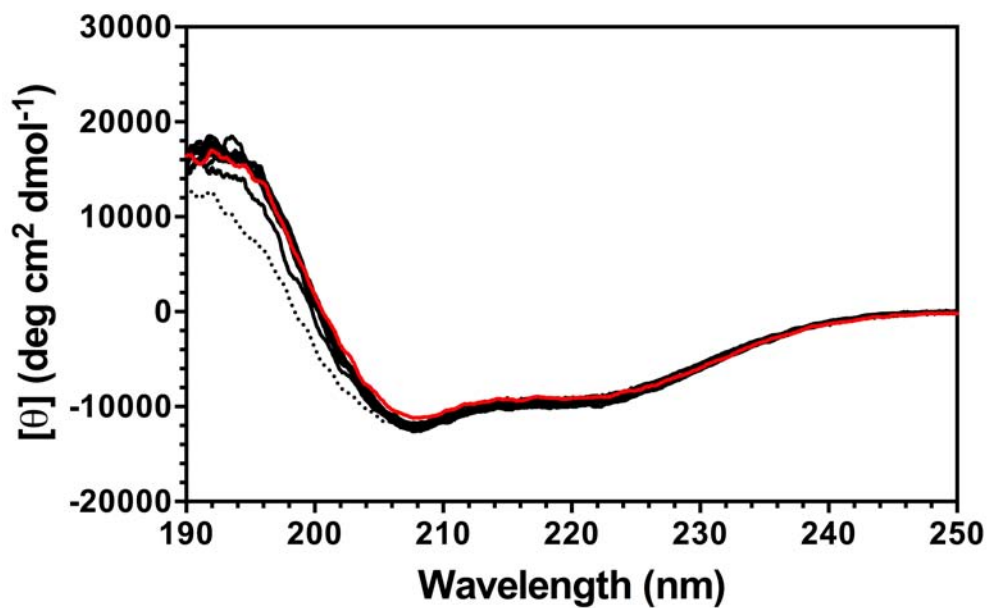


Figure 4.5. Far-UV circular dichroism spectra of KatP at low pH (4.5-3.0). Along with pH 7.0, the spectra at pH 4.5, 4.4, 4.0, 3.8, 3.6, 3.5, 3.4, 3.2 are shown in solid line, the spectrum at pH 3.0 is shown in dotted line. Spectra were recorded at 23 °C in 5 mM citrate buffer at different low pH, or in 5 mM phosphate buffer, pH 7.0.

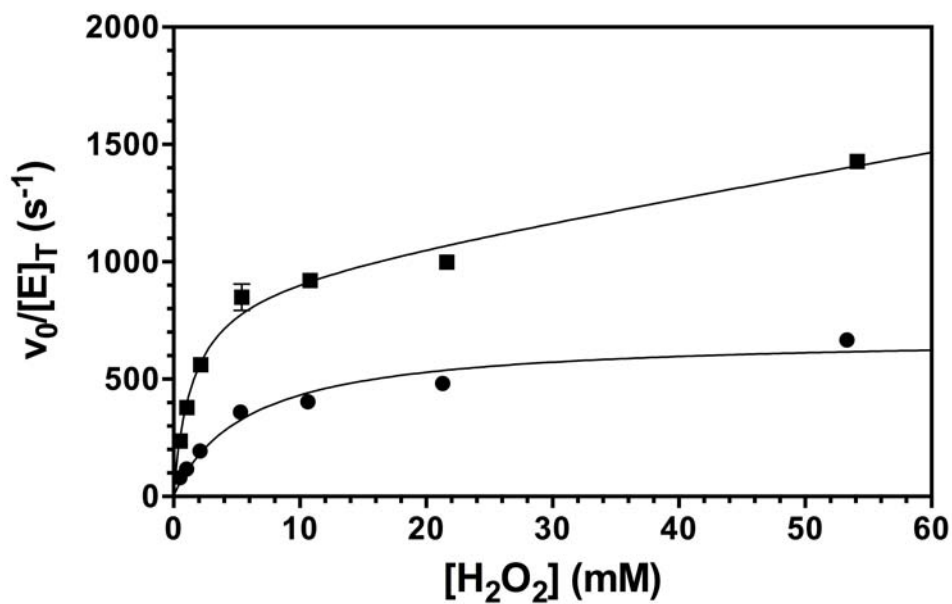


Figure 4.6. Effect of H_2O_2 concentration on the rate of O_2 production by KatP at pH 5.0 in the absence of PxEDs (●) and in the presence of 0.1 mM NADPH (■).

Table 4.4. Effect of NADPH on apparent catalase^a kinetic parameters of KatP at pH 5.0.

| PxEDs | Catalase Kinetic Parameters | | | |
|-------|--------------------------------------|------------------------------------|---|---|
| | Component 1 | | | Component 2 |
| | k_{cat} (s^{-1}) | K_M (mM H_2O_2) | k_{cat}/K_M ($10^5 \text{ M}^{-1} \text{ s}^{-1}$) | k_{app} ($10^5 \text{ M}^{-1} \text{ s}^{-1}$) |
| None | 680 ± 30 | 5.9 ± 0.7 | 1.2 | - |
| NADPH | 920 ± 50 | 1.5 ± 0.4 | 6.2 | 0.094 |

^a Assays included 5 nM KatP, 0.1 mM PxEDs when present, in 50 mM acetate buffer, pH 5.0, 23 °C.

Table 4.5. Comparison of peroxidase^a kinetic parameters of KatP with different PxEDs at pH 5.0.

| PxEDs | H ₂ O ₂ -dependent Peroxidase Kinetic Parameters | | |
|-------|--|---|---|
| | k_{cat} (s ⁻¹) | K_M (mM H ₂ O ₂) | k_{cat}/K_M (10 ⁵ M ⁻¹ s ⁻¹) |
| ABTS | 89.9±2.8 | 1.6±0.2 | 0.55 |
| TMB | 23.4±0.3 | 0.0071±0.0004 | 33.1 |
| NADPH | 1.00±0.02 | 0.070±0.005 | 0.14 |

^a Assays included 20 nM KatP and 0.1 mM PxEDs, in 50 mM acetate buffer, pH 5.0, 23 °C.

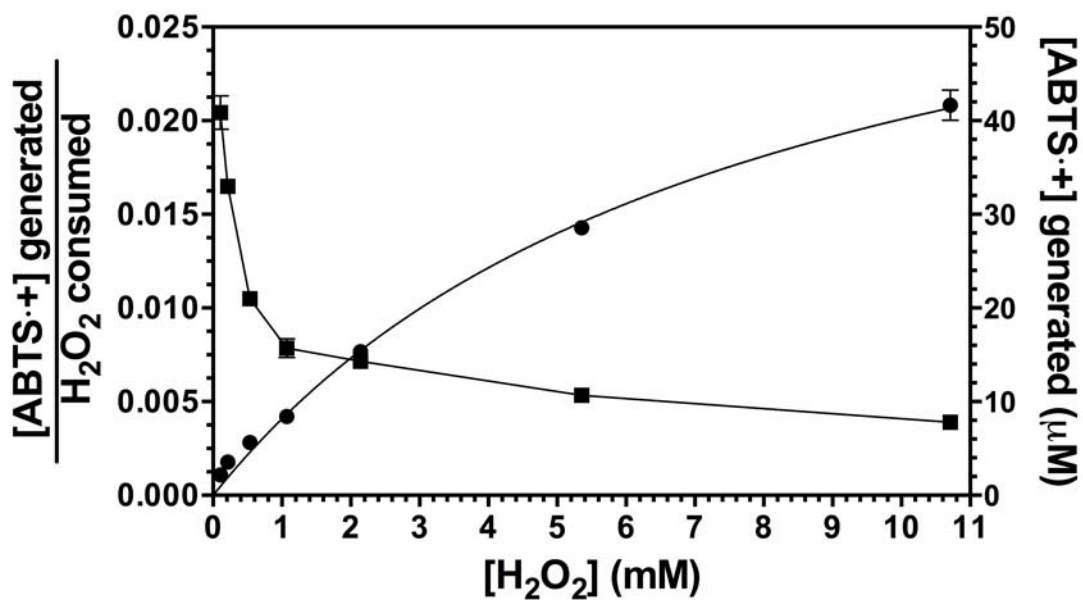


Figure 4.7. Production of ABTS^{•+} in comparison to H₂O₂ consumption by KatP. The extent of ABTS^{•+} produced (●) and the ratio of ABTS^{•+} generated to H₂O₂ consumed (■) are shown as a function of initial H₂O₂ concentrations. All assays were carried out with 20 nM KatP and 0.1 mM ABTS in 50 mM acetate buffer, pH 5.0, at 23 °C.

assaults in the periplasm. However, the doubt was casted away when we observed an over 30-fold drop of K_M in the hyperbolic component of ABTS-assisted catalase activity. Such a sensitive response to H_2O_2 , by virtue of ABTS not in spite of it, was intriguing given the anticipated inhibition effect.

Nonetheless, the stimulatory effect by PxEDs was most prominent under acidic conditions, 0.1 mM ABTS was able to increase the apparent k_{cat} by 10-fold and other commonly used PxEDs, such TMB and TMPD both showed to stimulate catalase activity to different extent manifested by lowered K_M and enhance k_{cat} . And when the pH profile was examined for the assisted catalase activity, it was clearly demonstrated that PxEDs substantially and specifically stimulated the catalase activity under acidic pH where the unassisted catalase activity is far from optimal. Adding to this striking stimulatory effect of PxEDs on catalatic turnover, when the production of $ABTS^+$ and the consumption of H_2O_2 was compared, it was found that less than 2 equivalents of $ABTS^+$ was generated for every 100 equivalents of H_2O_2 consumed which means theoretically over 99% of H_2O_2 was decomposed catalatically by releasing O_2 with minimal accumulation of $ABTS^+$.

On the other hand, at our attempt for seeking such an ever-elusive PxED, we discovered NADPH provided marginal stimulatory effect on the catalase activity even with a fairly low reduction potential and it also appeared to be a poor PxED for peroxidase activity, suggesting other than the necessary reduction potential, substrate binding for peroxidase activity is also required to bring about the stimulatory effect.

The pH-dependent stimulation of catalase activity by PxEDs is reminiscent of the arginine switch in KatG. The unassisted catalase activity of catalase-peroxidase has been

shown to be modulated by a mobile arginine 20 Å from the active site whose conformation is pH-dependent. The Y conformation in which the guanidinium side chain of the arginine points toward the active site and associates with the tyrosinate from the unique covalent adduct Met-Tyr-Trp is dominant at high pH, while at low pH the R conformation is predominantly adopted where the arginine side chain dissociates with the tyrosinate and turns away from active site (Figure 4.8). And the correlation between the conformation of the mobile arginine and the pH was well established from all the available crystal structures from different organisms resolved at different pH. For example, at pH 8.0, KatG from *Burkholderia pseudomallei* exhibited 100% Y conformation, decreasing the pH to 7.5 shifted the Y conformation to 70% while at pH 5.6, there were 30% Y and 70% R conformations populated (80). Given that Y conformation favors the Compound I reduction while R conformation favors Compound I formation, the optimum for catalase activity would correlate to the pH where Y and R conformations are equally populated. On the other hand, the arginine switch appears to be part of the proposed potential binding site for PxEDs (83).

Therefore, given the pH-dependent stimulatory effect observed for catalase activity of KatP, it is possible that the PxEDs facilitate the balance of the two conformations of the arginine switch thereby enhancing the catalytic turnover. And this hypothesis was supported by several of our observations. First, ABTS was even able to assist catalase activity at pH 7.0 suggesting at that pH the conformation states of the arginine switch is likely to be imbalanced. Second, the poor peroxidatic electron donor (PxED) for peroxidase activity but excellent electron donor in general, NADPH afforded very limited stimulation of catalase activity, suggesting substrate binding of PxED for peroxidatic

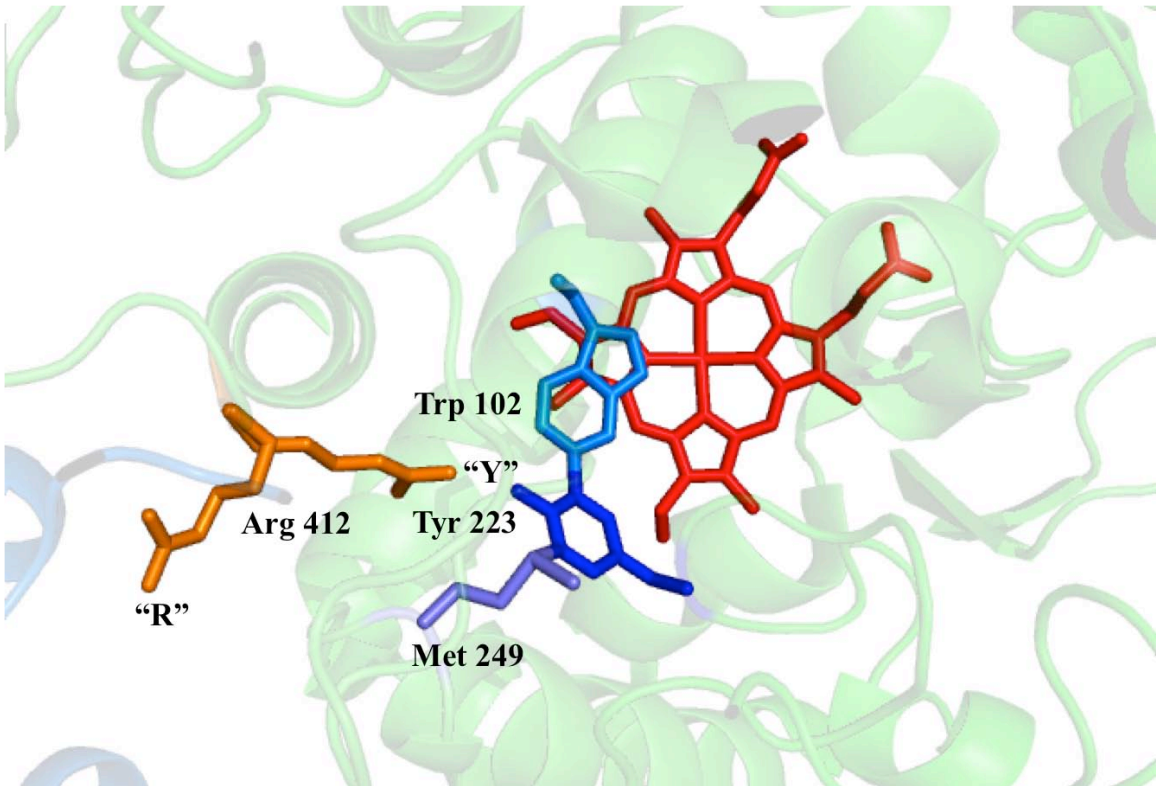


Figure 4.8. The arginine switch and covalent adduct in KatP. Coordinates from the structure of *Burkholderia pseudomallei* KatG were used (PDB accession number 1MWV). Numbering reflects *Escherichia coli* O157:H7 KatP sequence.

function might be a prerequisite for the stimulatory effect. Indeed, another generally good electron donor, ascorbate also exhibited little if any stimulatory effect on KatG from *M. tuberculosis* as we previously reported (86). Third, different PxEDs stimulated catalase activity to different extent suggesting the interaction between the bound PxED and the arginine switch and other vicinal residues possibly impart different extent of balance between the two conformations. Moreover, it is even possible for PxEDs to bind deeper into the cavity of the arginine switch to interact with the covalent adduct directly. In this respect, the PxED can serve as an alternative for the arginine switch. Indeed, it was shown that substitution of the mobile arginine to alanine still retained the stimulatory effect with some PxEDs but to a lesser extent (133). Based on this hypothesis, the observed inhibition effect for *o*-dianisidine can be explained by its presumably adverse interaction with the arginine switch which brings further imbalance of the two conformation states.

The second hypothesis we made is that, PxEDs prevent off-pathway electron transfer which is otherwise more prone to occur under acidic conditions. Given the high contents of Trp, Tyr and Met of N-terminal domain bearing the active site in KatP enzyme, the intramolecular electron transfer prevalently occurs. Indeed, several protein-based radicals such as Trp^{•+} and Tyr^{•+} has been identified in KatGs from different organisms and it has been suggested that the radical transfer from heme intermediate to the solvent-exposed protein surface is quite facile (125). Based on this propensity of protein-based radical formation, it is likely that the radical centered on the MYW covalent adduct would migrate to other oxidizable residue (Figure 4.9), once that happens unlike Compound III*, the return to the resting enzyme and releasing O₂ would become

difficult and slow. However, in the presence of PxEDs, the off-pathway electron transfer leading to such catalase-inactive intermediates can be prevented in the first place thereby promoting an efficient catalytic pathway. Our proposed mechanisms of catalase activity accounting for the observed stimulatory effect is shown in Figure 4.9 and identification and characterization of residues responsible for the off-pathway electron transfer is underway in Goodwin Laboratory.

The emerging face of PxED-assisted catalase activity not only invites us to re-evaluate the mechanisms of catalase-peroxidase but also provides an important link between catalase-peroxidase and bacterial virulence. It has been shown that *Legionella pneumophila* became less virulent without KatA and KatA is required for bacterial replication in macrophages (91, 134). Our observed stimulation of catalase activity by PxEDs under acidic conditions is well mirrored in the process of phagocytosis during host immune responses and our data present here implicate that the PxED, either intracellularly from the pathogen itself or extracellularly from the host cell, would afford catalase-peroxidase robust defenses against H₂O₂ assaults from the host and therefore contribute to the evasion and virulence of the bacterial pathogens.

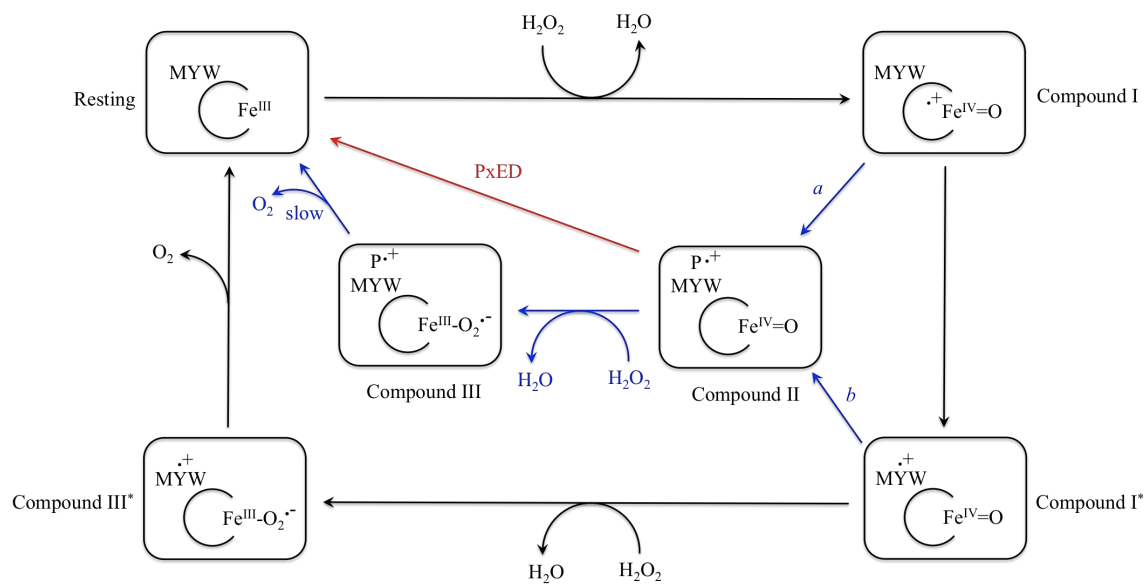


Figure 4.9. Proposed mechanism accounting for the stimulation of KatP catalase activity by PxEDs. The unassisted catalytic cycle is shown in black arrows. The off-pathway is shown in blue arrows. Reduction of Compound I (*a*) and Compound I* (*b*) produce catalase-inactive Compound II-like intermediate. Reaction of Compound II with H₂O₂ produces catalase-inactive Compound III-like intermediate. PxED is proposed to prevent subsequent reactions of Compound II by converting it to the resting state. MYW stands for the Met-Tyr-Trp covalent adduct, an unspecified oxidizable residue is designated as P.

CHAPTER FIVE
PEROXIDATIC ELECTRON DONORS ENHANCE BACTERIAL DEFENSES
AGAINST H₂O₂ DURING OXIDATIVE STRESS IN *ESCHERICHIA COLI*

5.1 Introduction

Hydrogen peroxide (H₂O₂) threatens the survival of virtually all organisms that fare in an aerobic habitat. Ever since its discovery in 1900 by Oscar Loew, the canonical catalase (KatE) has long been logically regarded as the key player in H₂O₂ detoxification given its striking turnover rate ($> 10^5 \text{ s}^{-1}$) (135). Catalases are not restricted to one protein type, another structurally unrelated bifunctional enzyme exhibits robust catalase activity along with peroxidase activity which gives rise to the name catalase-peroxidase (KatG). Recent studies with the model organism *Escherichia coli* have suggested that alkyl hydroperoxide reductase (AhpCF) is the primary scavenger of endogenous H₂O₂, thus three authentic enzymes have been identified to detoxify H₂O₂ in *E. coli*, i.e., AhpCF, KatG and KatE (50).

Despite the fact it is well known that respiratory chains generate H₂O₂ together with superoxide (O₂⁻), the main sources of endogenous H₂O₂ in *E. coli* have been revealed to be the autoxidation of the abundant flavoproteins and the turnover of committed oxidases and it is estimated that the steady-state concentration of H₂O₂ is maintained at about 50 nM (20-22). Nevertheless, the biggest threat of H₂O₂ posed to bacteria stems from the external environment, including microbial competitors and eukaryotic hosts (44). Especially when a phenomenon like neutrophil-based oxidative burst is considered, up to

100 mM H₂O₂ can be generated (94). Unlike the charged species, O₂⁻, H₂O₂ penetrates cell membranes with a permeability coefficient similar to that of water, and therefore, is lethal to bacteria lacking scavenging enzymes (136).

With a very low K_M for H₂O₂ (1.4 μM) and a very low k_{cat} (55 s⁻¹), AhpCF is responsible for degrading H₂O₂ in the low-micromolar range (47). However, because of these kinetic parameters, AhpCF can be easily overwhelmed upon exposure to higher H₂O₂ concentrations. Under these circumstances, scavenging activities from KatG and KatE start to predominate due to the saturation of AhpCF. Among the three scavengers, KatG is unique in its ability to decompose H₂O₂ by either catalatic or peroxidatic mechanisms. Canonical descriptions of catalatic and peroxidatic mechanisms suggest that the two should be mutually antagonistic (Figure 5.1), and the hypothesis was indeed supported by one of the earliest observations that the peroxidatic electron donor (PxED) *o*-dianisidine did inhibit catalase activity of *E. coli* KatG at pH 7.5 (59). Surprisingly, our *in vitro* studies have shown that instead of inhibiting catalase activity, PxEDs stimulate KatG catalase activity by up to 14-fold. This effect is particularly prominent under acidic pH conditions optimal for peroxidase activity instead, precisely those conditions where one would anticipate the greatest inhibitory effect of PxEDs (86). It is noteworthy that KatG also stands out as the only catalase carried by *Mycobacterium tuberculosis*, and in highly virulent bacterial pathogens such as *E. coli* O157:H7, *Yersinia pestis* and *Legionella pneumophila*, an additional periplasmic form of KatG is expressed, and in each case is observed to be associated with virulence factors unique to each organism (87-92). Our *in vitro* studies on periplasmic KatG from *E. coli* O157:H7 (also known as

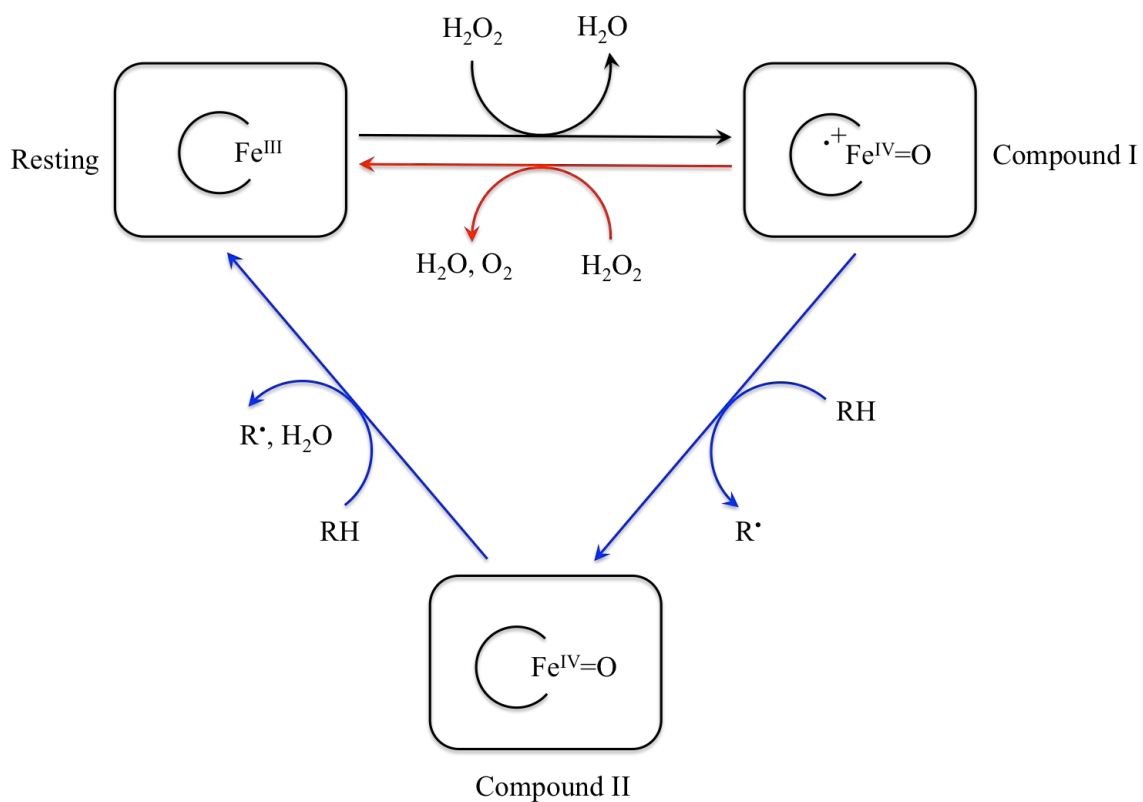


Figure 5.1. Divergence of catalase and peroxidase catalytic cycles in KatG. Both catalytic and peroxidatic cycles share the first step (black arrows), after which catalase (red arrows) and peroxidase pathways (blue arrows) diverge to complete each own catalytic cycle. RH and R• stand for peroxidatic electron donors (PxEDs) and PxED radicals, respectively.

KatP) demonstrated the PxED-enhanced catalase activity is also observed with these enzymes. Not only did PxEDs boost KatP catalase activity, but they also broadened the pH range of efficient H₂O₂ decomposition to acidic conditions. This could potentially be a great advantage for bacterial pathogens to survive oxidative burst and related phenomena, and escape the host immune responses.

With all these *in vitro* findings, this study was undertaken to appraise whether PxEDs enhance bacterial defenses against H₂O₂ and thus potentially contribute to bacterial virulence and also determine by what mechanisms the KatG-dependent PxED effect is achieved during H₂O₂ stress in the model organism *E. coli*.

5.2 Materials and Methods

5.2.1 Reagents

Hydrogen peroxide (30%), 2,2'-azino-bis(3-ethylbenzthiazoline-6-sulfonic acid) (ABTS), 3,3',5,5'-tetramethylbenzidine dihydrochloride hydrate (TMB), L-arabinose, ampicillin, chloramphenicol, kanamycin, sodium citrate dehydrate were purchased from Sigma-Aldrich (St. Louis, MO). LB broth, Miller (Luria-Bertani) was obtained from BD Biosciences (San Jose, CA). Tetracycline hydrochloride, sodium acetate trihydrate, calcium chloride dihydrate and magnesium sulfate were purchased from Fisher Scientific (Pittsburgh, PA). *PfuTurbo* DNA polymerase was obtained from Agilent Technologies (La Jolla, CA). All oligonucleotide primers were purchased from Invitrogen (Carlsbad, CA). All restriction enzymes and DNA modification enzymes were obtained from New England Biolabs (Beverly, MA). All buffers and media were prepared using water purified through a Barnstead EASYpure II system (18.2 MΩ/cm resistivity).

5.2.2 Strain constructions

Plasmids were purified with QIAprep Spin Miniprep Columns (Qiagen, Valencia, CA). DNA fragments were excised from agarose gels and purified using QIAquick Gel Extraction Kit (Qiagen, Valencia, CA) according to the manufacturer's instructions. Bacterial strains and plasmids used in this study are listed in Table 5.1; isogenic strains were used in all experiments. To generate *ahpCF* single mutant, the suicide plasmid pHD002 which carries the Δ *ahpCF::cat* null allele was constructed by the method of splicing by overlap extension by the polymerase chain reaction (SOE by PCR) (Figure 5.2) (137, 138). Briefly, a DNA sequence containing 1038 bp upstream and 1044 bp downstream of the *ahpCF* coding sequence was amplified from *E. coli* MG1655 genomic DNA using two pairs of primers: the upstream forward primer (pUF) 5'-GTAATAGAGAGCTCGCGTGACATTTGCCCCCAGATC-3' and the upstream reverse primer (pUR) 5'-GGCTAAGCAATTGCAGGTGAATCTTACTAGTTCTATACTTCCTCCGTGTTTTTCG-3'; the downstream forward primer (pDF) 5'-CATCTCATCGAAAACACGGAGGAAGTATAGAACTAGTAAGATTCACCTGC-3' and the downstream reverse primer (pDR) 5'-CGCCACAAGCATGCACGAACGGAATTACC-3'. The oligonucleotide primers were designed to engineer SacI and SpeI, SpeI and SphI sites at the 5' and 3' ends of the upstream and downstream gene, respectively. The overlap of 42 bp between the two fragments of DNA allowed the splicing of the upstream and downstream gene via SOE by PCR. The Δ *ahpCF* DNA fragment was then cloned as a SacI/SphI fragment into the ampicillin resistance suicide vector pGP704 digested with the same enzymes to form pHD001 (139, 140). The selection and propagation of newly generated suicide plasmid

Table 5.1. Strains and plasmids used in this study.

| Strain or plasmid | Genotype or characteristics | Source or reference |
|------------------------|---|-------------------------------------|
| <i>E. coli</i> strains | | |
| MG1655 | wild-type | <i>E. coli</i> Genetic Stock Center |
| JW1721-1 | $\Delta katE731::kan$ | <i>E. coli</i> Genetic Stock Center |
| UM197 | <i>katG17::Tn10</i> | <i>E. coli</i> Genetic Stock Center |
| DG001 | MG1655 $\Delta katE731::kan$ | P1(JW1721-1) × MG1655 |
| DG002 | MG1655 <i>katG17::Tn10</i> | P1(UM197) × MG1655 |
| DG003 | DG002 $\Delta katE731::kan$ | P1(JW1721-1) × DG002 |
| DG004 | DG003 pBAD30 (<i>katG</i>) | This study |
| DG005 | DG003 pBAD30 (<i>katG</i> ^{Y229F}) | This study |
| DG006 | MG1655 $\Delta ahpCF::cat$ | This study |
| DG007 | DG001 $\Delta ahpCF::cat$ | P1(DG006) × DG001 |
| DG008 | DG006 <i>katG17::Tn10</i> | P1(DG002) × DG006 |
| DG009 | DG003 $\Delta ahpCF::cat$ | P1(DG006) × DG003 |
| DG011 | DG009 pBAD30 (<i>katG</i>) | This study |
| DG012 | DG009 pBAD30 (<i>katG</i> ^{Y229F}) | This study |
| Plasmids | | |
| pGP704 | Plasmid for <i>ahpCF</i> mutant construction | 139 |
| pHD001 | pGP704 derivative for <i>ahpCF</i> deletion | This study |
| pHD002 | pHD001 derivative with <i>cat</i> | This study |
| pBAD30 | Plasmid for <i>katG</i> complementation | 142 |

were achieved by transformation of *E. coli* DH5 α λ *pir* strain. The chloramphenicol cassette was cloned into pHD001 at the site of *SpeI* to generate the final vector pHD002 transforming *E. coli* MG1655 for allelic exchange. The Δ *ahpCF* mutants were isolated as chloramphenicol resistant but ampicillin sensitive colonies via double-crossover event by homologous recombination. Deletion of *ahpCF* was confirmed by PCR analysis. The single mutation *ahpCF* along with *katE* and *katG* was then introduced into other strains via P1 transduction to generate single, double and triple mutants and verified by antibiotic resistance(s) and PCR analysis (141). Complementation of the *katE/katG* and *ahpCF/katE/katG* mutant strains was achieved with the fully active wild-type *katG* gene from *Mycobacterium tuberculosis* as well as with a mutant *katG* wherein the expressed KatG would be the peroxidase-active but catalase-inactive Y229F protein (86). The *katG* gene (wild-type and mutant) was cloned in pBAD30 vector with restriction sites *XbaI/HindIII* that also carries ampicillin resistance to place the gene under tightly controlled, titratable expression using L-arabinose (142).

5.2.3 Bacterial growth studies

Bacteria were routinely cultured in LB broth, Miller at 37 °C supplemented with 100 μ g/mL ampicillin when appropriate. To avoid the photochemical formation of H₂O₂, LB medium was shielded from light with aluminum foil. All protocols were designed to ensure experiments were conducted upon exponentially growing cells. For growth curve assays, overnight cultures were diluted 1:100 into LB medium and grown to early log phase with optical density at 600 nm (OD₆₀₀) of 0.1 to 0.2. The cultures were then diluted 1:100 into new medium of the same composition in a Corning Costar 96 well flat bottom cell culture plate (Corning, NY) and grown for 24 hours with shaking in a BioTek

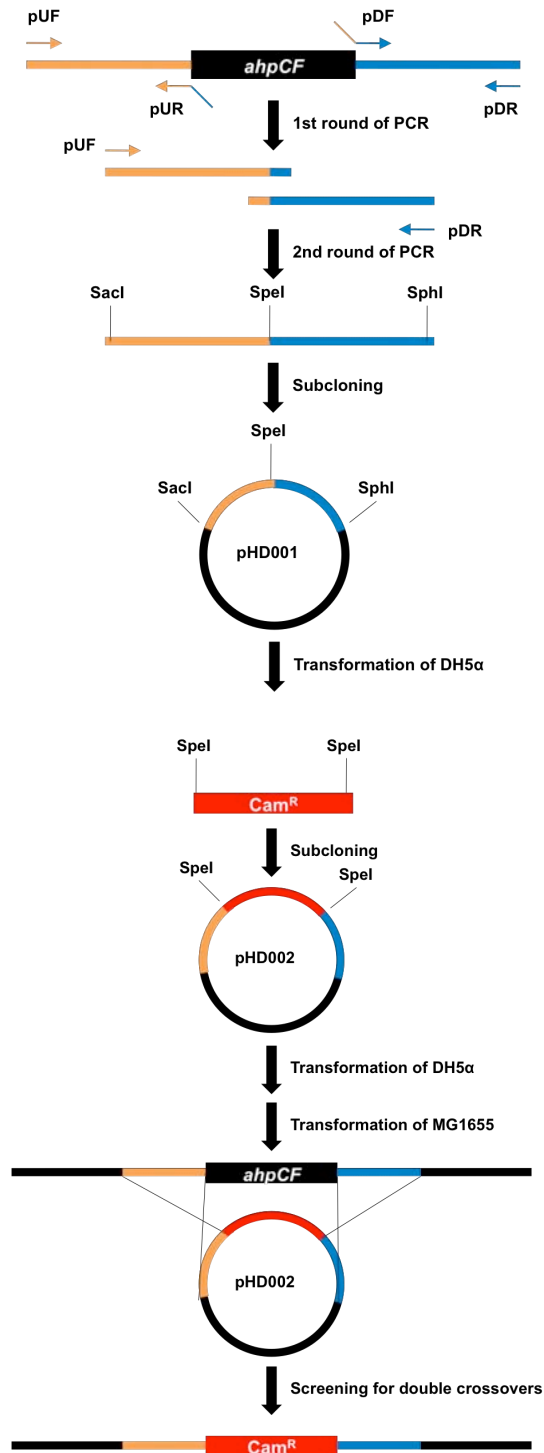


Figure 5.2. Construction of $\Delta ahpCF$ mutant. pUF, pUR and pDF, pDR are the two pairs of primers for splicing by overlap extension PCR. pHD0001 and pHD002 are both suicide plasmids derived from pGP704.

Synergy HT plate reader (Winooski, VT). Cell growth was monitored as OD₆₀₀ and both neutral (pH 7.0) and acidic (pH 5.0) growth conditions were assessed. The effect of PxEDs on the growth of *katE/katG* double mutants and *ahpCF/katE/katG* triple mutants complemented with wild-type *katG* and Y229F *katG* gene was determined by growing DG004, DG005, DG011 and DG012 (Table 5.1) in LB medium supplemented with 0.1 mM ABTS and 0.1 mM TMB, respectively.

5.2.4 KatG expression analysis

To evaluate the expression of complemented *katG* gene via plasmid pBAD30, 0.01% (0.66 mM) and 0.1% (6.66 mM) of L-arabinose were used to induce mid-log phase cells and the cultures were monitored hourly to ensure growth. Expression analysis was performed by TCA protein precipitation. Briefly, a quantity of cells sufficient to yield a 0.05 OD₆₀₀ reading when diluted to 1 mL was treated with an equal volume of 10% trichloroacetic acid stored at 4°C followed by centrifugation. The pellet was washed with 1 mL acetone, then dried and resuspended in SDS-PAGE loading buffer, appropriate pH was adjusted with Tris base. Samples were then separated by SDS-PAGE using a 7.6% polyacrylamide resolving gel. The solubility of expressed protein was also confirmed by SDS-PAGE.

5.2.5 H₂O₂ challenge assays

The effect of PxEDs on bacterial defenses against H₂O₂ was appraised by *katE/katG* double mutants and *ahpCF/katE/katG* triple mutants with wild-type *katG* and Y229F *katG* gene provided through plasmid-mediated complementation. To perform the assays, overnight cultures were diluted 1:100 into acidic LB medium (pH 5.0) supplemented with 100 µg/mL ampicillin and grown to early log phase with OD₆₀₀ of 0.1 to 0.2. The cultures

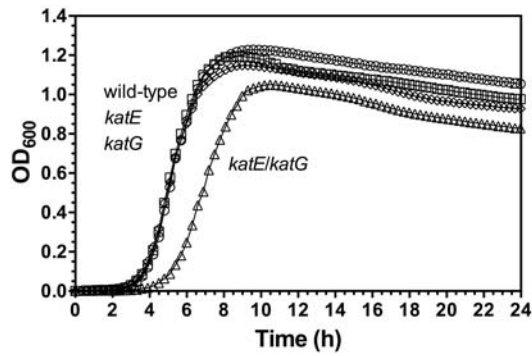
were then transferred to a Corning Costar 96 well flat bottom cell culture plate (Corning, NY) which was supplemented with varying concentrations of L-arabinose, 0.01% (0.66 mM), 0.005% (0.33 mM), 0.002% (0.13 mM) and 0.001% (0.06 mM) for different levels of expression. 0.1 mM each of PxEDs, ABTS and TMB, was also added into the cultures followed by the treatment with 1.0 mM H₂O₂. The cells were then allowed to recover for 24 hours with shaking in a BioTek Synergy HT plate reader and the recovery was monitored as OD₆₀₀. Any background absorbance was corrected by the uninoculated medium of the same composition under the same condition (130, 131).

5.3 Results

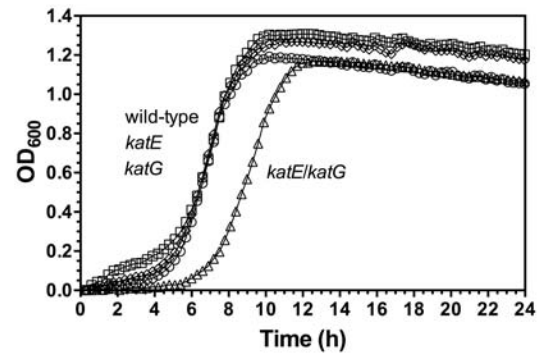
5.3.1 KatG plays the critical role for bacterial defenses against H₂O₂ during aerobic metabolism.

Given the low K_M of AhpCF compared to the concentrations of H₂O₂ used in our assays, we initiated our studies with single mutants *katE*, *katG* and double mutant *katE/katG* constructed by transducing the null mutations into the wild-type strain MG1655 (47). When the four strains were grown in LB medium both at pH 7.0 and pH 5.0 without inclusion of exogenous H₂O₂, neither of the single mutants showed a growth defect, but the *katE/katG* double mutant exhibited a modestly extended lag phase (Figure 5.3A and 5.3B). These data suggest that AhpCF is sufficient to afford protection from endogenously generated H₂O₂. Not surprisingly, vulnerability to endogenous H₂O₂ was increased in AhpCF null mutants. Although *ahpCF* single mutant and *ahpCF/katE* double mutant grew as well as did the wild-type in neutral LB medium, the growth defect started to be evident under acidic condition in *ahpCF/katE* double mutant with delayed entrance into the log phase (Figure 5.3C and 5.3D), whereas *katE* single mutant showed no

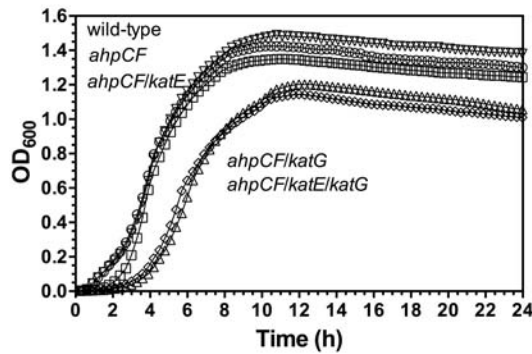
A



B



C



D

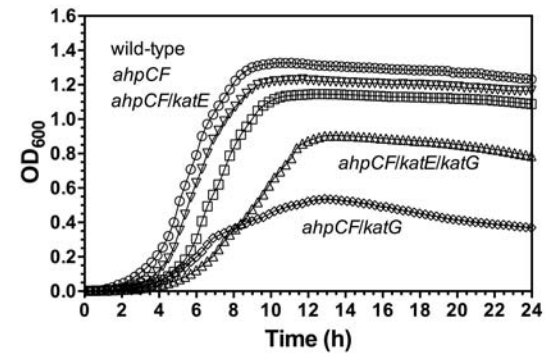


Figure 5.3. Growth curves of wild-type and mutant strains in LB medium. Wild-type (○), the single mutants *katE* (□) and *katG* (◇), and the double mutant *katE/katG* (△) were grown in LB at pH 7.0 (A) and pH 5.0 (B); Wild-type (○), the single mutant *ahpCF* (▽), the double mutants *ahpCF/katE* (□) and *ahpCF/katG* (◇), and the triple mutant *ahpCF/katE/katG* (△) were grown in LB at pH 7.0 (C) and pH 5.0 (D).

observable difference compared to the wild-type strain. This suggests AhpCF played an essential role in scavenging endogenous H₂O₂ thus allowed rapid transition from the lag phase to exponential phase. The effect of lacking AhpCF was more detrimental in *ahpCF/katG* double mutant and *ahpCF/katE/katG* triple mutant. At neutral pH, *ahpCF/katG* double mutant grew as poorly as *ahpCF/katE/katG* triple mutant (Figure 5.3C) consistent with the observations of Seaver and Imlay wherein both *ahpCF/katG* and *ahpCF/katE/katG* mutants failed to scavenge H₂O₂ (50). These results unequivocally suggest that KatG is the key scavenger of H₂O₂ in aerobic growth and it is able to compensate for the loss of AhpCF, whereas KatE provides no additional protection against H₂O₂ when both AhpCF and KatG are absent.

The *ahpCF/katG* mutant grew even more poorly in acidic LB medium with substantially decreased growth rates and only 1/3 of final cell density achieved as the wild-type signifying the critical role of KatG in bacterial fitness (Figure 5.3D). As shown at neutral pH, the role of KatE is enigmatic by the fact there was no discernable phenotype change from *ahpCF/katG* to *ahpCF/katE/katG* mutant strain. Interestingly, compared to the double mutant *ahpCF/katG*, the triple mutant *ahpCF/katE/katG* appeared less vulnerable to H₂O₂ under acidic growth conditions (Figure 5.3D) making the already elusive role of KatE, the canonical catalase in *E. coli* more perplexing. This was also evidenced by our observation that *ahpCF/katG* mutant grew much slower on LB agar plates with noticeably smaller colonies than *ahpCF/katE/katG* triple mutant.

5.3.2 Peroxidatic electron donors ABTS and TMB pose no adverse effect on aerobic growth of *katG* complemented strains.

ABTS and TMB are two widely used artificial peroxidatic electron donors (PxEDs) in *in vitro* studies of KatG enzymes as the physiological PxEDs remain unidentified. Before evaluating the effect of PxEDs on resistance to H₂O₂ toxicity *in vivo*, it was important to establish that the donors themselves had no toxic effects on *E. coli*. Based on our *in vitro* experiments, 0.1 mM of each PxEDs, ABTS and TMB, was supplemented into pH 5.0 LB medium, the mutants being tested, *katE/katG* and *ahpCF/katE/katG* strains all exhibited unaltered growth behavior, suggesting 0.1 mM ABTS and TMB did not pose a toxic threat to aerobic growing *E. coli* (data not shown).

Given the conspicuous stimulatory effect observed in *M. tuberculosis* KatG, the wild-type and Y229F mutant *katG* gene from *M. tuberculosis* were complemented to *katE/katG* and *ahpCF/katE/katG* mutant strains through pBAD30 vector (86). Regulated by the arabinose operon, pBAD30 is a tightly controlled expression vector that allows for precise targeting of levels of gene expression. This was especially desirable as it avoids potential interference with normal bacterial metabolism. Complemented mutant strains were induced with 0.1% (6.66 mM) and 0.01% (0.66 mM) of L-arabinose, and the resulting protein expression was analyzed by SDS-PAGE (Figure 5.4). The protein bands around 80 kDa only appeared after induction and were more intense when higher concentration of L-arabinose, i.e., 0.1%, was used, moreover, the expressed wild-type KatG and Y229F KatG both appeared to be soluble.

5.3.3 PxEDs afford a more effective and quick response to oxidative stress for mutant strains complemented with the fully active wild-type *katG* gene.

The *katE/katG* double mutant (DG004) and *ahpCF/katE/katG* triple mutant (DG011) grown under acidic conditions were induced by L-arabinose as low as 0.001% for the

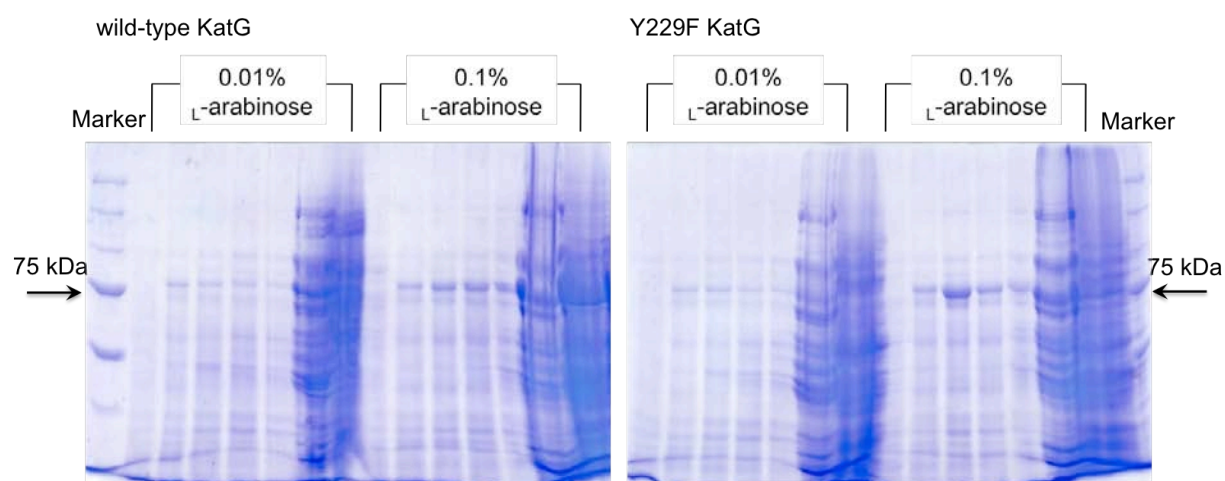


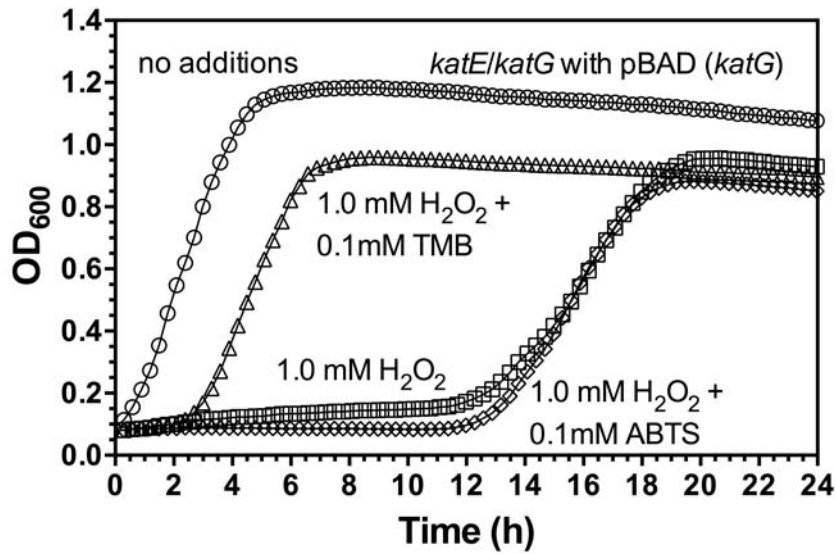
Figure 5.4. Protein expression analyses of wild-type KatG and Y229F KatG. From left to right excluding the marker lane, each set of 7 lanes are 0 hour (pre-induction), 1 hour, 2 hours, 3 hours, 4 hours (post-induction), insoluble fraction and soluble fraction.

expression of wild-type KatG. When challenged with 1.0 mM H₂O₂, a lag of growth up to 12 hours was observed in both strains before log phase was re-established concomitant with a slower growth rate compared to the unchallenged cells. By contrast, the unchallenged cells continued their exponential growth and entered stationary phase after about 6 hours (Figure 5.5A). Inclusion of ABTS had little impact on either strain as each showed the same long lag period preceding log phase growth. In contrast, inclusion of 0.1 mM TMB resulted in a much diminished lag period in the *katE/katG* strain (2 hours) and in the *ahpCF/katE/katG* strain (6 hours) accompanied by comparable growth rates in log phase with unchallenged cells (Figure 5.5 and 5.6), indicating an enhanced scavenging activity of H₂O₂ by virtue of PxEDs. The level of KatG expression afforded by induction with 0.001% L-arabinose appeared sufficient to protect cells from H₂O₂ stress. Increasing the concentration of L-arabinose up to 0.01% did little to increase the protective effect (Figure 5.5B and 5.6B).

5.3.4 PxEDs enhance bacterial defenses against H₂O₂ by stimulating the *catalase* activity of KatG.

KatG also possesses a peroxidase activity that scavenges H₂O₂ and depends on PxEDs. It was possible that the observed PxED-enhanced H₂O₂ defenses may not be necessarily attributed to PxED-stimulated *catalase* activity of KatG, but instead, may simply be the result of its standard peroxidase activity. To address this matter, a mutant gene Y229F *katG* was also complemented in *katE/katG* and *ahpCF/katE/katG* mutant strains. Unlike wild-type KatG, the Y229F protein has a greater peroxidase activity but no catalase activity even in the presence of PxEDs (86, 107, 157). When Y229F *katG* complemented *katE/katG* strain was stressed with 1.0 mM H₂O₂, no recovery of growth was observed

A



B

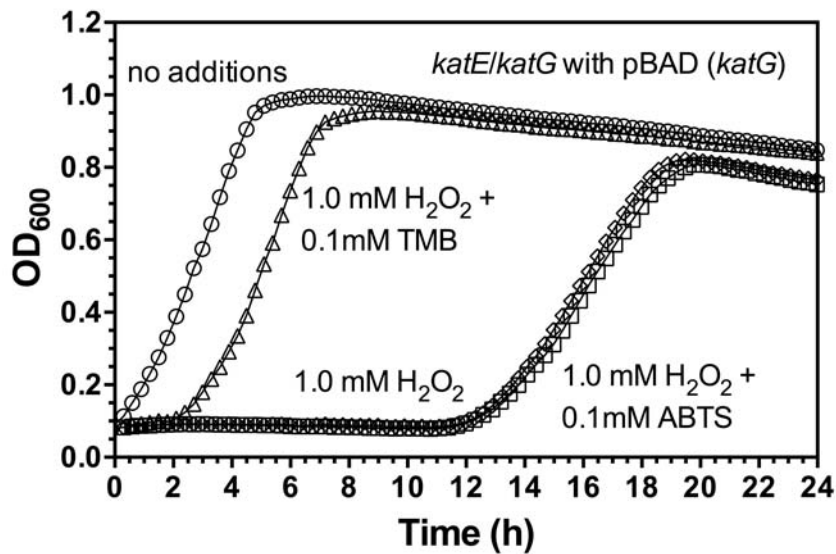
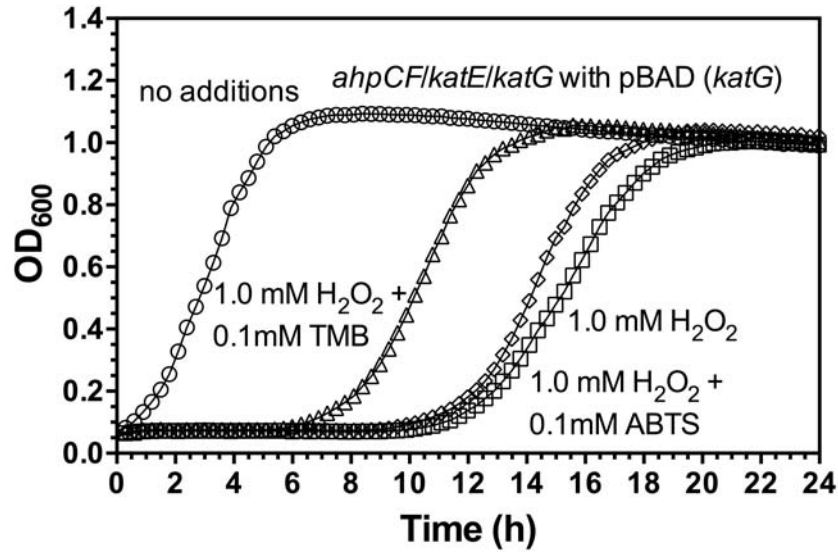


Figure 5.5. Effect of PxEDs on recovery of the growth of *katE/katG* double mutant complemented with wild-type *katG* from *M. tuberculosis* (DG004) at pH 5.0. With no additions (○), 1.0 mM H₂O₂ (□), 1.0 mM H₂O₂ + 0.1 mM ABTS (◇), and 1.0 mM H₂O₂ + 0.1 mM TMB (△), induced by 0.001% (A) and 0.01% (B) L-arabinose.

A



B

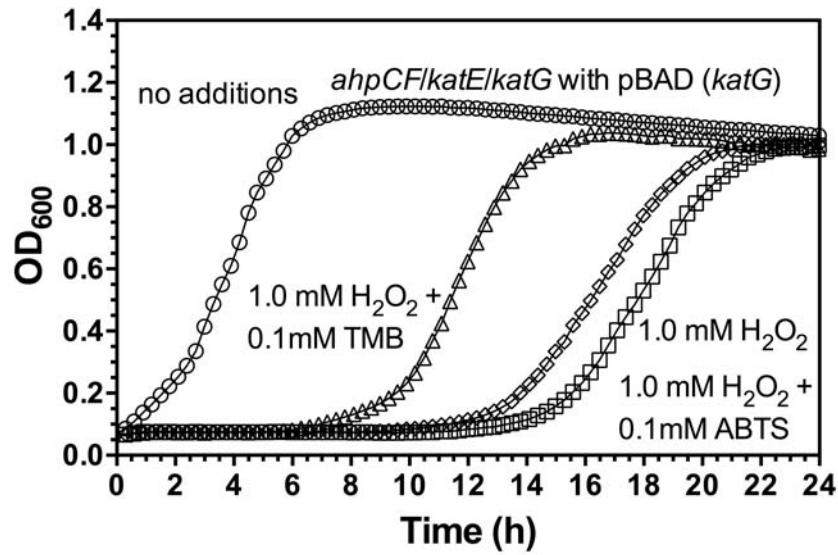


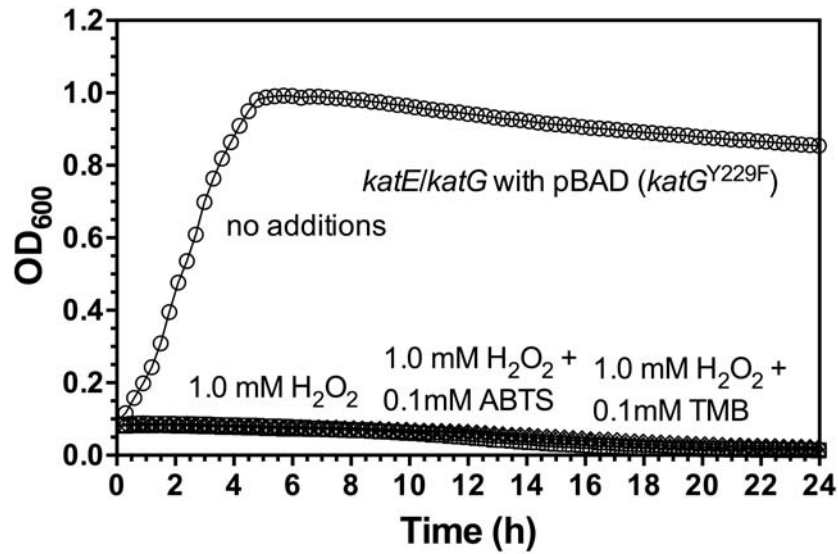
Figure 5.6. Effect of PxEDs on recovery of the growth of *ahpCF/katE/katG* triple mutant complemented with wild-type *katG* from *M. tuberculosis* (DG011) at pH 5.0. With no additions (○), 1.0 mM H₂O₂ (□), 1.0 mM H₂O₂ + 0.1 mM ABTS (◇), and 1.0 mM H₂O₂ + 0.1 mM TMB (△), induced by 0.001% (A) and 0.005% (B) L-arabinose.

within 24 hours (Figure 5.7A). The inclusion of PxEDs imparted no ability to alleviate growth inhibition due to H₂O₂, and increasing the levels of expression of Y229F KatG was also ineffective for relieving H₂O₂-dependent growth inhibition (Figure 5.7B). These results suggest that the peroxidase activity of the catalase-inactive Y229F KatG, which is in fact greater than that of the wild-type, was incapable of protecting bacteria from H₂O₂ stress. In the Y229F KatG complemented *ahpCF/katE/katG* triple mutant strain, PxEDs were still unable to facilitate H₂O₂ scavenging, however, the recovery of growth was detected about 16 hours after the treatment with H₂O₂ (Figure 5.8).

5.4 Discussion

Two catalases are produced and independently regulated in *E. coli*. The expression of bifunctional KatG is transcriptionally induced by OxyR in a H₂O₂-dependent manner during logarithmic growth. Conversely, the expression of the canonical monofunctional KatE is insensitive to concentrations of H₂O₂ and is instead induced by the alternative sigma factor RpoS, upon entry into stationary phase (143, 144). KatE in *E. coli* has a robust observed catalase k_{cat} of 151,000 s⁻¹, however its K_M is also very high, at 64 mM of H₂O₂ at neutral pH (158). KatE also remains maximally active over a broad pH range of 4-11 and is remarkably resistant to denaturation (58, 146). It would be reasonable to anticipate that KatE would be superior to KatG in protecting bacteria from H₂O₂-dependent toxicity. Nevertheless, our study suggests that the presence or absence of *katE* has no impact on cell aerobic growth at neutral pH (Figure 5.3A and 5.3C). The same phenomenon was also observed with *E. coli* serotype O157:H7 by G. Uhlich in which KatE did not scavenge H₂O₂ in either the exponential or the stationary phase (147).

A



B

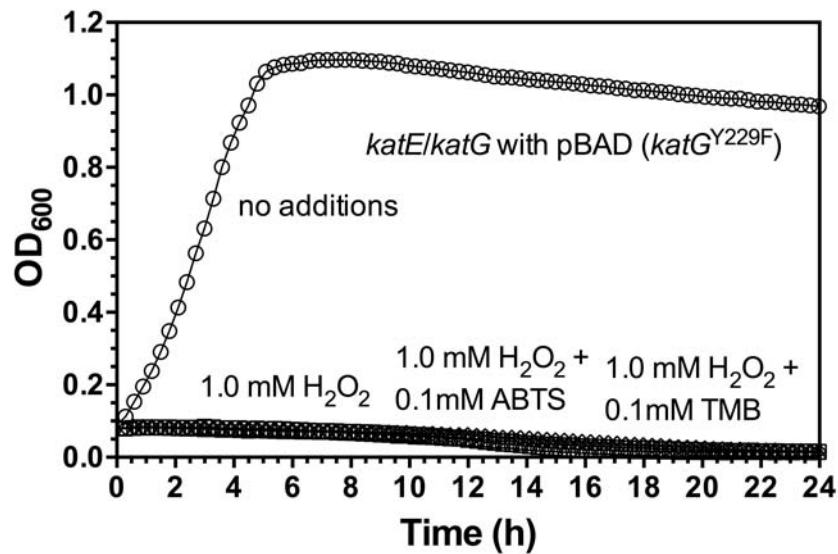


Figure 5.7. Effect of PxEDs on recovery of the growth of *katE/katG* double mutant complemented with Y229F *katG* from *M. tuberculosis* (DG005) at pH 5.0. With no additions (○), 1.0 mM H₂O₂ (□), 1.0 mM H₂O₂ + 0.1 mM ABTS (◇), and 1.0 mM H₂O₂ + 0.1 mM TMB (△), induced by 0.001% (A) and 0.01% (B) L-arabinose.

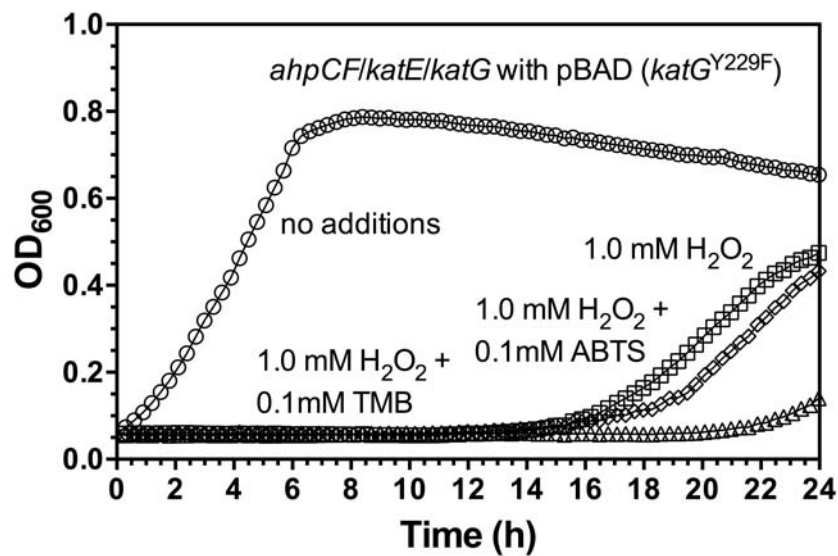


Figure 5.8. Effect of PxEDs on recovery of the growth of *ahpCF/katE/katG* triple mutant complemented with Y229F *katG* from *M. tuberculosis* (DG012) at pH 5.0. With no additions (○), 1.0 mM H₂O₂ (□), 1.0 mM H₂O₂ + 0.1 mM ABTS (◇), and 1.0 mM H₂O₂ + 0.1 mM TMB (△), induced by 0.001% L-arabinose.

A lack of impact of *katE* on H₂O₂ resistance was also seen at pH 5.0. Indeed, the presence of *katE* appeared to be a *disadvantage* for aerobic growth (Figure 5.3D). It is not entirely clear why *katE* exerted an adverse effect on growth under acidic conditions. The expression of RpoS is likely to be upregulated by acid stress, thus one would anticipate the increased transcription and availability of KatE (148). In any case, pH seemed to play an important role given the adverse effect was not observed at pH 7.0 (Figure 5.3C vs 5.3D). It has been shown that during aerobic growth under mild acid stress, there is an upregulation of selected components of the electron transport chain, and thus a higher rate of proton export is expected under these conditions than under growth conditions at neutral pH (149). Moreover, ATPase can also be involved in pumping protons against thermodynamic gradient with consumption of ATP (150, 151). In both cases, elevated respiration is likely to occur in order to support those activities. This, in turn, would contribute to greater production of reactive oxygen species. Although the role of KatE remains unclear, it leaves no doubt that KatG plays the pivotal role in protecting the bacteria that produce it from H₂O₂-dependent oxidative stress under both neutral and acidic growth conditions.

The first characterization of *E. coli* KatG by Claiborne and Fridovich showed that the enzyme exhibits both a peroxidase activity acting upon different PxEDs and an efficient catalase activity (59). However the physiological identity of PxEDs remains unrevealed after more than three decades. Therefore, to determine the effect of PxEDs on bacterial defenses against H₂O₂ using exogenous PxEDs raises two concerns. One is that whether PxEDs cause cytotoxicity, and thus influence normal metabolism, and the other is whether the PxEDs can be successfully taken up by the cell in order to function. At

presence of 0.1 mM PxEDs no apparent growth defect was shown in the strains tested suggesting both ABTS and TMB are innocuous for *E. coli* growth. However, ABTS and TMB were distinct in their ability to produce recovery of bacterial growth (Figure 5.5 and 5.6), while TMB afforded the challenged cells an efficient response to H₂O₂ assaults by reducing the lag nearly 6-fold, the supplementation with ABTS did not appear to aid the recovery compared to the control without PxEDs added. Our *in vitro* studies have shown that both ABTS and TMB are very effective for stimulating KatG catalase activity by up to 9-fold under the same concentration and condition (86). The discrepancy in terms of PxEDs in our *in vivo* studies can be reconciled by the fact that ABTS is highly charged but TMB is not. It is reasonable to suggest that transport of ABTS across the cell membrane may be problematic. In addition, the porin channels located on the outer membrane of *E. coli* can only mediate non-specific, diffusion-based passage of hydrophilic molecules up to approximately 600 Da. Thus a high molecular weight of more than 500 of ABTS would also contribute to the difficulty of its uptake by *E. coli* cells (153).

In terms of k_{cat} , the peroxidase activity of KatG is generally 100-fold lower than the catalase activity. Our results show that peroxidase activity alone even enhanced as in Y229F KatG is not sufficient to detoxify exogenous H₂O₂ regardless of PxEDs. Our data show that the protective effect of PxEDs arise due to the stimulation of KatG catalase activity thus render an advantage to bacteria growing under acidic conditions. It is important to emphasize that KatG catalase activity is very poor under these conditions in the absence of PxEDs. The effect of PxEDs is somehow attenuated as shown in

ahpCF/katE/katG triple mutant (Figure 5.6), and the reason why *ahpCF/katE/katG* mutants were able to recover (Figure 5.8) remains poorly understood.

The broadened pH range into acidic conditions for more efficient catalase activity of KatG by virtue of PxEDs may have profound implications. Unlike KatE, KatG has a near neutral pH optimum for catalase activity whereas the peroxidase activity is optimal under acidic conditions. In this regard, the stimulatory effect for catalase activity of KatG by PxEDs may impart a great advantage for bacterial pathogens to survive the acidic environment such as phagolysosomes, in which copious H₂O₂ is generated, and elude the host immune responses consequently. Although a physiological PxED has yet to be identified, our *in vitro* studies with KatP, a second copy of KatG located in the periplasm of *E. coli* O157:H7 have shown that KatP still retains an efficient catalase activity under acidic pH in the presence of PxEDs. Taken together, while elucidation of the physiological PxEDs of KatG would be tremendously helpful, our study presented here provides the evidence that such PxEDs are conducive to bacterial survival under H₂O₂-induced oxidative stress by specifically enhancing the catalase activity of the KatG enzyme.

CHAPTER SIX SUMMARY

The oxygen paradox dictates that while oxygen is indispensable and an efficient electron acceptor for aerobic life, nevertheless, oxygen derived reactive oxygen species are constantly threatening the integrity of the biomolecules in living organisms. Life on Earth embarked on an evolutionary journey with oxygen circa three billion years ago, and it was not until three decades ago did the toxicity of reactive oxygen species (ROS) become appreciated. Among all the scavengers of ROS, catalase-peroxidase (KatG) has been the center of this dissertation and intrigued and haunted both biochemists and microbiologists ever since its first discovery.

What makes KatG an attractive object to study and how can KatG contribute to science advances and human welfare? Throughout the devolvement in this ever fermenting field, the answers to these questions have become more and more clear. At first glance, KatG, the enzyme found in bacteria, archaea and fungi, does not seem too impressive, it decomposes H_2O_2 and evolves O_2 just as the canonical catalase discovered more than 100 years ago. However, when one gazes into the active site of KatG and compares it with that of both canonical catalase and peroxidase, the fascinating conundrum implied by KatG starts to surface. With nearly superimposable active site structure with peroxidases such cytochrome *c* peroxidase and ascorbate peroxidase, KatG fit squarely into Class I of non-animal peroxidase, now known as peroxidase-catalase superfamily and it bears virtually no sequence similarity with the canonical catalase.

Given none of other members in the entire superfamily has appreciable catalase activity, it really begs the question, how is KatG able to achieve robust catalytic turnover with a peroxidase core?

Much progress has been made in addressing this fundamental question so far. There are several unique features that make KatG stand out from other peroxidases. First, instead of being monomeric, KatG exists as either a homodimer or a homotetramer. Moreover, each subunit of KatG is almost twice the size of the monomeric peroxidase due to the extra gene-duplicated C-terminal domain. Studies have shown that the seemingly redundant C-terminal domain, albeit devoid of active site, is indispensable for both catalase and peroxidase activity for KatG. Second, two important large loop structures of the active site harboring N-terminal domain have been identified and characterized in KatG and demonstrated to be essential for the catalase but not peroxidase activity. Third, a novel covalent adduct adjacent to the active site heme, namely Met-Tyr-Trp covalent adduct has also been shown to be crucial for the catalase activity as substitution of any member of the adduct abolishes the catalase activity. Last but not least, a mobile arginine also known as the arginine switch located 20 Å from the active site appears to modulate the catalase activity of KatG with two different conformations in a pH-dependent manner.

Our previous studies have demonstrated that without C-terminal domain, the active site in the N-terminal domain collapses due to the coordination of the distal histidine to the heme iron shifting the active form of high-spin heme to its inactive low-spin state. In efforts to elucidate the mechanisms by which the C-terminal domain modulates KatG active site architecture and function, the interface between N- and C-terminal domain

within each subunit was examined and it revealed strictly conserved H-bond interactions involving two networks, namely the distant- and near-network based on the distance of the residues from the active site.

The conserved H-bond interactions in the distant-network involve Arg 117 from N-terminal domain forming H-bonds with both Asp 597 and Gln 600 from C-terminal domain. We capitalized on the ability of C-terminal domain to reactivate the stand-alone inactive N-terminal domain and generated variants targeting these residues and characterized these altered interactions. The work presented here demonstrated that while the apparent rate constant of reactivation was largely unaffected by substitutions of distant-network residues, the effect on the coordination state of the heme iron and the catalase activity of these domain variants after the reactivation process was remarkable. Substitution of Arg 117 in the domain variants all resulted a shift from predominantly narrow rhombic high-spin heme as observed in reactivated unmodified domain proteins to substantial broad rhombic high-spin heme. While peroxidase activity was not much influenced by substitutions, catalase activity was diminished to different extent, in particularly, R117D^N+D597R^C showed over 80% loss of catalase k_{cat} . More importantly, our data suggest that the loss of catalase activity observed in the distant-network variants has little correlation with low-spin contribution in these reactivated domain proteins.

The near-network residues include Arg 479 which forms H-bonds with adjacent Asp 482 also from the C-terminal domain, while Asp 482 in turn interacts with Tyr111 from the N-terminal domain. Similarly with Arg 117 in the distant-network, substitution of Arg 479 also resulted a considerable shift from narrow to broad rhombic high-spin heme species. An even greater loss of catalase activity were observed in reactivated near-

network variants. In particular, double substitution of Tyr 111 and Asp 482 with alanine caused an over 90% loss of catalase k_{cat} , and only 1% of catalase k_{cat} remained with double substitution of Tyr 111 and Arg 479. These results highlight the indispensable role of near-network residues for the catalase activity in KatG. Moreover, a substantial loss of peroxidase k_{cat} of KatG by C-terminal domain residue substitution was also observed, suggesting that Arg 479 and Asp 482 play an essential role in KatG peroxidase activity. A greater contribution of low-spin species is generally detected in the reactivated near-network variants compared to distant-network variants, nonetheless, no significant correlation can be established between observed catalase activity and low-spin contribution. Taken together, our work points toward a multifaceted role of C-terminal domain in KatG, it not only supports the active site configuration by preventing the formation of hexacoordinate low-spin heme, but also modulates both catalase and peroxidase activity by low-spin-independent mechanisms.

The peroxidase activity of KatG generally received less attention, nevertheless, the physiological PxED remains unidentified. The questions surrounding KatG as a peroxidase may seem less relevant, but as to how the presence of PxEDs of peroxidase activity influences the catalytic turnover is appealing in that such scenarios are most likely to occur under physiological conditions. When PxEDs were included in the catalase reactions of KatP, a periplasmic catalase-peroxidase from *E. coli* O157:H7, we observed a stimulation of catalase activity by up to 10-fold. PxEDs assisted the catalase activity by lowering the apparent K_M and enhancing the apparent k_{cat} and such a stimulatory effect was especially prominent under acidic conditions. More strikingly, when we quantified the amount of ABTS oxidized at pH 5.0, it was found that for every

100 equivalents of H₂O₂ consumed, there were less than 2 equivalents of ABTS radical generated even at substrate and pH conditions optimal for the peroxidase activity. Most importantly, for a highly virulent bacterial pathogen *E. coli* O157:H7, PxEDs expanded the pH range for catalase function to acidic conditions and enhanced the catalatic turnover to an extent that rivaled or surpassed the unassisted catalase activity at its optimal conditions. We proposed two hypotheses accounting for the PxED-assisted catalase activity, one considers that PxEDs facilitate and even serve as an alternative to the arginine switch who adopts two pH-dependent conformations and modulates the catalase activity, the other based on the propensity of facile intramolecular electron transfer in KatG proposes that PxEDs enhance catalatic turnover by preventing the formation of catalase-inactive intermediates. The pH- and PxED-dependent catalase activity observed in KatP not only supplements our current understanding of the mechanisms of KatG but also sheds light on the potential strategies which bacterial and even fungal pathogens utilize for their survival.

The conditions under which PxED-assisted catalase activity occurred are reminiscent of the environment inside a phagocyte in the process of host immune responses. In light of this, our initial efforts were made to seek evidence for PxED-assisted bacterial defenses against H₂O₂. In particular, we constructed isogenic *E. coli* strains with null mutation of AhpCF, KatE, KatG, the three authentic H₂O₂ scavengers *in vivo*, in single, double and triple mutants. We also complemented the *katE/katG* and *ahpCF/katE/katG* mutants with both fully active wild-type *katG* and catalase-inactive but peroxidase-active mutant Y229F *katG* gene. Our results suggest that KatG was the pivotal scavenger of H₂O₂ in aerobic growth and was able to compensate for the absence

of AhpCF. On the other hand, KatE afforded little if any protection against H₂O₂ in the absence of both AhpCF and KatG. More importantly, we demonstrated that, Y229F *katG* complemented double mutant *katE/katG* was unable to sustain 1.0 mM H₂O₂ stress even in the presence of 0.1 mM PxEDs. The *katE/katG* mutant complemented with wild-type *katG* gene was able to recover after 12 hours, and in the presence of one of the PxEDs, 0.1 mM TMB facilitated an efficient response to the H₂O₂ assaults and allowed the cells to enter exponential phase within 2 hours. These results suggest that TMB specifically stimulated the catalase activity of KatG while peroxidase activity alone was insufficient to protect cells from the H₂O₂-dependent growth inhibition. A similar but attenuated effect from TMB was also observed for the *katG* complemented *ahpCF/katE/katG* triple mutant. Our results provide the first *in vivo* evidence that PxEDs enhance bacterial defenses against H₂O₂ by stimulating the *catalytic* turnover of KatG and bring us one step further on the mechanisms by which KatG contributes to bacterial and even fungal survival, in a broader scope.

Based on these, two directions are on the horizon. The work presented here negates that C-terminal domain prevents the formation of low-spin species through the highly conserved intrasubunit interactions. However, our results are striking in that they point toward a new facet of C-terminal domain of KatG. In this regard, X-ray crystallographic studies could potentially shed light on the mechanisms by which these conserved intrasubunit interactions modulate both catalase and peroxidase activities. The discovery that PxED contributes to bacterial resistance against H₂O₂ by enhancing the catalase activity of KatG, necessitates the identification of the physiological PxED for the KatG enzyme. Once the physiological PxED is identified, host-bacteria interactions can be

further studied to elucidate the mechanisms by which bacterial pathogens elude host immune responses.

REFERENCES

1. **Cadenas E.** 1989. Biochemistry of oxygen toxicity. *Annu. Rev. Biochem.* **58**:79-110.
2. **Sharma P, Jha AB, Dubey RS, Pessarakli M.** 2012. Reactive oxygen species, oxidative damage, and antioxidative defense mechanism in plants under stressful conditions. *J. Bot.* **2012**:1-26.
3. **Gerschman R, Gilbert DL, Nye SW, Dwyer P, Fenn WO.** 1954. Oxygen poisoning and X-irradiation: a mechanism in common. *Science.* **119**:623-626.
4. **Imlay JA, Linn S.** 1988. DNA damage and oxygen radical toxicity. *Science.* **240**:1302-1309.
5. **Oleinick NL, Chiu SM, Ramakrishnan N, Xue LY.** 1987. The formation, identification, and significance of DNA-protein cross-links in mammalian cells. *Br. J. Cancer Suppl.* **8**:135-140.
6. **Brot N, Weissbach H.** 1982. The biochemistry of methionine sulfoxide residues in proteins. *Trends Biochem. Sci.* **7**:137-139.
7. **Davies KJ.** 1987. Protein damage and degradation by oxygen radicals. I. general aspects. *J. Biol. Chem.* **262**:9895-9901.
8. **Gardner PR, Fridovich I.** 1991. Superoxide sensitivity of the *Escherichia coli* 6-phosphogluconate dehydratase. *J. Biol. Chem.* **266**:1478-1483.

9. **Mehler AH.** 1951. Studies on reactions of illuminated chloroplasts. I. Mechanism of the reduction of oxygen and other Hill reagents. Arch. Biochem. Biophys. **33**:65-77.
10. **Asada K, Kiso K, Yoshikawa K.** 1974. Univalent reduction of molecular oxygen by spinach chloroplasts on illumination. J. Biol. Chem. **249**:2175-2181.
11. **Telfer A, Bishop SM, Phillips D, Barber J.** 1994. Isolated photosynthetic reaction center of photosystem II as a sensitizer for the formation of singlet oxygen. Detection and quantum yield determination using a chemical trapping technique. J. Biol. Chem. **269**:13244-13253.
12. **Hideg E, Kálai T, Hideg K, Vass I.** 1998. Photoinhibition of photosynthesis in vivo results in singlet oxygen production detection via nitroxide-induced fluorescence quenching in broad bean leaves. Biochemistry. **37**:11405-11411.
13. **Pospíšil P.** 2009. Production of reactive oxygen species by photosystem II. Biochim. Biophys. Acta. **1787**:1151-1160.
14. **Asada K.** 2006. Production and scavenging of reactive oxygen species in chloroplasts and their functions. Plant Physiol. **141**:391-396.
15. **Imlay JA, Fridovich I.** 1991. Superoxide production by respiring membranes of *Escherichia coli*. Free Radic. Res. Commun. **12-13**:59-66.
16. **Boveris A, Chance B.** 1973. The mitochondrial generation of hydrogen peroxide. General properties and effect of hyperbaric oxygen. Biochem. J. **134**:707-716.
17. **Kussmaul L, Hirst J.** 2006. The mechanism of superoxide production by NADH:ubiquinone oxidoreductase (complex I) from bovine heart mitochondria. Proc. Natl. Acad. Sci. **103**:7607-7612.

18. **Murphy MP.** 2009. How mitochondria produce reactive oxygen species. *Biochem. J.* **417**:1-13.
19. **Messner KR, Imlay JA.** 1999. The identification of primary sites of superoxide and hydrogen peroxide formation in the aerobic respiratory chain and sulfite reductase complex of *Escherichia coli*. *J. Biol. Chem.* **274**:10119-10128.
20. **Seaver LC, Imlay JA.** 2004. Are respiratory enzymes the primary sources of intracellular hydrogen peroxide? *J. Biol. Chem.* **279**:48742-48750.
21. **Korshunov S, Imlay JA.** 2010. Two sources of endogenous H₂O₂ in *Escherichia coli*. *Mol. Microbiol.* **75**:1389–1401.
22. **Imlay JA.** 2013. The molecular mechanisms and physiological consequences of oxidative stress: lessons from a model bacterium. *Nat. Rev. Microbiol.* **11**:443–454.
23. **Imlay JA.** 1995. A metabolic enzyme that rapidly produces superoxide, fumarate reductase of *Escherichia coli*. *J. Biol. Chem.* **270**:19767-19777.
24. **Kohanski MA, Dwyer DJ, Hayete B, Lawrence CA, Collins JJ.** 2007. A common mechanism of cellular death induced by bactericidal antibiotics. *Cell.* **130**:797-810.
25. **Dwyer DJ, Kohanski MA, Collins JJ.** 2009. Role of reactive oxygen species in antibiotic action and resistance. *Curr. Opin. Microbiol.* **12**:482-489.
26. **Liu Y, Imlay JA.** 2013. Cell death from antibiotics without the involvement of reactive oxygen species. *Science.* **339**:1210-1213.

27. **Keren I, Wu Y, Inocencio J, Mulcahy LR, Lewis K.** 2013. Killing by bactericidal antibiotics does not depend on reactive oxygen species. *Science*. **339**:1213-1216.
28. **Babior BM, Kipnes RS, Curnutte JT.** 1973. Biological defense mechanisms. The production by leukocytes of superoxide, a potential bactericidal agent. *J. Clin. Invest.* **52**:741-744.
29. **Lam GY, Huang J, Brumell JH.** 2010. The many roles of NOX2 NADPH oxidase-derived ROS in immunity. *Semin. Immunopathol.* **32**:415-430.
30. **Yang Y, Bazhin AV, Werner J, Karakhanova S.** 2013. Reactive oxygen species in the immune system. *Int. Rev. Immunol.* **32**:249-270.
31. **Lambeth JD.** 2004. NOX enzymes and the biology of reactive oxygen. *Nat. Rev. Immunol.* **4**:181-189.
32. **McCord JM, Fridovich I.** 1969. Superoxide dismutase. An enzymic function for erythrocyte hemocuprein (hemocuprein). *J. Biol. Chem.* **244**:6049-6055.
33. **Edward RA, Whittaker MM, Whittaker JW, Jameson GB, Baker EN.** 1998. Distinct metal environment in Fe-substituted manganese superoxide dismutase provides a structural basis of metal specificity. *J. Am. Chem. Soc.* **120**:9684–9685.
34. **Yamakura F, Sugio S, Hiraoka BY, Ohmori D, Yokota T.** 2003. Pronounced conversion of the metal-specific activity of superoxide dismutase from *Porphyromonas gingivalis* by the mutation of a single amino acid (Gly155Thr) located apart from the active site. *Biochemistry.* **42**:10790-10799.

35. **Kroll JS, Langford PR, Wilks KE, Keil AD.** 1995. Bacterial [Cu,Zn]-superoxide dismutase: phylogenetically distinct from the eukaryotic enzyme, and not so rare after all! *Microbiology*. **141**:2271-2279.
36. **Miller AF.** 2004. Superoxide dismutases: active sites that save, but a protein that kills. *Curr. Opin. Chem. Biol.* **8**:162-168.
37. **Gort AS, Ferber DM, Imlay JA.** 1999. The regulation and role of the periplasmic copper, zinc superoxide dismutase of *Escherichia coli*. *Mol. Microbiol.* **32**:179-191.
38. **San Mateo LR, Toffer KL, Orndorff PE, Kawula TH.** 1999. Neutropenia restores virulence to an attenuated Cu,Zn superoxide dismutase-deficient *Haemophilus ducreyi* strain in the swine model of chancroid. *Infect. Immun.* **67**:5345-5351.
39. **Sansone A, Watson PR, Wallis TS, Langford PR, Kroll JS.** 2002. The role of two periplasmic copper- and zinc-cofactored superoxide dismutases in the virulence of *Salmonella choleraesuis*. *Microbiology*. **148**:719-726.
40. **Fee JA.** 1991. Regulation of *sod* genes in *Escherichia coli*: relevance to superoxide dismutase function. *Mol. Microbiol.* **5**:2599-2610.
41. **Wuerges J, Lee JW, Yim YI, Yim HS, Kang SO, Djinovic Carugo K.** 2004. Crystal structure of nickel-containing superoxide dismutase reveals another type of active site. *Proc. Natl. Acad. Sci.* **101**:8569-8574.
42. **Barondeau DP, Kassmann CJ, Bruns CK, Tainer JA, Getzoff ED.** 2004. Nickel superoxide dismutase structure and mechanism. *Biochemistry*. **43**:8038-8047.

43. **Sheng Y, Abreu IA, Cabelli DE, Maroney MJ, Miller A-F, Teixeira M, Valentine JS.** 2014. Superoxide dismutases and superoxide reductases. *Chem. Rev.* **114**:3854–3918.
44. **Mishra S, Imlay J.** 2012. Why do bacteria use so many enzymes to scavenge hydrogen peroxide? *Arch. Biochem. Biophys.* **525**:145-160.
45. **Christman MF, Morgan RW, Jacobson FS, Ames BN.** 1985. Positive control of a regulon for defenses against oxidative stress and some heat-shock proteins in *Salmonella typhimurium*. *Cell.* **41**:753-762.
46. **Poole LB.** 2005. Bacterial defenses against oxidants: mechanistic features of cysteine-based peroxidases and their flavoprotein reductases. *Arch. Biochem. Biophys.* **433**:240-254.
47. **Parsonage D, Youngblood DS, Sarma GN, Wood ZA, Karplus PA, Poole LB.** 2005. Analysis of the link between enzymatic activity and oligomeric state in AhpC, a bacterial peroxiredoxin. *Biochemistry.* **44**:10583-10592.
48. **Hall A, Karplus PA, Poole LB.** 2009. Typical 2-Cys peroxiredoxins--structures, mechanisms and functions. *FEBS J.* **276**:2469-2477.
49. **Parsonage D, Karplus PA, Poole LB.** 2008. Substrate specificity and redox potential of AhpC, a bacterial peroxiredoxin. *Proc. Natl. Acad. Sci.* **105**:8209-8214.
50. **Seaver LC, Imlay JA.** 2001. Alkyl hydroperoxide reductase is the primary scavenger of endogenous hydrogen peroxide in *Escherichia coli*. *J. Bacteriol.* **183**:7173–7181.

51. **Klotz MG, Klassen GR, Loewen PC.** 1997. Phylogenetic relationships among prokaryotic and eukaryotic catalases. *Mol. Biol. Evol.* **14**:951-958.
52. **Murshudov GN, Grebenko AI, Barynin V, Dauter Z, Wilson KS, Vainshtein BK, Melik-Adamyan W, Bravo J, Ferrán JM, Ferrer JC, Switala J, Loewen PC, Fita I.** 1996. Structure of the heme d of *Penicillium vitale* and *Escherichia coli* catalases. *J. Biol. Chem.* **271**:8863-8868.
53. **Bravo J, Verdaguer N, Tormo J, Betzel C, Switala J, Loewen PC, Fita I.** 1995. Crystal structure of catalase HPII from *Escherichia coli*. *Structure.* **3**:491-502.
54. **Hillar A, Nicholls P, Switala J, and Loewen PC.** 1994. NADPH binding and control of catalase compound II formation: comparison of bovine, yeast, and *Escherichia coli* enzymes. *Biochem. J.* **300**:531–539.
55. **Díaz A, Loewen PC, Fita I, Carpena X.** 2012. Thirty years of heme catalases structural biology. *Arch. Biochem. Biophys.* **525**:102-110.
56. **Loewen P.** 1996. Probing the structure of catalase HPII of *Escherichia coli*-a review. *Gene.* **179**:39-44.
57. **Chelikani P, Fita I, Loewen PC.** 2004. Diversity of structures and properties among catalases. *Cell. Mol. Life Sci.* **61**:192-208.
58. **Switala J, O'Neil JO, Loewen PC.** 1999. Catalase HPII from *Escherichia coli* exhibits enhanced resistance to denaturation. *Biochemistry.* **38**:3895-3901.
59. **Claiborne A, Malinowski DP, Fridovich I.** 1979. Purification and characterization of hydroperoxidase II of *Escherichia coli* B. *J. Biol. Chem.* **254**:11664-11668.

60. **Kolattukudy PE, Mohan R, Bajar MA, Sherf BA.** 1992. Plant peroxidase gene expression and function. *Biochem. Soc. Trans.* **20**:333-337.
61. **Sutherland GR, Zapanta LS, Tien M, Aust SD.** 1997. Role of calcium in maintaining the heme environment of manganese peroxidase. *Biochemistry.* **36**:3654-3662.
62. **Sundaramoorthy M, Kishi K, Gold MH, Poulos TL.** 1997. Crystal structures of substrate binding site mutants of manganese peroxidase. *J. Biol. Chem.* **272**:17574-17580.
63. **Choinowski T, Blodig W, Winterhalter KH, Piontek K.** 1999. The crystal structure of lignin peroxidase at 1.70 Å resolution reveals a hydroxy group on the cbeta of tryptophan 171: a novel radical site formed during the redox cycle. *J. Mol. Biol.* **286**:809-827.
64. **Doyle WA, Blodig W, Veitch NC, Piontek K, Smith AT.** 1998. Two substrate interaction sites in lignin peroxidase revealed by site-directed mutagenesis. *Biochemistry.* **37**:15097-15105.
65. **Timofeevski SL, Nie G, Reading NS, Aust SD.** 1999. Addition of veratryl alcohol oxidase activity to manganese peroxidase by site-directed mutagenesis. *Biochem. Biophys. Res. Commun.* **256**:500-504.
66. **Kaothien P, Shimokawatoko Y, Kawaoka A, Yoshida K, Shinmyo A.** 2000. A *cis*-element containing PAL-box functions in the expression of the wound-inducible peroxidase gene of horseradish. *Plant Cell Rep.* **19**:558-562.

67. **Howes BD, Feis A, Raimondi L, Indiani C, Smulevich G.** 2001. The critical role of the proximal calcium ion in the structural properties of horseradish peroxidase. *J. Biol. Chem.* **276**:40704-40711.
68. **Gajhede M, Schuller DJ, Henriksen A, Smith AT, Poulos TL.** 1997. Crystal structure of horseradish peroxidase C at 2.15 Å resolution. *Nat. Struct. Biol.* **4**:1032-1038.
69. **Veitch NC.** 2004. Horseradish peroxidase: a modern view of a classic enzyme. *Phytochemistry.* **65**:249-259.
70. **Huyett JE, Doan PE, Gurbiel R, Houseman ALP, Sivaraja M, Goodin DB, Hoffman BM.** 1995. Compound ES of cytochrome *c* peroxidase contains a Trp pi-cation radical: characterization by continuous wave and pulsed Q-band external nuclear double resonance spectroscopy. *J. Am. Chem. Soc.* **117**:9033–9041.
71. **Patterson WR, Poulos TL.** 1995. Crystal structure of recombinant pea cytosolic ascorbate peroxidase. *Biochemistry.* **34**:4331-4341.
72. **Fishel LA, Villafranca JE, Mauro JM, Kraut J.** 1987. Yeast cytochrome *c* peroxidase: mutagenesis and expression in *Escherichia coli* show tryptophan-51 is not the radical site in compound I. *Biochemistry.* **26**:351-360.
73. **Welinder KG.** 1991. Bacterial catalase-peroxidases are gene duplicated members of the plant peroxidase superfamily. *Biochim. Biophys. Acta.* **1080**:215-220.
74. **Baker RD, Cook CO, Goodwin DC.** 2004. Properties of catalase-peroxidase lacking its C-terminal domain. *Biochem. Biophys. Res. Commun.* **320**:833-839.
75. **Baker RD, Cook CO, Goodwin DC.** 2006. Catalase-peroxidase active site restructuring by a distant and "inactive" domain. *Biochemistry.* **45**:7113-7121.

76. **Li Y, Goodwin DC.** 2004. Vital roles of an interhelical insertion in catalase-peroxidase bifunctionality. *Biochem. Biophys. Res. Commun.* **318**:970-976.
77. **Kudalkar SN.** 2012. Roles of large loops in catalytic versatility of catalase-peroxidases: significance of peripheral structures in improvising enzyme functions. Ph.D. dissertation. Auburn University, Auburn, AL.
78. **Jakopitsch C, Kolarich D, Petutschnig G, Furtmüller PG, Obinger C.** 2003. Distal side tryptophan, tyrosine and methionine in catalase-peroxidases are covalently linked in solution. *FEBS Lett.* **552**:135-140.
79. **Zhao X, Yu S, Rangelova K, Suarez J, Metlitsky L, Schelvis JP, Magliozzo RS.** 2009. Role of the oxyferrous heme intermediate and distal side adduct radical in the catalase activity of *Mycobacterium tuberculosis* KatG revealed by the W107F mutant. *J. Biol. Chem.* **284**:7030-7037.
80. **Carpaena X, Wiseman B, Deemagarn T, Singh R, Switala J, Ivancich A, Fita I, Loewen PC.** 2005. A molecular switch and electronic circuit modulate catalase activity in catalase-peroxidases. *EMBO Rep.* **6**:1156-1162.
81. **Kudalkar SN, Campbell RA, Li Y, Varnado CL, Prescott C, Goodwin DC.** 2012. Enhancing the peroxidatic activity of KatG by deletion mutagenesis. *J. Inorg. Biochem.* **116**:106-115.
82. **Jakopitsch C, Droghetti E, Schmuckenschlager F, Furtmüller PG, Smulevich G, Obinger C.** 2005. Role of the main access channel of catalase-peroxidase in catalysis. *J. Biol. Chem.* **280**:42411-42422.

83. **Carpena X, Loprasert S, Mongkolsuk S, Switala J, Loewen PC, Fita I.** 2003. Catalase-peroxidase KatG of *Burkholderia pseudomallei* at 1.7 Å resolution. *J. Mol. Biol.* **327**:475-489.
84. **Jakopitsch C, Wanasinghe A, Jantschko W, Furtmüller PG, Obinger C.** 2005. Kinetics of interconversion of ferrous enzymes, compound II and compound III, of wild-type *synechocystis* catalase-peroxidase and Y249F: proposal for the catalytic mechanism. *J. Biol. Chem.* **280**:9037-9042.
85. **Zhao X, Suarez J, Khajo A, Yu S, Metlitsky L, Magliozzo RS.** 2010. A radical on the Met-Tyr-Trp modification required for catalase activity in catalase-peroxidase is established by isotopic labeling and site-directed mutagenesis. *J. Am. Chem. Soc.* **132**:8268-8269.
86. **Ndontsa EN, Moore RL, Goodwin DC.** 2012. Stimulation of KatG catalase activity by peroxidatic electron donors. *Arch. Biochem. Biophys.* **525**:215-222.
87. **Klotz MG, Loewen PC.** 2003. The molecular evolution of catalytic hydroperoxidases: evidence for multiple lateral transfer of genes between prokaryota and from bacteria into eukaryota. *Mol. Biol. Evol.* **20**:1098-1112.
88. **Brunder W, Schmidt H, Karch H.** 1996. KatP, a novel catalase-peroxidase encoded by the large plasmid of enterohaemorrhagic *Escherichia coli* O157:H7. *Microbiology.* **142**:3305-3315.
89. **Varnado CL, Hertwig KM, Thomas R, Roberts JK, Goodwin DC.** 2004. Properties of a novel periplasmic catalase-peroxidase from *Escherichia coli* O157:H7. *Arch. Biochem. Biophys.* **421**:166-174.

90. **Garcia E, Nedialkov YA, Elliott J, Motin VL, Brubaker RR.** 1999. Molecular characterization of KatY (antigen 5), a thermoregulated chromosomally encoded catalase-peroxidase of *Yersinia pestis*. *J. Bacteriol.* **181**:3114-3122.
91. **Bandyopadhyay P, Steinman HM.** 2000. Catalase-peroxidases of *Legionella pneumophila*: cloning of the *kata* gene and studies of KatA function. *J. Bacteriol.* **182**:6679-6686.
92. **Amemura-Maekawa J, Mishima-Abe S, Kura F, Takahashi T, Watanabe H.** 1999. Identification of a novel periplasmic catalase-peroxidase KatA of *Legionella pneumophila*. *FEMS Microbiol. Lett.* **176**:339-344.
93. **Kobayashi SD, Voyich JM, Burlak C, DeLeo FR.** 2005. Neutrophils in the innate immune response. *Arch. Immunol. Ther. Exp.* **53**:505-517.
94. **Loewen PC, Klotz MG, Hassett DJ.** 2000. Catalase—an “old” enzyme that continues to surprise us. *ASM News.* **66**:76-82.
95. **Klebanoff SJ.** 1968. Myeloperoxidase-halide-hydrogen peroxide antibacterial system. *J. Bacteriol.* **95**:2131-2138.
96. **Nauseef WM.** 1990. Myeloperoxidase deficiency. *Hematol. Pathol.* **4**:165-178.
97. **Lucht W.** 2011. Earth systems: Shaped by life. *Nature.* **470**:460-461.
98. **Vlasits J, Jakopitsch C, Schwanninger M, Holubar P, Obinger C.** 2007. Hydrogen peroxide oxidation by catalase-peroxidase follows a non-scrambling mechanism. *FEBS Lett.* **581**:320-324.
99. **Bonagura CA, Bhaskar B, Shimizu H, Li H, Sundaramoorthy M, McRee DE, Goodin DB, Poulos TL.** 2003. High-resolution crystal structures and

- spectroscopy of native and compound I cytochrome *c* peroxidase. *Biochemistry*. **42**:5600-5608.
100. **Wada, K, Tada, T, Nakamura, Y, Kinoshita, T, Tamoi, M, Shigeoka, S, Nishimura, K.** 2002. Crystallization and preliminary X-ray diffraction studies of catalase-peroxidases from *Synechococcus* PCC 7942. *Acta. Crystallogr. D Biol. Crystallogr.* **58**:157-159.
 101. **Yamada, Y, Fujiwara, T, Sato, T, Igarashi, N, Tanaka, N.** 2002. The 2.0 Å crystal structure of catalase-peroxidase from *Haloarcula marismortui*. *Nat. Struct. Biol.* **9**:691-695.
 102. **Bertrand T, Eady NA, Jones JN, Jesmin, Nagy JM, Jamart-Grégoire B, Raven EL, Brown KA.** 2004. Crystal structure of *Mycobacterium tuberculosis* catalase-peroxidase, *J. Biol. Chem.* **279**:38991-38999.
 103. **Kamachi S, Wada K, Tamoi M, Shigeoka S, Tada T.** 2014. The 2.2 Å resolution structure of the catalase-peroxidase KatG from *Synechococcus elongatus* PCC7942. *Acta. Crystallogr. F Struct. Biol. Commun.* **70**:288-293.
 104. **Zámocký M, Regelsberger G, Jakopitsch C, Obinger C.** 2001. The molecular peculiarities of catalase-peroxidases. *FEBS Lett.* **492**:177-182.
 105. **Carpaena X, Melik-Adamyan W, Loewen PC, Fita I.** 2004. Structure of the C-terminal domain of the catalase-peroxidase KatG from *Escherichia coli*. *Acta. Crystallogr. D Biol. Crystallogr.* **60**:1824-1832.
 106. **Jakopitsch C, Auer M, Ivancich A, Rüker F, Furtmüller PG, Obinger C.** 2003. Total conversion of bifunctional catalase-peroxidase (KatG) to

- monofunctional peroxidase by exchange of a conserved distal side tyrosine. J. Biol. Chem. **278**:20185-20191.
107. **Yu S, Giroto S, Zhao X, Magliozzo RS.** 2003. Rapid formation of compound II and a tyrosyl radical in the Y229F mutant of *Mycobacterium tuberculosis* catalase-peroxidase disrupts catalase but not peroxidase function. J. Biol. Chem. **278**:44121-44127.
 108. **Moore S.** Accessed in 2008. 'Round-the-horn site-directed mutagenesis. On http://openwetware.org/wiki/Round-the-horn_site-directed_mutagenesis.
 109. **Falk JK.** 1964. In Smith KM (ed) Porphyrins and metalloporphyrins, p 804-807, Elsevier Publishing, New York.
 110. **Hagen WR.** Accessed in 2012. Biomolecular EPR spectroscopy. On <http://www.bt.tudelft.nl/biomolecularEPRspectroscopy>.
 111. **Chouchane S, Giroto S, Kapetanaki S, Schelvis JP, Yu S, Magliozzo RS.** 2003. Analysis of heme structural heterogeneity in *Mycobacterium tuberculosis* catalase-peroxidase (KatG). J. Biol. Chem. **278**:8154-8162.
 112. **Ivancich A, Jakopitsch C, Auer M, Un S, Obinger C.** 2003. Protein-based radicals in the catalase-peroxidase of *synechocystis* PCC6803: a multifrequency EPR investigation of wild-type and variants on the environment of the heme active site. J. Am. Chem. Soc. **125**:14093-14102.
 113. **Svistunenko DA, Worrall JA, Chugh SB, Haigh SC, Ghiladi RA, Nicholls P.** 2012. Ferric haem forms of *Mycobacterium tuberculosis* catalase-peroxidase probed by EPR spectroscopy: Their stability and interplay with pH. Biochimie. **94**:1274-1280.

114. **Kaessmann H.** 2010. Origins, evolution, and phenotypic impact of new genes. *Genome Res.* **20**:1313-1326.
115. **Singh R, Wiseman B, Deemagarn T, Jha V, Switala J, Loewen PC.** 2008. Comparative study of catalase-peroxidases (KatGs). *Arch. Biochem. Biophys.* **471**:207-214.
116. **Hiner AN, Hernández-Ruiz J, Rodríguez-López JN, García-Cánovas F, Brisset NC, Smith AT, Arnao MB, Acosta M.** 2002. Reactions of the class II peroxidases, lignin peroxidase and *Arthromyces ramosus* peroxidase, with hydrogen peroxide. Catalase-like activity, compound III formation, and enzyme inactivation. *J. Biol. Chem.* **277**:26879-26885.
117. **Moore RL.** 2009. Toward the understanding of complex biochemical systems: the significance of global protein structure and thorough parametric analysis. Ph.D. dissertation. Auburn University, Auburn, AL.
118. **Jakopitsch C, Auer M, Regelsberger G, Jantschko W, Furtmüller PG, Rüker F, Obinger C.** 2003. Distal site aspartate is essential in the catalase activity of catalase-peroxidases. *Biochemistry.* **42**:5292-5300.
119. **Santoni E, Jakopitsch C, Obinger C, Smulevich G.** 2004. Comparison between catalase-peroxidase and cytochrome *c* peroxidase. The role of the hydrogen-bond networks for protein stability and catalysis. *Biochemistry.* **43**:5792-5802.
120. **Baker CJ, Deahl K, Domek J, Orlandi EW.** 2000. Scavenging of H₂O₂ and production of oxygen by horseradish peroxidase. *Arch. Biochem. Biophys.* **382**:232-237.

121. **Hernández-Ruiz J, Arnao MB, Hiner AN, García-Cánovas F, Acosta M.** 2001. Catalase-like activity of horseradish peroxidase: relationship to enzyme inactivation by H₂O₂. *Biochem. J.* **354**:107-114.
122. **Ohno S.** 1970. Evolution by gene duplication. Springer-Verlag, New York.
123. **Mildvan AS.** 2004. Inverse thinking about double mutants of enzymes. *Biochemistry.* **43**:14517-14520.
124. **Chelikani P, Carpena X, Fita I, Loewen PC.** 2003. An electrical potential in the access channel of catalases enhances catalysis. *J. Biol. Chem.* **278**:31290-31296.
125. **Njuma OJ, Ndontsa EN, Goodwin DC.** 2014. Catalase in peroxidase clothing: Interdependent cooperation of two cofactors in the catalytic versatility of KatG. *Arch. Biochem. Biophys.* **544**:27-39.
126. **Wiseman B, Carpena X, Feliz M, Donald LJ, Pons M, Fita I, Loewen PC.** 2010. Isonicotinic acid hydrazide conversion to Isonicotinyl-NAD by catalase-peroxidases. *J. Biol. Chem.* **285**:26662-26673.
127. **Hillar A, Van Caesele L, Loewen PC.** 1999. Intracellular location of catalase-peroxidase hydroperoxidase I of *Escherichia coli*. *FEMS Microbiol. Lett.* **170**:307-312.
128. **Singh R, Wiseman B, Deemagarn T, Donald LJ, Duckworth HW, Carpena X, Fita I, Loewen PC.** 2004. Catalase-peroxidases (KatG) exhibit NADH oxidase activity. *J. Biol. Chem.* **279**:43098-43106.
129. **Moore RL, Powell LJ, Goodwin DC.** 2008. The kinetic properties producing the perfunctory pH profiles of catalase-peroxidases. *Biochim. Biophys. Acta.* **1784**:900-907.

130. **Josephy PD, Eling T, Mason RP.** 1982. The horseradish peroxidase-catalyzed oxidation of 3,5,3',5'-tetramethylbenzidine. Free radical and charge-transfer complex intermediates. *J. Biol. Chem.* **257**:3669-3675.
131. **Scott SL, Chen W-J, Bakac A, Espenson JH.** 1993. Spectroscopic parameters, electrode potentials, acid ionization constants, and electron exchange rates of the 2,2'-azinobis(3-ethylbenzothiazolone-6-sulfonate) radicals and ions. *J. Phys. Chem.* **97**:6710-6714.
132. **Faguy DM, Doolittle WF.** 2000. Horizontal transfer of catalase-peroxidase genes between archaea and pathogenic bacteria. *Trends Genet.* **16**:196-197.
133. **Ndontsa EN.** 2013. Synergy not antagonism in antioxidant defenses: the unanticipated effect of electron donors on catalase-peroxidase function. Ph.D. dissertation. Auburn University, Auburn, AL.
134. **Bandyopadhyay P, Byrne B, Chan Y, Swanson MS, Steinman HM.** 2003. *Legionella pneumophila* catalase-peroxidases are required for proper trafficking and growth in primary macrophages. *Infect. Immun.* **71**:4526-4535.
135. **Loew, O.** 1900. A new enzyme of general occurrence in organisms. *Science.* **11**:701-702.
136. **Winterbourn CC, Hampton MB, Livesey JH, Kettle AJ.** 2006. Modeling the reactions of superoxide and myeloperoxidase in the neutrophil phagosome: implications for microbial killing. *J. Biol. Chem.* **281**:39860-39869.
137. **Warrens AN, Jones MD, Lechler RI.** 1997. Splicing by overlap extension by PCR using asymmetric amplification: an improved technique for the generation of hybrid proteins of immunological interest. *Gene.* **186**:29-35.

138. **Murphy KC, Campellone KG, Poteete AR.** 2000. PCR-mediated gene replacement in *Escherichia coli*. *Gene*. **246**:321-330.
139. **Herrero M, de Lorenzo V, Timmis KN.** 1990. Transposon vectors containing non-antibiotic resistance selection markers for cloning and stable chromosomal insertion of foreign genes in gram-negative bacteria. *J. Bacteriol.* **172**:6557-6567.
140. **Miller VL, Mekalanos JJ.** 1988. A novel suicide vector and its use in construction of insertion mutations: osmoregulation of outer membrane proteins and virulence determinants in *Vibrio cholerae* requires *toxR*. *J. Bacteriol.* **170**:2575-2583.
141. **Thomason LC, Costantino N, Court DL.** 2007. *E. coli* genome manipulation by P1 transduction. *Curr. Protoc. Mol. Biol.* **Chapter 1**:Unit 1.17.
142. **Guzman LM, Belin D, Carson MJ, Beckwith J.** 1995. Tight regulation, modulation, and high-level expression by vectors containing the arabinose PBAD promoter. *J. Bacteriol.* **177**:4121-4130.
143. **Storz G, Tartaglia LA, Ames BN.** 1990. Transcriptional regulator of oxidative stress-inducible genes: direct activation by oxidation. *Science*. **248**:189-194.
144. **Mulvey MR, Switala J, Borys A, Loewen PC.** 1990. Regulation of transcription of *katE* and *katF* in *Escherichia coli*. *J. Bacteriol.* **172**:6713-6720.
145. **Sevinc MS, Ens W, Loewen PC.** 1995. The cysteines of catalase HPII of *Escherichia coli*, including Cys438 which is blocked, do not have a catalytic role. *Eur. J. Biochem.* **230**:127-132.
146. **Loewen PC, Switala J.** 1986. Purification and characterization of catalase HPII from *Escherichia coli* K12. *Biochem. Cell. Biol.* **64**:638-646.

147. **Uhlich GA.** 2009. KatP contributes to OxyR-regulated hydrogen peroxide resistance in *Escherichia coli* serotype O157:H7. *Microbiology*. **155**:3589-3598.
148. **Foster JW.** 2004. *Escherichia coli* acid resistance: tales of an amateur acidophile. *Nat. Rev. Microbiol.* **2**:898-907.
149. **Kanjee U, Houry WA.** 2013. Mechanisms of acid resistance in *Escherichia coli*. *Annu. Rev. Microbiol.* **67**:65-81.
150. **Richard H, Foster JW.** 2004. *Escherichia coli* glutamate- and arginine-dependent acid resistance systems increase internal pH and reverse transmembrane potential. *J. Bacteriol.* **186**:6032-6041.
151. **Sun Y, Fukamachi T, Saito H, Kobayashi H.** 2011. ATP requirement for acidic resistance in *Escherichia coli*. *J. Bacteriol.* **193**:3072-3077.
152. **Putnam CD, Arvai AS, Bourne Y, Tainer JA.** 2000. Active and inhibited human catalase structures: ligand and NADPH binding and catalytic mechanism. *J. Mol. Biol.* **296**:295-309.
153. **Condemine G, Berrier C, Plumbridge J, Ghazi A.** 2005. Function and expression of an *N*-acetylneuraminic acid-inducible outer membrane channel in *Escherichia coli*. *J. Bacteriol.* **187**:1959-1965.
154. **Wang Y, Goodwin DC.** 2013. Integral role of the I'-helix in the function of the "inactive" C-terminal domain of catalase-peroxidase (KatG). *Biochim. Biophys. Acta.* **1834**:362-371.
155. **Uhlich GA, Chen CY, Cottrell BJ, Irwin PL, Phillips JG.** 2012. Peroxide resistance in *Escherichia coli* serotype O157 : H7 biofilms is regulated by both RpoS-dependent and -independent mechanisms. *Microbiology.* **158**:2225-2234.

156. **Benjamin MM, Datta AR.** 1995. Acid tolerance of enterohemorrhagic *Escherichia coli*. *Appl. Environ. Microbiol.* **61**: 1669–1672.
157. **Ghiladi RA, Medzihradzky KF, Rusnak FM, Ortiz de Montellano PR.** 2005. Correlation between isoniazid resistance and superoxide reactivity in *Mycobacterium tuberculosis* KatG. *J. Am. Chem. Soc.* **127**:13428-13442.
158. **Switala J, Loewen PC.** 2002. Diversity of properties among catalases. *Arch. Biochem. Biophys.* **401**:145-154.